

University of Nottingham

UK | CHINA | MALAYSIA

Polymer nanomedicine: Understanding activity at the cellular and molecular level using metabolomics

Mohammad Ahmad Al-Natour; MSc

Thesis submitted to the University of Nottingham for the degree of Doctor of Philosophy

January 2019

Abstract

Nanomedicine can be defined as the science and application of therapeutic entities which have dimensions in the 10-1000 nm range. Polymer nanomedicine involves using polymers to aid drug delivery at the nanoscale, the research underlying this discipline employs nanotechnology methods to prevent, diagnose and treat diseases. In attempt to understand the biological effects of polymer nanomedicine on living tissues, a global metabolic profiling approach was utilised to study the impact of different polymeric nanoparticles on various cell lines. In this project, Poly (lactic-co-glycolic acid) (PLGA) was adopted to fabricate Nanoparticles (NPs). This choice was made because PLGA is a versatile synthetic co-polymer that is already widely used in pharmaceutical applications. Cell-based metabolomics were applied to investigate the metabolic changes in human-like macrophages and lung carcinoma cell lines after the exposure to different types of PLGA NPs. The studies revealed that the plain PLGA NPs perturbed metabolism of some important amino acids, including arginine and proline and altered membrane lipids levels in different degrees. The next phase in the study was to evaluate the metabolic effects of drug loaded NPs. Methotrexate (MTX) was selected as the model drug, as it is a folate analogue antimetabolite, and has been widely used for the

treatment of rheumatoid arthritis and cancer. MTX loaded NPs were thus prepared and tested in metabolomics assays in comparison with free MTX. The data showed that MTX loaded NPs had less impact on the macrophages than free MTX, and the effects of the NPs containing MTX were limited to changes of nucleotide metabolism and suppressing the tricarboxylic acid cycle (TCA). In comparison, MTX loaded NPs showed a higher impact on A549 cells, compared to the free drug, which was again in accord similar to other cell lines in literature. Finally, DNA loaded NPs in the form of polyplexes made of cationic polymers and plasmid DNA were studied. The study revealed that the polyplexes downregulated metabolites associated with glycolysis and the TCA cycle and induced oxidative stress in both cell lines. The fold changes of the metabolites indicated that the polyplexes of polyethyleneimine and hyperbranched polylysine affected the metabolism much more than the polyplexes of hyperbranched polylysine-co-histidine. This was in line with transfection results, suggesting a correlation between the toxicity and transfection efficiency of these polyplexes. These results highlight the importance of the metabolomics approach not just to assess the potential toxicity of polyplexes but also to understand the molecular mechanisms underlying their actions, which could help in designing more efficient drug delivery systems.

Acknowledgement

I would like to express my sincere appreciations and gratitude to my principal supervisor Prof. Cameron Alexander for all his guidance and inspiration throughout my studies. I am truly thankful to my co-supervisors, Dr Dong-Hyun Kim and Prof. Amir Ghaemmaghami for all the support and help. I would also like to thank Dr Vincenzo Taresco and Dr Francesca Mastrotto for their valuable assistance in polymer synthesis especially at the beginning of my project.

Special thanks to our collaborators Dr Ali Alazzo, Dr Snow Stolnik-Trenkic and Dr Keith Spriggs for their contribution and helping in the polyplexes study. I gratefully acknowledge Dr Yousif Deifallah, Dr Veeren Chauhan and Dr Jonathan Aylott for their contribution and helping in C elegans work. Also, thanks to all of the students and postdoctoral researchers in B-15 lab for their company and useful discussion.

I would like to thank the University of Petra in Jordan for awarding me the PhD Scholarship and sponsoring my study.

Most importantly, I would like to express my appreciation and thanks to my parents, my wife and my daughter for all their love and support.

List of Publications

- Ali Alazzo, **Mohammad Al-natour**, Keith Spriggs, Snjezana Stolnik, Amir Ghaemmaghami, Dong-Hyun Kim and Cameron Alexander. Investigating the molecular effects of hyperbranched polycation-DNA complexes on lung cancer cells using LC-MS-based metabolite profiling. Molecular Omics. 2019;15(1):77-87

Under revision by ACS Macro letters

- **Mohammad Al-natour**, Veeren M Chauhan, Vincenzo Taresco, Mohamed D Yousif, Amir Ghaemmaghami, Dong-Hyun Kim, Jonathan W Aylott and Cameron Alexander. A Facile Dye-Initiated Polymerisation of Lactide-Glycolide Generates Highly Fluorescent PLGA for Enhanced Characterisation of Cellular Delivery

Contents

Abstract i
Acknowledgement iii
List of Publications iv
Contents v
List of Abbreviations vii
Chapter one 1
1 General Introduction 1
1.1 Nanomedicine 2
1.1.1 Nanoparticles (NPs) 4
1.1.2 Biodistribution and processing of nanomaterials 8
1.1.3 Toxicity of nanomedicines 10
1.2 Metabolomics 12
1.2.1 Targeted and untargeted metabolomics 13
1.2.2 Instrumentation 14
1.2.3 Metabolomics and effects of NPs 19
1.3 Aim of the study 24
Chapter two 26
2 A Facile Dye-Initiated Polymerisation of Lactide-Glycolide Generates Highly Fluorescent PLGA for Enhanced Characterisation of Cellular Delivery 26
2.1 Introduction 27
2.2 Materials and methods 30
2.2.1 Materials 30
2.2.2 Polymer synthesis 31
2.2.3 NPs formation and characterisation 33
2.2.4 Impact of NPs on cells viability 35
2.2.5 Cellular uptake of NPs 35
2.2.6 *In vitro* release 36
2.2.7 Caenorhabditis elegans growth 37
2.2.8 Caenorhabditis elegans NPs uptake 37
2.3 Results and discussion 38
2.3.1 Polymer synthesis 38
2.3.2 NPs formation and characterisation 40
2.3.3 NPs cellular uptake 42
2.3.4 Caenorhabditis elegans NPs uptake 47
2.4 Conclusion 49
2.5 Supporting information 50
Chapter three 56
3 Studying the impact of PGLA nanoparticles on activated THP-1 cells at the molecular level using LC-MS-based metabolomics 56
3.1 Introduction 57
3.2 Materials and methods 62
3.2.1 Materials 62
3.2.2 Polymer synthesis 62
3.2.3 NPs synthesis 64
3.2.4 Cell culture, activation and treatment 65
3.2.5 Metabolic activity (AlamarBlue®) assay. 66
3.2.6 Cellular uptake of NPs by activated THP-1 cells 66
3.2.7 Metabolite extraction 67
3.2.8 Liquid chromatography-mass spectrometry (LC-MS) 68

3.2.9 Data analysis and metabolite identification 69
3.3 Results and discussion 70
3.3.1 Polymer synthesis 70
3.3.2 NPs formation and characterisation 71
3.3.3 Metabolic activity (AlamarBlue®) assay 72
3.3.4 NPs cellular uptake 72
3.3.5 Multivariate analysis of LC-MS profiling data 73
3.3.6 Metabolic pathway analysis 75
3.4 Conclusion 3
3.5 Supporting information 4
Chapter four 11
4 LC-MS metabolomics comparisons of cancer cell and macrophage responses to polymer-encapsulated methotrexate and free drug 11
4.1 Introduction 12
4.2 Materials and methods 14
4.2.1 Materials 14
4.2.2 Cell culture 15
4.2.3 Metabolic activity (AlamarBlue®) assay. 15
4.2.4 Cellular uptake study 16
4.2.5 Metabolomic analysis 16
4.3 Results and discussion 19
4.4 Conclusion 28
4.5 Supporting information 29
Chapter five 37
5 Investigating the molecular effects of hyperbranched polycation-DNA complexes on lung cancer cells using LC-MS-based metabolite profiling 37
5.1 Introduction 38
5.2 Materials and methods 41
5.2.1 Materials 41
5.2.2 Preparation of polyplexes 42
5.2.3 Cell culture 42
5.2.4 Metabolic activity (MTT) assay. 42
5.2.5 Lactate dehydrogenase (LDH) detection assay 43
5.2.6 Annexin-V/PI apoptosis assay 44
5.2.7 *In vitro* Transfection study 45
5.2.8 Cellular uptake study 45
5.2.9 Metabolomic analysis 46
5.3 Results and discussion 50
5.4 Conclusion 67
5.5 Supporting information 69
Chapter six 78
6 Conclusion and future work 78
6.1 Conclusion 79
6.2 Future work 84
References 88
Appendix 118
Proton nuclear magnetic resonance (1H-NMR) spectroscopy 118
Particle size and Zeta potential measurement 118
Transmission electron microscopy (TEM) 118

List of Abbreviations

ABC	ATP-binding cassette
AFM	Atomic force microscope
ALL	Acute lymphoblastic leukemia
AMD	Age-related macular degeneration
ANOVA	Analysis of variance
CKD	Chronic kidney disease
DLS	Dynamic Light scattiring
DMEM	Dulbecco's modified Eagle's medium
DNA	Deoxyribonucleic acid
DSC	Differential scanning calorimetry
dTMP	Deoxythymidine monophosphate
dUMP	Deoxyuridine-5-monophosphate
EPR	Enhanced Permeability and Retention
ER	Extended release
FBS	Foetal bovine serum
FDA	Food and Drug Administration
FDR	False discovery rate
FGAR	5'-phosphoribosyl-N-formylglycinamide
FITC	Fluorescein isothiocyanate
FPGS	Folylpolyglutamyl synthetase
FT-IR	Fourier transform-infrared spectroscopy
GAR	5'-phosphoribosyl-glycinamide
GART	Phosphoribosylglycinamide formyltransferase
GSH	Reduced glutathione
GSSG	Oxidised glutathione
hb-polyK	Hyperbranched polylysine
hb-polyKH	Hyperbranched polylysine-co-Histidine
HCl	Hydrochloric acid
HEPES	4-(2-hydroxyethyl)-1-piperazineethanesulfonic acid
IDO	Indoleamine 2,3 dioxygenase
LC-MS	Liquid chromatography mass spectrometry
LDH	Lactate dehydrogenase
Mn	Average number molecular weight
MTT	Methylthiazolyldiphenyl-tetrazolium bromide
MTX	Methotrexate
Mw	Average weight molecular weight
MWCO	Molecular weight cut-off
NAC	N-acetylcysteine
NADH	Nicotinamide adenine dinucleotide reduced form
NADPH	Nicotinamide adenine dinucleotide phosphate
NHS	N-hydroxysuccinimide
NMR	Nuclear magnetic resonance
NO	Nitric oxide
NP	Nanoparticle

OPLS-DA	Orthogonal partial least squares discriminant analysis
PBS	Phosphate buffer saline
PDI	Polydispersity index
PEG	Polyethylene glycol
PEI	Polyethylenimine
PGs	Polyglutamates
RFC	Reduced folate carrier
RGD	Arginylglycylaspartic acid
RISC	RNA-inducing silencing complex
RNAi	RNA interference
ROS	Reactive oxygen species
RPMI	Roswell Park Memorial Institute media
SCID	Severe combined immunodeficiency disease
TCA	Tricarboxylic acid
TiO2	Titanium dioxide
TS	Thymidylate synthetase
VIP	Variable importance in projection scores

Chapter one

General Introduction

1.1 Nanomedicine

Nanomedicine is a branch of medicine that applies the knowledge and tools of nanotechnology to the prevention and treatment of disease. Nanomedicine involves the use of nanoscale materials, such as biocompatible nanoparticles and nanorobots, for diagnosis, delivery, sensing or actuation purposes in a living organism (1). Nanotechnology approaches to medicine have been considered as repairing, constructing, observing and regulating human biological systems at the molecular level (2). The broader applications of nanomedicine include early disease diagnosis as well as therapeutics which will increase our ability to treat challenging diseases, such as cancer (1, 3-5), cardiovascular diseases (5), neurodegenerative brain diseases (Alzheimer's and Parkinson's Diseases) (6, 7), diabetes (6), tuberculosis (8) and cystic fibrosis (7). The European Medicines Agency (EMA), defines nanomedicine as "a system designed for clinical applications that is composed of at least one nanoscale component, resulting in specific advantageous characteristics, such as better targeting and bioavailability of therapeutics, new modes of therapeutic action, and nanostructured surfaces/scaffolds for engineered tissues" (9). In this case, the nanoscale is defined as typically 1-1000 nm, Figure 1-1 (10). The definition highlights the main aims and advantages of nanomedicine, however, the applications of

nanomedicine are not limited to drug delivery for the purpose of treating or managing the symptoms of a certain ailment, but also efficient disease diagnosis and prevention (11-14). Polymer based nanomedicine involves using polymers to aid drug delivery at the nanoscale, this can done be either by physically entrapment, surface adsorption or covalent linkage. The term "Polymer therapeutics" is a subdivision of polymer nanomedicine that encompasses polymer-protein conjugates, drug-polymer conjugates, and supramolecular drug-delivery systems.

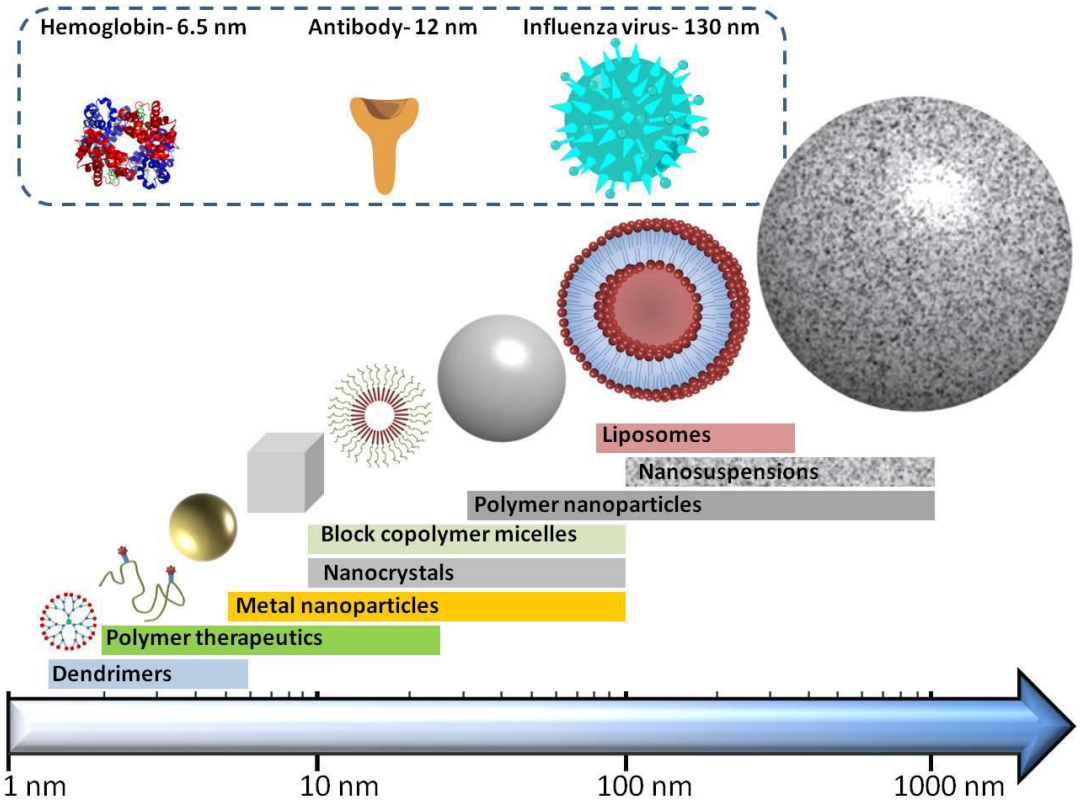


Figure 1-1: Schematic representation of different structures of nanomedicines and their approximate sizes. Biological nanostructures are shown at the top of the figure to facilitate the comparison. Adapted from reference (10).

1.1.1 Nanoparticles (NPs)

NPs are a principal component of nanomedicine, ranging in size from 1 to 100 nm (at least one dimension). They can have different shapes such as spheres, hemispheres, cylinders, tubes, cones, and wires (15), and can be either solid, hollow or porous (16). They can be made of polymers (17), lipids (18), proteins (19), nucleic acids (20), carbon (21), inorganic materials (22, 23) or mixtures of these materials (24). NPs are considered to be promising for cancer treatment, owing to reports of innate tumour targeting ability. In particular, NPs have been developed to exploit the enhanced permeation and retention effect (EPR); a phenomenon in which the vasculature surrounding tumours are leaky enough to allow ingress of NPs of <200 nm size, while at the same time the poor lymphatic drainage results in their accumulation in tumour cells (25). Although extensively cited in literature, and demonstrated conclusively to occur in mouse models of cancers, the EPR effect does not occur for all cancers, and examples in humans are not numerous in the literature (26, 27). In general, the size of NPs gives them transitional properties between molecules and their bulk counterparts, independent of their chemistry. For example, the surface area to volume ratio is very high in NPs, making surface modification or loading drugs by surface adsorption more efficient (28), NPs can be equipped with molecular recognition moieties to enhance retention at disease sites, which can improves

drug dosing at the target location and reduce unwanted side effects (29). In addition, chemistries can be installed in NPs to allow site-mediated drug release, or activation of the NPs can be triggered externally by certain stimuli (Heat, magnetic fields or radiation) (30, 31). One of the main advantages of using NPs in drug delivery over the conventional systems is improving therapeutic window of a drug: i.e. more accumulates at its target site without increasing the initial dose or causing toxicity or severe side effects. NPs can be further designed and modified to overcome specific obstacles which otherwise confound the conventional dosage formulations (32). For instance, the blood-brain barrier (BBB) is considered as the major obstacle facing the delivery of all large molecular weight therapeutics, and most small molecular weight drugs to the central nervous system (CNS) (33). For example, enzymes are unable to cross the BBB (34), which makes enzyme replacement therapy for CNS diseases very hard, however, 7-aminoacid glycopeptide modified PLGA NPs were able to deliver FITC-albumin as a model drug to mice brain (35). Polymers are versatile and have various applications in all aspects of life, they have tunable chemistry, topology, dimensions and physical properties which makes them widely applicable in nanomedicine (36), Figure 1-2. Nanoparticles fabricated from polymers (polymeric NPs) demonstrate efficient drug encapsulation and provide protection from the dynamic extra and intracellular environments (*e.g.* peptidases, nucleases) (37).

Polymeric NPs can modify drug pharmacokinetics by providing sustained drug release to decrease the dosing frequency and maintain therapeutic blood levels (38). Most importantly, polymeric NPs can be fabricated from biocompatible and biodegradable materials, which is advantageous from the safety and regulatory viewpoint (39-41). Many polymer nanomedicines have found their way to the market (42) (see Table 1-1). The safety and efficacy of polymeric NPs have been extensively studied, hence, polymeric NPs are widely used in nanomedicines. One of the most widely used biodegradable polymers is poly lactic-co-glycolic acid (PLGA, Figure 1-3). PLGA biodegradability can be controlled by altering the relative composition of lactic acid and glycolic acid (43). PLGA has been used to form NPs loaded with chemotherapeutics (44-47), and related polymers such as polylactic acid and polycaprolactone are employed in nanomedicine technologies as well (48, 49). In order for a polymer to be of use in nanomedicine preparation, it must be bio compatable and readily eliminated from the body, some polymers such as PLGA, poly lactic acid and poly glutamic acid are biodegradable, and some polymers such as PEG can be eliminated by te kidneis. In addition, the polymer rate of degradation can be optimised by changing either the polymer's molecular weight or size of the fabricated nanomedicne, in order to make the release either imidiate or sustained.

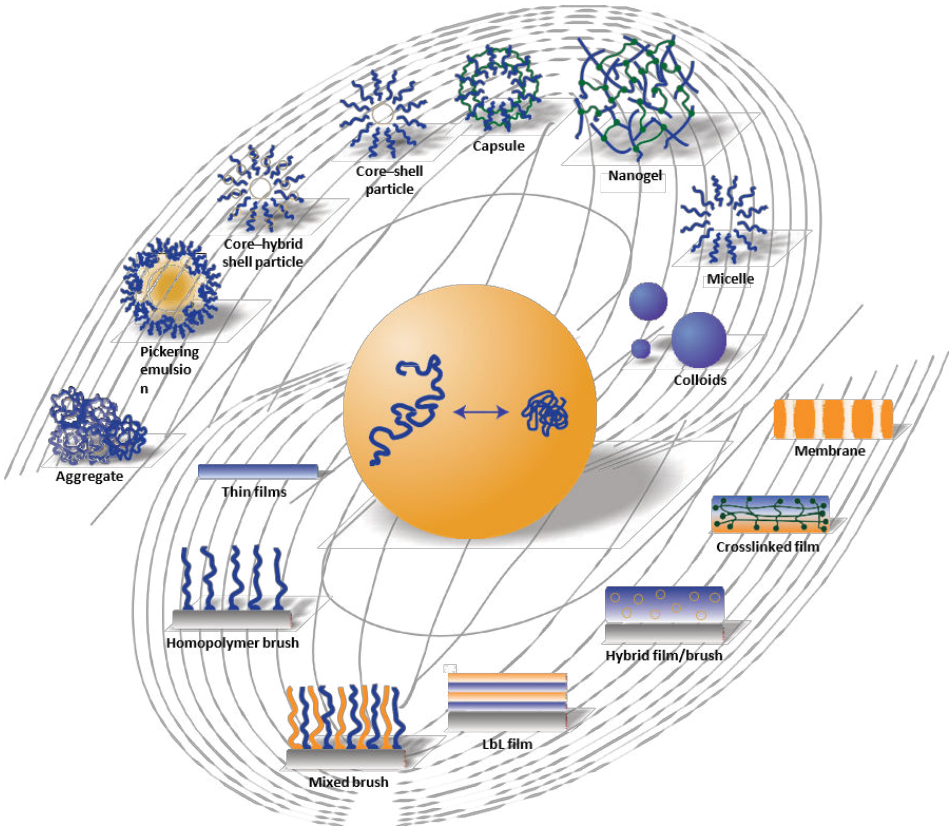


Figure 1-2: Various polymeric nanostructures. Adapted from reference (50).

Table 1-1: FDA approved polymer nanomedicine.

Trade Name (Manufacturer)	Generic Name	Indication(s)*	Polymer involved
Adynovate (Shire)	Antihemophilic factorpegylated	Hemophilia	PEG
Cimzia (UCB)	Certolizumab pegol	Crohn's disease, rheumatoid arthritis, psoriatic arthritis, ankylosing spondylitis	PEG
Eligard (Tolmar)	Leuprolide acetate and polymer	Prostate cancer	ATRIGEL
Krystexxa (Horizon)	Pegloticase	Chronic gout	PEG
Macugen (Bausch and Lomb)	Pegaptinib	Neovascular AMD	PEG
Mircera (Vifor)	Methoxy polyethylene glycol-epoetin beta	Anemia associated with CKD	PEG
Neulasta (Amgen)	Pegfilgrastim	Chemotherapy-induced neutropenia	PEG
Pegasys (Genentech)	Pegylated IFN alpha-2a	Hepatitis B, hepatitis C	PEG
PegIntron (Merck)	Pegylated IFN alpha-	Hepatitis C	PEG

	2b		
Plegridy (Biogen)	Pegylated IFN beta-1a	Multiple sclerosis	PEG
Rebinyn (Novo Nordisk) (available in 2018)	Coagulation factor IX (recombinant), glycopegylated	Hemophilia B	PEG
Somavert (Pfizer)	Pegvisomant	Acromegaly	PEG
Zilretta (Flexion Therapeutics)	Triamcinolone acetonide ER injectable suspension	Osteoarthritis knee pain	PLGA

ALL = acute lymphoblastic leukemia; AMD = age-related macular degeneration;

CKD = chronic kidney disease; ER = extended release;

HCl = hydrochloride; IFN = interferon;

SCID = severe combined immunodeficiency disease.

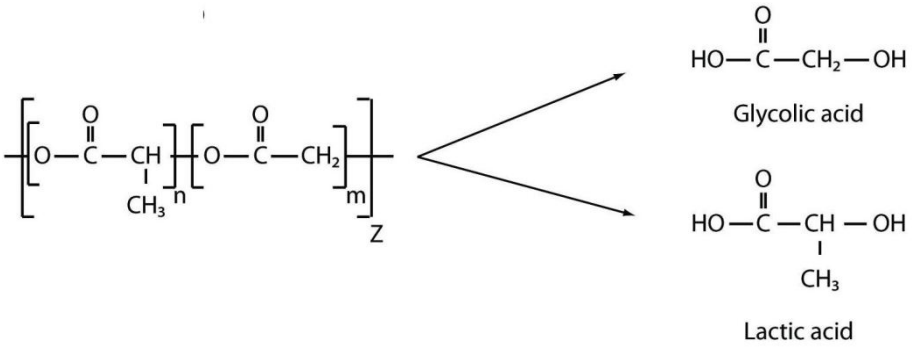


Figure 1-3: The structures of PLGA and its monomers glycolic acid and lactic acid.

1.1.2 Biodistribution and processing of nanomaterials

The mononuclear phagocyte system (MPS), which includes the circulating monocytes and the tissue resident macrophages, are the main cells responsible for NPs clearance by phagocytosis (51, 52). The distribution and clearance of the NPs are highly dependent on the adsorption of plasma proteins to their surfaces once they are in

the blood circulation (53); these adsorbed plasma proteins have been described as protein coronae (Figure 1-4) (54).

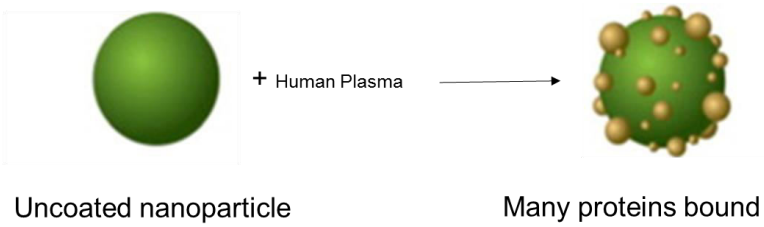


Figure 1-4: The adsorption of protein corona onto the surface of the nanoparticles upon the contact with the bloodstream. Adapted from reference (55).

NPs coated with protein coronae complexes can be recognised and cleared by the MPS, and eventually accumulate in the liver (56). If the protein coronae enhances the uptake of the nanoparticles by the phagocytes they are called opsonins, but if the contrary happens and the adsorption of the protein coronae minimizes their uptake they are called dysopsonins (57). The nature of the nanoparticles determines the type and the amount of the adsorbed proteins; neutrally charged and hydrophilic nanoparticles usually have lower opsonisation rates than the charged and hydrophobic ones resulting in longer circulation times (58). Coating NPs with certain materials affects their biodistribution and clearance. Coating is usually done either by chemical bonding or physical adsorption, one common example is grafting or coating the NPs with polyethylene glycol (PEG). It was reported that coating NPs with PEG reduces the adsorption of plasma proteins to their surfaces

(Figure 1-5) by steric hindrance which in turn leads to increased circulation times (56).

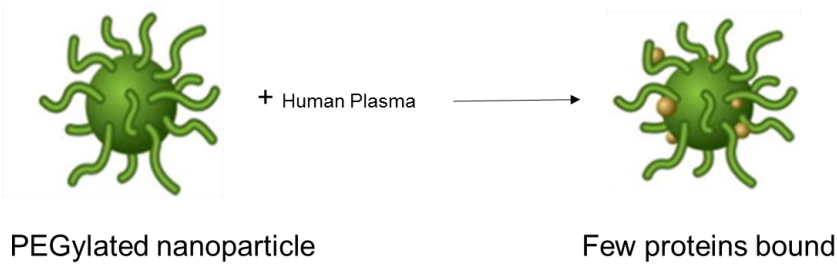


Figure 1-5: Coating the surface of the particle with PEG prevents the adsorption of protein corona onto the surface of the particle. Adapted from reference (55).

Coating the NPs with non-ionic surfactants, such as pluronics, was reported to overcome multidrug resistance mechanisms by inhibiting the excretion of NPs by efflux pumps, especially P-glycoproteins (59). Pluronics are triblock copolymers in structure composed of central hydrophobic polypropylene glycol (PPG) block flanked by two hydrophilic PEG blocks (60). Coating with pluronics is expected to inhibit the opsonisation of NPs as they have PEG blocks (61). Lipids can also be utilised as coatings specifically to improve the biocompatibility of some NPs, Quantum dots are semiconductor NPs made of metals or metal oxides (62). Lipid coated QDs have shown better applicability and improved pharmacokinetics than bare QDs in mice, especially the higher circulation time and lower aggregation in blood capillaries (63).

1.1.3 Toxicity of nanomedicines

Even though nanomedicines might provide advantages over traditional drug delivery systems, the potential toxicity associated with nanomaterials is still a growing concern (64, 65). NPs may have the ability to adversely affect the physiology or directly interrupt the normal structure of human tissue or organs (66). Toxicity of NPs is highly dependent on their physiochemical properties, especially particle size, surface charge, shape, composition, chemistry, and their stability (67). It is widely accepted that the mechanisms of their interaction with the biological system can be either physical or chemical (68). The physical mechanisms of the NPs result mainly from their specific surface properties and size (69). This covers changing protein conformation/folding which leads to loss of function (70), protein aggregation and precipitation (71), disruption of cell membranes and cellular activity (72, 73), and blocking of transport processes (74). Chemical mechanisms of NPs toxicity include electrolyte imbalance resulting from their dissolution and releasing toxic ions which leads to disturbance of the cellular membrane transport activity (75) and the formation of free radicals which directly impacts cell integrity (76). However, increasing the oxidative stress by producing reactive oxygen species (ROS) is considered the main cause of nanotoxicity among the other chemical processes (77); as it has consequences that could cause further damage and lead to

cell death (78). However, the specific proteins and metabolic pathways that are involved in the toxicity and oxidative stress mediated by NPs are not fully known (79). The responses of biological systems after exposure to NPs have been studied thoroughly, however owing to the enormous variety of nanomaterials and consequently the impossibility of defining a 'nano' effect, there is much research work needed (67). While conventional *in vitro* cytotoxicity assays are used to assess the activity of different compounds, however, it has been reported by many researchers that it is difficult to use these assays to study NPs cytotoxicity (80). The health risks of long-term exposure of NPs require further research and this is considered one of the major concerns surrounding nanomedicines in general (79).

1.2 Metabolomics

Metabolomics is an emerging field in 'omics' studies as first defined in 1998 (81). Since then this field has expanded rapidly (82), Figure 1-6. It differs from other omics studies (genomics, transcriptomics and proteomics) as it can evaluate a biochemical activity by measuring the starting substrates and the end products during the metabolic process, which makes it easier to correlate the metabolic and phenotypic changes (83). Moreover, metabolomics can measure hundreds or thousands of metabolites

which are the end products of gene expression or cellular metabolic activities (35). A metabolome is the set of all small metabolites that have a molecular weight of 1500 Daltons or lower (84), this includes the amino acids, peptides, organic acids, alkaloids, vitamins, carbohydrates and inorganic species that are present in a biological specimen (85). Metabolomic analysis is usually conducted to examine the changes in these small metabolites either during development, upon certain treatment with a drug, modifying a gene or resulting from changing the environment (35, 86). The complete measurement of biological sample low molecular weight metabolites is defined as global metabolic profiling (87).

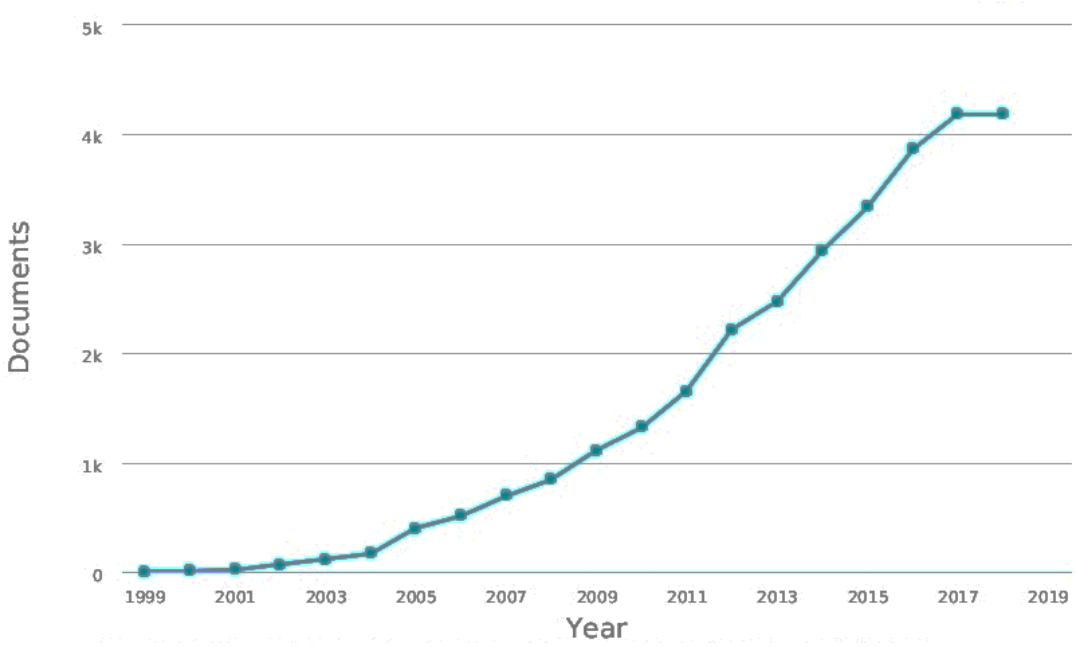


Figure 1-6: The graph was extracted from the online analysis tool of Scopus searching platform. The search is performed on the term metabolomics or metabonomics and the publication year is from 1999 to 2018 (88).

1.2.1 Targeted and untargeted metabolomics

There are two main paths for metabolomic analysis. The first method is global metabolic profiling, measuring all the metabolites that can be quantified in the sample, which also known as the untargeted metabolomics approach (89). The second method involves identifying and measuring preselected metabolites (tens to hundreds of metabolites) that are expected to change under certain circumstances, considered as biomarkers, involved in a particular metabolic pathway or belong to the same class of compounds, this is also known as the targeted metabolomics approach (90). The advanced analytical techniques that are available now are making it possible for untargeted metabolomics to be performed with higher accuracy and sensitivity even for biological samples which are very complicated in nature (91, 92).

1.2.2 Instrumentation

The analytical instruments that are most commonly used in metabolomics are mass spectrometry (MS) and nuclear magnetic resonance spectroscopy (NMR) (93). NMR has many advantages that attract the scientists to employ it in metabolomics research; it is quantitative, reproducible, non-destructive, non-invasive and simple such that it does not need complicated sample preparation. However, the sensitivity of NMR is a major drawback, despite that there are some promising emerging sensitivity enhancements that

use; higher field strength, cryo and microprobes and dynamic nuclear polarisation (94, 95). Mass spectrometry analytical platform is more commonly used; it can detect metabolites in the nanomolar, picomolar and recently femtomolar concentrations, while NMR is limited to the micromolar level (96, 97). Table 1-2 summarises the advantages and disadvantages of using LC-MS and NMR in metabolomics.

1.2.2.1 Liquid chromatography

Usually, an effective chromatographic separation technique such as gas chromatography GC (mainly for volatile metabolites) or high-performance liquid chromatography (HPLC) is coupled with MS to make the spectra less complex (93). In liquid chromatography (LC)-MS approach, the choice of column chromatography depends mainly on the chemical properties of the metabolites of interest; hydrophilic interaction liquid chromatography (HILIC) is used widely for polar metabolites and reversed phase (C-18) is used for the nonpolar ones (98).

Table 1-2: Summary of the advantages and limitations of LC-MS spectrometry in comparison with NMR spectroscopy as analytical tools for metabolomics research.

Parameter	LC-MS	NMR
Sensitivity	High	Low
Reproducibility	Moderate	Very high
Experimental time	More than 10 min for typical LC-MS run	5 min for 1D proton NMR
Sample recovery	Destructive	Non-destructive
Sample preparation	Needs extraction and purification	Need minimal sample preparation
Sample	Needs different columns	The entire sample analysed

measurement	depending on metabolites partition coefficient	in one measurement
Tissue samples	No, requires tissue extraction,	Yes
Number of detectable metabolites (urine sample)	More than 400	40–100 depending on spectral resolution
In-vivo studies	No	Yes

1.2.2.2 Ionisation sourses

MS operates by ionising uncharged molecules to produce negatively and positively charged ions, then it analyses the formed mass ions on the basis of mass to charge ratio (*m/z*) (99). There are quite a few technologies for ionisation and analysis, and different combinations of these processes are available for different applications. Ionisation sources including atmospheric pressure chemical ionisation, atmospheric pressure matrix-assisted laser desorption atmospheric pressure photo-ionisation and electrospray ionisation (ESI), are widely used in LC-MS systems, however, ESI is the most commonly used ionisation source in metabolomics application. ESI is a soft ionisation technique, it results in minimal insource fragmentation compared to other ionisation techniques, it is suitable for organic and inorganic compounds and covers wide mass range, by changing the polarity of the ionisation the number of detected metabolites can be raised (99). ESI is performed by applying high voltage to a liquid passing through a capillary tube, which produces highly charged fine droplets. Due to coulombic repulsion, the charges tend to go to the surface of the droplets,

after that a hot nitrogen gas desolvates the droplets, and as the droplets shrink in size the surface charge density increases which increase the repulsion until the droplets explode producing charged mass ions (100). ESI is prone to pronounced ion suppression, which results in loss of detector linear response and lower number of detected mass ions, ion suppression is usually caused by either endogenous component e.g. co-elution, high concentration and high mass, (matrix effect) or exogenous material that can get introduced throughout sample preparation e.g. plasticisers, ion pairing reagents and polymers (101).

1.2.2.3 Mass analysers

The final step in LC-MS analysis is analysing the ionised analytes on bases of *m/z*, high sensitivity and resolution metabolite detection is generally required. There are different mass analysers suitable for different metabolomics approaches, for instance, tandem triple quadrupole and tandem Q-Trap are most commonly used for targeted metabolomics (102-105) because they provide the desired sensitivity and accuracy in quantification of preselected metabolites (106). On the other hand, the resolving power is very important for untargeted metabolomics approach, due to the complexity of the samples and the high number of detected mass ions, therefore high-resolution mass analysers such as quadrupole-time of flight (Q-Tof) and Orbitrap are more commonly used (107-109). Orbitrap was introduced commercially by Thermo scientific in

2005. It can be briefly described as follows, it consists of three electrodes, two outer electrodes in the shape of two cups facing each other and a centre spindle shaped electrode, Figure 1-7, voltage difference between the outer and the central electrodes generates a linear electric field along the axis. Mass ions enter to the space between the inner and outer electrodes through a slot with a compensation electrode, mass ions will be electrically attracted to the central electrode, but their tangential velocity induces centrifugal force that opposes the electric field. Due to the conical shapes the electrodes, the mass ions remain in a continuous helical movement inside the trap generating three oscillation frequencies: axial, radial and rotational. Unlike the other frequencies, the frequency of the axial oscillations depends only on *m/z*, the outer electrodes record this frequency and then it gets Fourier-transformed to *m/z* (110).

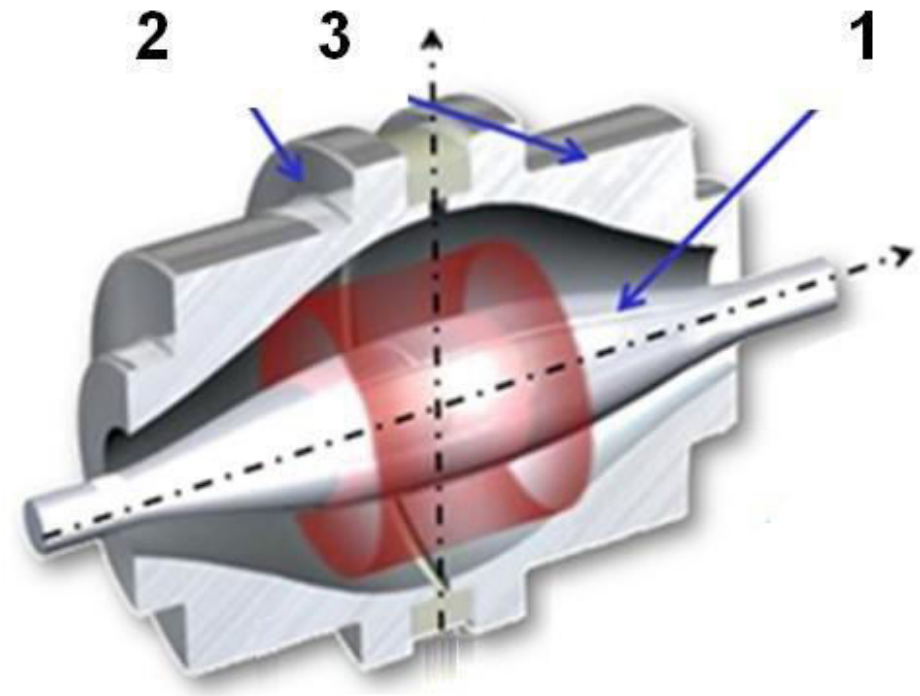


Figure 1-7: Cross section of Orbitrap mass analyser. 1) central electrode and 2,3) two halves of the outer, Adapted from reference (111).

1.2.3 Metabolomics and effects of NPs

A large number of polymeric nanomaterials have been designed and investigated to develop efficient drug delivery systems in the last few decades, one of the most important steps is to assess the biocompatibility of these materials. However, the toxicity of these nanomaterials has been routinely evaluated in *in vitro* cell culture based on simple cell viability assays, such as MTT and LDH (112-118). Although these conventional tools give insights on toxicity, they have several limitations and do not provide sufficient information on potential mechanisms of cell toxicity to inform the

design of new polymeric materials (119). These assays also give indications of the crude toxicity of materials but not the safety of these materials at subtoxic concentrations. The need to understand the potential toxicity of nanomedicine has urged the scientist to look for other analytical approaches that can describe nanotoxicology comprehensively at the cellular and molecular levels. Cellular metabolites involved in various metabolic pathways and biological processes have been playing important roles in explaining the metabolic biochemistry of organisms in response to various stimuli (120). The assembly of cellular metabolites typically termed as metabolome offer a snapshot of cellular state (121). Development in mass spectrometry makes it possible to rapidly detect thousands of small molecules simultaneously from minimal amounts of biological samples. Recent innovations in instrumentation, bioinformatics and software allow unbiased profiling of diverse small molecules (e.g., amino acids, lipids, sugars and organic acids). By comprehensively tracking the altered expression patterns of small molecules, metabolomics offers a systems approach to better understanding global metabolism of living things and has been widely accepted to deal with various biological questions such as toxicity assessment, preclinical screening and mechanistic exploration (122-124). Compared with other 'omics' technologies (genomics, transcriptomics, proteomics), metabolomics holds certain advantages in nanotoxicity research.

First, the number of reported small molecule metabolites is far less than genes, transcripts and proteins (123). Second, metabolomics could qualitatively and quantitatively describe the net results of genomic, transcriptomic and proteomic variability, and changes in metabolome could be regarded as the best indicator of an organism's phenotype (125). Third, information obtained from metabolomics is more generic, as a given metabolite, unlike a gene, a transcript or a protein, is the same for every organism that possesses it (126). The above characteristics make metabolomics an ideal choice for investigating nanoparticle–organism interaction at different molecular levels. Therefore, in the last few years, there has been an increasing interest in utilising metabolomics to study nanotoxicology. Figure 1-8 shows a schematic representation of the workflow for metabolomics study of NPs toxicity. The recent developments in metabolomics and bioinformatics analysis platforms made the application of metabolomics in studying nanotoxicology efficient.

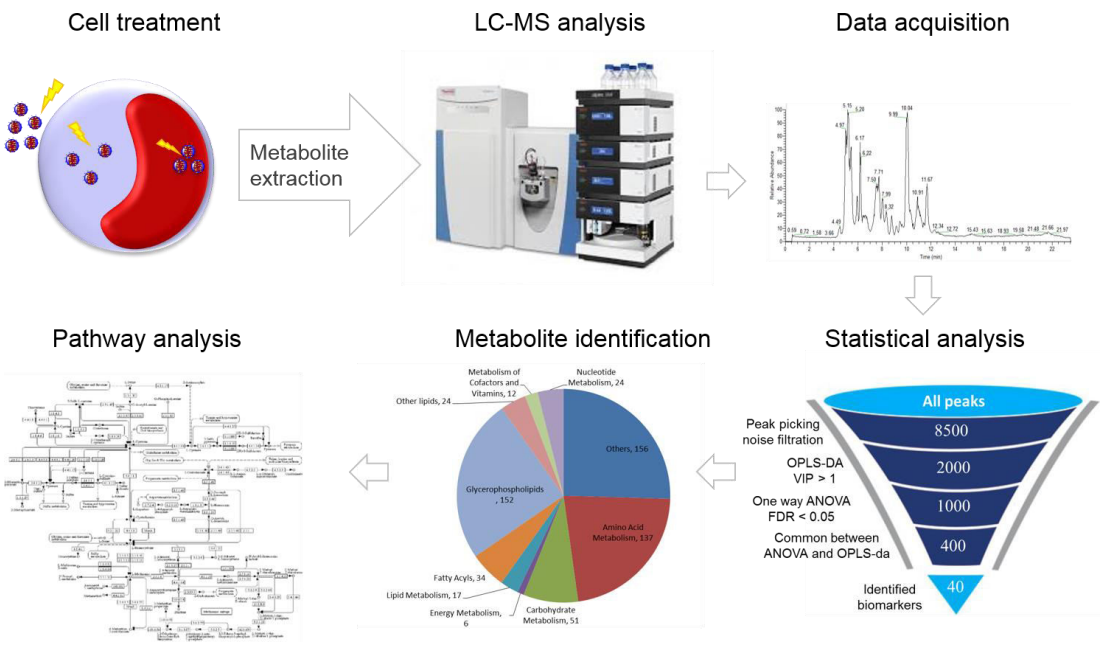


Figure 1-8: Workflow of metabolomics study of NPs toxicity.

At the beginning of this project, there were very limited number metabolomics studies regarding nanotoxicology; the available studies were mostly concerned in eco-toxicological effects of metallic NPs. For example, it was reported that cerium oxide NPs altered the energy metabolism of *Chlamydomonas reinhardtii* (a freshwater alga) by downregulating photosynthesis (127). Silver NPs (AgNPs) have increased the anaerobic metabolism and oxidative stress in *Daphnia Magna* (128). AgNPs are widely used in cosmetics and medical products for their anti-bacterial activity, studying their effects on humane keratinocytes, although AgNPs didn't affect the keratinocytes viability, changes in the membrane components, increased oxidative stress, downregulation in tricarboxylic acid cycle activity and ATP depletion were detected

(129). Titanium dioxide NPs (TiO_2 NPs) are incorporated into the dental cement to enhance their antibacterial and mechanical properties. It has been shown that these NPs can enhance gingival inflammatory reactions as they increase the production of prostaglandins and COX-1, COX-2 proteins expression (130). Metabolomics techniques for nanotoxicity investigations were thoroughly reviewed by Lv et al (126).

In late 2015, metabolomics methods were used to assess the biological effects of PEG-PLGA NPs, PEG-PLGA NPs loaded with doxorubicin (DOX) and paclitaxel (TAX) and free DOX/TAX on a mice model. The results showed that the PEG-PLGA NPs induced slight and temporary metabolic changes to the host, and decreased the toxic side effects for the chemotherapeutics (131), however, in this study, serum and tissue samples were collected after seven days of administering the NPs, this might have omitted the acute toxic effects of NPs and the loaded chemotherapeutics which are expected to manifest in the first few hours or days of exposure, nevertheless, if the chronic toxic effects of the NPs and the loaded chemotherapeutics where under investigation, multiple dosing for long periods would be needed. Saborano et al (132) studied macrophages metabolic reprogramming upon exposure to silk, PLGA and silica NPs, the macrophages reacted in the same manner to all of the NPs groups despite the different chemistries, however silica NPs had the strongest impact on the basis of metabolite fold

change. In this study, high concentrations of NPs (500μg/ml) were used because smaller doses (10μg/ml) did not induce metabolic changes. 500μg/ml of NPs is higher than the expected doses of nanomedicine, it is mostly used for potent drugs due to the low loading capacity. Armiñán et al (133), studied the biochemical alterations caused by free and polymer conjugated doxorubicin *in vitro* and *in vivo.* The results of *in vitro* experiment MCF7 cells revealed the effect of cell entry pathways on the activities of both free and polymer conjugated doxorubicin and the in vivo experiment suggested that the polymer conjugated chemotherapeutics had better pharmacokinetics and biodistribution profiles. Despite the fact that this study was well planned and involved *in vitro* cell culture and *in vivo* mice experiments, using ^{1}H NMR which has limited sensitivity in comparison to MS makes detecting and identifying metabolites very hard, as a result only 35 and 45 metabolites were identified in cell culture and tissue samples respectively, the small numbers of identified metabolites makes assessing the NPs biocompatibility and inferring their possible toxic effects very hard, and suggests that there might be many important metabolites and metabolic pathways that are not investigated.

The ever-increasing research, production and application of nanomaterials in biomedical and other fields, and the absences of a standardised safety and biocompatibility assessment have resulted

in a gap between nanotechnology and nanotoxicology. Using metabolomics to discover the uncertainties surrounding nanomaterials should reduce this gap which attracted many researchers in the last five years Figure 1-9, these numbers are expected to rise in the next few years, especially with the advances in NMR and MS analytical platforms.

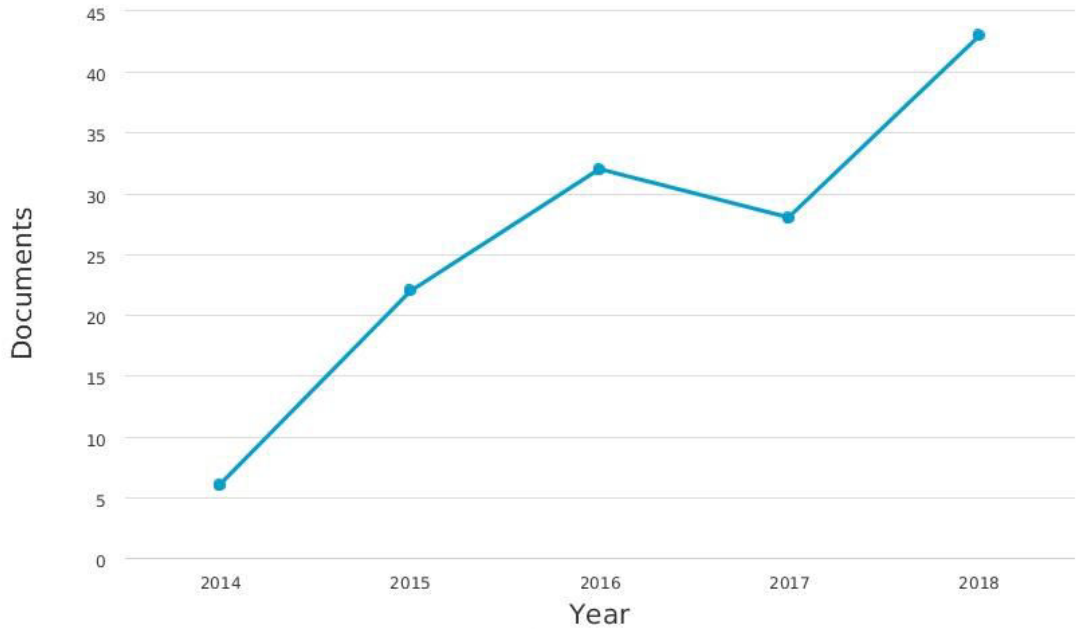


Figure 1-9: The graph was extracted from the online analysis tool of Scopus searching platform. The search is performed on the term metabolomics and nanoparticles and the publication year is from 2014 to 2018 (88).

1.3 Aim of the study

The aim of this PhD project involves development and optimisation of a high throughput, robust and comprehensive cell based global metabolic profiling approach to study the effects of polymer nanomedicine at the cellular and molecular level using advanced

metabolomics. Poly lactic-co-glycolic acid (PLGA) will be the main studied polymer and the LC-MS analysis will be following the previously described method (134, 135).

The main objectives of the work:

- Synthesis and characterisation of fluorescently labelled PLGA copolymer in order to use it for NPs fabrication. Studying the cellular uptake of the fabricated NPs (Chapter 2).

- Developing an efficient cellular metabolite extraction protocol that covers metabolites related to amino acids metabolism, redox homeostasis, glycolysis, tricarboxylic acid (TCA) cycle, nucleotide metabolism and different lipid classes and using the optimised protocol to study the impact of coating PLGA NPs on their biocompatibility (Chapter 3).

- Discrimination of the molecular effects of free and nanoparticle loaded methotrexate on proliferative and non-proliferative cancer cells (Chapter 4).

- Investigating the intracellular effects of hyperbranched polycation–DNA complexes on lung cancer cells using LC-MS-based metabolite profiling (Chapter 5).

Chapter two

A Facile Dye-Initiated Polymerisation of Lactide-Glycolide Generates Highly Fluorescent PLGA for Enhanced Characterisation of Cellular Delivery

2.1 Introduction

Poly (lactic-co-glycolic acid) (PLGA) is a synthetic biocompatible copolymer, approved by the United States Food and Drug Administration (US FDA) and widely used for biomedical applications (37, 136-138). PLGA particulate carriers have been used to deliver therapeutics ranging from low molecular weight drugs, peptides and proteins, through to nucleic acids, vaccines and cells (136, 139-143). In addition, PLGA-based scaffolds based on colloidal particles, hydrogels and fibres have been extensively explored for regenerative medicine (144-146).

Recently, the desire to develop biodegradable polymers with imaging capabilities has increased, especially to study biomolecules, analyze biological processes, and track diseases and therapeutic efficacy (147, 148). In particular, real-time monitoring of biodegradable materials, assessment of targeted drug delivery are emerging fields that demand biodegradable fluorescent polymers. Till now, huge efforts have been made to conjugate or mix semiconducting quantum dots or organic dyes with biodegradable polymers to create photoluminescent biodegradable materials (149). However, the toxicity of quantam dost which are usually made of heavy metals and the unavoidable photobleaching and poor dye-to-polymer labeling ratios of organic dyes render their practical use *in vivo* very hard (150). One common alternative

is Green fluorescent protein (GFP), it has intrinsic photoluminescence, however, it induces cell toxicity either by causing protein aggregation or due to over-expression (151). Thus, the development of brightly fluorescent, biocompatible and biodegradable polymers for imaging supported drug delivery systems still considered a major challenge (152). For therapeutic applications, it is essential to monitor the kinetics of tissue and cellular drug uptake, specific organ accumulation after systemic administration, *in vivo* bio-distribution and intracellular fate of these therapeutics (153). For *in vitro* studies, the most common strategy used is to load PLGA nanoparticles with fluorophores, which can then be imaged with widefield or confocal fluorescence microscopy to determine polymer biodistribution (154). However, the major drawback associated with this approach has been the separation and leakage of the fluorophore from the PLGA nanoparticles, which can result in measurement and experimental artefacts. This is because it is extremely challenging to distinguish between the signal from the loaded nanoparticles and unbound leaking fluorophores (155), which can lead to an overestimation of the nanoparticle uptake (136). Furthermore, free fluorophores may interact with biological systems and can induce unwanted biochemical processes and toxicity (156). To enhance fluorescence imaging of PLGA nanoparticle biodistribution and to overcome the challenges associated with fluorophore leaching, PLGA can be

covalently linked to fluorophores (157). However, PLGA itself has a limited number of easily modifiable functional groups, i.e. the hydroxyl and carboxyl termini, which restricts the efficacy of fluorophore labelling. In a typical example, a labelling efficiency of 65% was achieved when 5-aminofluorescein was reacted with PLGA (158). Other routes to functionalised PLGA have required multiple steps and were performed in organic solvents, which in turn renders scale-up challenging and uneconomical (159).

The free-living soil nematode *Caenorhabditis elegans*, which typically feeds on *Escherichia coli* in a laboratory setting (160), was first introduced into laboratory practices as model organism to study complex biochemical process by Brenner *et al* in the earlier 1960s (161). Due to its low cost of cultivation, short generation time, transparent body and a completed genetic and neuronal maps, *C. elegans* has been exploited to sophisticated processes such as genetics, neurology and toxicology as well as validation of pharmacologically active compounds (161, 162). More recently, it has been described as an ideal model for drug delivery studies and finding potential targets for new therapeutics (163). In this chapter with the aim of utilising *C. elegans* as a model organism for drug delivery, fluorescent NPs made from a fluorescent labelled PLGA were synthesised and successfully compared to dye loaded NPs. The effect of loaded and unloaded nanoparticles on organism viability was investigated, in order to use a sub-lethal treatment

concentration for the study. Unloaded and Rhodamine-B base loaded nanoparticles were successfully delivered to the nematode, and the release of the model drug from the cargo drug carrier and its internal distribution was confirmed microscopically.

In this chapter I aim to synthesis a brightly fluorescent PLGA polymers that are suitable for drug delivery applications, the biocompatibility of all synthesised polymers will be tested using typical cell viability assays and will be compared to the commertially available PLGA, the synthesised polymers will be used to fabricate NPs and their utility will be evaluated in terms of their visibility under fluorescent microscopy inside cells and nematodes gastric lumen, and their ability to deliver active pharmaceutical agents to cells.

2.2 Materials and methods

2.2.1 Materials

Lactide (LA), glycolide (GA) 99%, 5-aminofluorescein (AF), rhodamine 6G (R6G), 2-aminoanthracene (AA), tin(II) 2-ethylhexanoate ($Sn(Oct)_2$) 92.5-100.0%, deuterated chloroform ($CDCl_3$), deuterated dimethyl sulfoxide (DMSO-d6), Roswell Park Memorial Institute (RPMI) 1640 medium, heat-inactivated fetal bovine serum (FBS), penicillin, streptomycin, L-glutamine, phorbol 12-myristate 13-acetate, paraformaldehyde and Resomer® RG 502, poly(D,L-lactide-co-glycolide) lactide:glycolide 50:50, ester

terminated (7,000-17,000 MW) were purchased from Sigma-Aldrich (Gillingham, UK). Ammonium carbonate was purchased from Fluka (Bucharest, Romania). Alexa Fluor™ 488 Phalloidin (AF488) and Alexa Fluor™ 647 Phalloidin (AF647) were purchased from Thermo Fisher Scientific (Loughborough, UK). Dichloromethane (DCM), methanol, diethyl ether and acetone were HPLC grade provided by Fisher Scientific (Loughborough, UK). All the materials and solvents were used as received unless stated otherwise.

2.2.2 Polymer synthesis

PLGA-2-aminoanthracene (PLGA-2AA, blue), PLGA-5-aminofluorescein (PLGA-5AF, green) and PLGA-rhodamine-6G (PLGA-R6G, red) were synthesised by ROP of LA and GA as shown in Figure 2-1A, where 2-aminoanthracene, 5-aminofluorescein and rhodamine-6G and were used as initiators.

2-Aminoanthracence labelled PLGA (PLGA-AA)

The synthesis was carried out by melting LA (30 mmol, 4.323 g, 30 eq), GA (20 mmol, 2.32 g, 20 eq) and 2-aminoanthracence (1 mmol, 0.193 g, 1eq) at 130°C under a nitrogen atmosphere. Sn $(Oct)_2$ (0.5% wt/wt) was added and the reaction continued for 3 hrs. Sn $(Oct)_2$ is one of the most widely used catalysts for ROP reactions, it provides high reaction rate, high conversion rate, and high molecular weights, even under rather mild polymerization conditions(164), in addition, $Sn(Oct)_2$ has been approved by the US

FDA as to be used as a food additive(165). Hereafter, the reaction mixture was cooled to room temperature. The synthesised copolymer was dissolved in acetone and precipitated in methanol four times to remove remaining unreacted monomers, free dye and short polymer chains. The filtered precipitate was dried under reduced pressure to produce a grey solid (4 g, 60% yield).

^{1}H NMR (400 MHz, $CDCl_3$) δ 7.4-8.5 (ArC-*H*, 9H), 5.25 (m, 1H, OCO-*CH*(CH_3)-COO), 4.91 (m, 2H OCO-*CH_2*-COO), 1.61 (q, 3H, OCO-CH(C*H_3*)-COO).

5-Aminofluorescein labelled PLGA (PLGA-5AF)

The synthesis was carried out by melting LA (30 mmol, 4.323 g, 30 eq), GA (20 mmol, 2.32 g, 20 eq) and 5-aminofluorescein (1 mmol, 0.347 g, 1eq) at 130°C under a nitrogen atmosphere. $Sn(Oct)_2$ (0.5% wt/wt) was added and the reaction was proceeded for 3 hrs after which, the reaction mixture was cooled to room temperature. The synthesised co-polymer was dissolved in acetone and precipitated in cold methanol four times to remove remaining unreacted monomers, free dye and short polymer chains. The filtered precipitate was dried under reduced pressure to generate of a deep orange product (4.3 g, 64% yield).

^{1}H NMR (400 MHz, $CDCl_3$) δ 6.5-7.25 (ArC-*H*, 9H), 5.25 (m, 1H, OCO-*CH*(CH_3)-COO), 4.91 (m, 2H OCO-*CH_2*-COO), 1.61 (q, 3H, OCO-CH(C*H_3*)-COO).

Rhodamine 6 G labelled PLGA (PLGA-R6G)

The synthesis was carried out by melting LA (30 mmol, 4.323 g, 30 eq), GA (20 mmol, 2.32 g, 20 eq) and rhodamine-6G (1 mmol, 0.479 g, 1eq) at 130°C under a nitrogen atmosphere. $Sn(Oct)_2$ (0.5% wt/wt) was added and the reaction continued for 3 hrs after which, the reaction mixture was cooled to room temperature. The synthesised copolymer was dissolved in acetone and precipitated in methanol four times to remove the unreacted monomers, free dye and short polymer chains. The filtered precipitate was dried under reduced pressure to generate of a light red product (1.7 g, 26% yield).

^{1}H NMR (400 MHz, DMSO-d6) δ (m, 1H, OCO-*CH*(CH_3)-COO), 4.91 (m, 2H OCO-*CH_2*-COO), 1.61 (q, 3H, OCO-CH(C*H_3*)-COO), 1.3 (q, 3H, CH-C(C*H_3*)-C).

2.2.3 NPs formation and characterisation

Green and blue fluorescent PLGA NPs were prepared using PLGA-AF and PLGA-AA respectively by nanoprecipitation (166). Briefly, a solution of each labelled PLGA (25 mg) in 10 ml of acetone was added to 10 ml of the anti-solvent (Milli-Q deionised water, 18.2 mΩ,) using a syringe pump (0.7 mL/min). The mixture was stirred at room temperature overnight, to ensure the complete evaporation of acetone. Whereas, PLGA-R6G NPs were prepared using a solution of PLGA-R6G (25 mg) in 10 ml of DMSO, which was added to 10 ml of the anti-solvent (deionised water) using a syringe pump (0.7 mL/min). DMSO was removed with dialysis

against 1 L of deionised water for 24 hrs. The NPs suspensions were filtered using 0.45 μm syringe filters to remove any aggregates and maintain system sterility.

Nanoparticles loaded with 5-aminofluorescein

A solution of PLGA (25 mg) and AF (2mg) in 10 ml of acetone was added to 10 ml of the anti-solvent (Milli-Q water) using a syringe connected to a pump (rate of addition 0.7 mL/min). The mixture was stirred at room temperature, overnight, to ensure the complete evaporation of acetone.

Nanoparticles loaded with doxorubicin

Nanoparticles were synthesised using a double emulsion–solvent evaporation method. Solutions of PLGA-AF (1 mL, 10 mg/ml, DCM) and doxorubicin (100 μl, 1mg/ml, DI water) were prepared. The aqueous doxorubicin (0.1 mL) phase was added to the organic PLGA-AF phase (1 mL) and sonicated for (1 min, 3W, Sonicator 3000, Misonix, USA) by a microtip probe to produce an emulsion. This emulsion was added to a PVA solution (0.5% w/v, deionised water) and sonicated (5 min, 3 W). The organic solvent was eliminated via mechanical stirring (4 hrs) and purified using PD10 columns. The production process yield was evaluated by weighing the solid residue after freeze-drying known volumes of nanoparticle suspension.

Particle size and zeta potential measurement

Mean NP hydrodynamic diameters were obtained by measuring the light scattering at 173° angle to incident radiation at 25 °C after diluting the samples with DI water using Malvern (TM) Zetasizer equipped with 10 mW He-Ne laser operating at a wavelength of 633 nm. The zeta potential for the NPs was measured in water using the same Malvern (TM) Zetasizer. Transmission electron microscopy (TEM) - NPs morphology was evaluated by using a Tecnai G2 (FEI, Oregon, USA) Transmission Electron Microscopy (TEM). 17µl of 2m/ml NPs suspended in water were pipetted onto a copper grid and wicked off after 10 minutes, subsequently, the grid was treated with 3% w/v of uranyl acetate.

2.2.4 Impact of NPs on cells viability

The AlamarBlue® metabolic activity assay was used to assess the effects of the green, red and blue PLGA NPs on the cells. Activated cells were incubated with media containing 50, 100, 250 and 500 µg/ml of NPs for 24 hrs. Hereafter, the media was removed, and the cells were washed with phosphate buffered saline (PBS) and incubated in fresh media containing 10% AlamarBlue® for 3 hrs. Supernatants (100µL) were transferred to 96 opaque black well plates and the fluorescence was recorded (Optima FLUOstar®) at excitation/emission of 540/580 nm. The results were plotted as mean % viability vs control ± standard error of the mean (SEM).

2.2.5 Cellular uptake of NPs

Cells were seeded on 8 well chambered (37 °C, 5% CO_2, 24 hrs). The media was then changed with fresh media or media containing 100 µg/mL of green, red and blue NPs (37 °C, 5% CO_2, 3 hrs). Following treatment, cells were washed twice with PBS and then exposed to 5 µM DRAQ5™ (blue NPs) or 1µM Hoechst® (green NPs & red NPs) for 15 min in the dark at 37 °C to stain the nucleus. After nucleic acid staining, cells were washed twice with PBS and then exposed to AF488 (blue NPs) or AF647 (green & red NPs) for 30 min in the dark at 37 °C to stain the cytoskeleton. The cells were washed twice with PBS and fixed in paraformaldehyde (4% v/v, PBS, 300 µL) for 15 min in the dark at room temperature. The plates were finally washed twice with PBS and stored with mounting media (Fluoromount™ Aqueous, Sigma-Aldrich, 4 °C) ready for imaging. Cells were imaged using an inverted Nikon Eclipse T1 and QIMAGING optiMOS camera equipped with CoolLED pE-4000 fluorescence illumination and pE-100 brightfield illumination and Nikon Plan Fluor 10 x (0.30 NA) objective and 40 x (0.75 NA). Fluorescence was captured through excitation at 405, 490, 550, 635 nm collecting at emission at 410-500, 500-550, 550-650, and 650-750 nm, using an exposure time of 100 ms. Brightfield was captured at an exposure time of 10 ms. Blank sample of deionised water was imaged for control. All fluorescence and bright field images were corrected to a 12-bit image (0-4095).

2.2.6 *In vitro* release

Freeze-dried doxorubicin loaded NPs were resuspended in PBS (5mg, 0.5 mL) and placed in a dialysis tube (Slide-A-Lyzer™ MINI Dialysis Devices, 3.5K membrane MWCO, Thermo Scientific) and dialysed against 14 mL of PBS at 37 °C for 24 hrs. Samples from the release media were collected after 3 and 24 hrs. The amount of doxorubicin release was calculated using fluorimeter (λex 480 nm, λem 590 nm) using a calibration curve of doxorubicin in PBS.

2.2.7 Caenorhabditis elegans growth

C. elegans nematodes (Bristol N2) were maintained on nematode growth medium (NGM) agar and *Escherichia coli* (OP50) at 20 °C(167). Synchronised growth cycles of *C. elegans* were prepared by harvesting eggs from gravid females, which were collected by rinsing an NGM growth plate with sterile deionised water (3.5 mL). Sodium hydroxide (5 M, 0.5 mL) and sodium hypochlorite (5%, 1 mL) were added to the worm suspension and vortexed (10 min) to separate nematodes from the eggs. The eggs were initially collected using centrifugation (1500 rpm, 1 min), and subsequently washed once with 5 mL of sterile deionised water and collected with centrifugation (1500 rpm, 1 min). The centrifuged egg suspension was aspirated to 0.1 mL and plated onto a fresh plate of NGM agar, seeded overnight with an *E. coli* lawn. The generation time of *C. elegans* using these conditions was 4 to 5 days.

2.2.8 Caenorhabditis elegans NPs uptake

NGM agar plates containing synchronised cycles of *C. elegans* (L_4-young adult stages) were harvested using sterile ultra-pure deionised water (18.2 MΩ). The nematodes were washed with sterile deionised water (1 mL, 3 times) and collected using centrifugation (2500 rpm, 1 min). *C. elegans* (~300 nematodes) were dosed with PLGA nanoparticles at 100 µg/mL (n = 3) for 3 hrs and washed prior to imaging (3 times, 5 mL of sterile deionised water, centrifugation 1500 rpm, 1 min). Regions of interest containing *C. elegans* that had ingested fluorescent nanoparticles were imaged using a Nikon Eclipse TS100, Nikon 4× 0.10 NA (air) objective.

2.3 Results and discussion

2.3.1 Polymer synthesis

Our motivation was to overcome fluorophore leakage and the low efficiency of PLGA labelling through a simple, solvent free, one-step reaction to prepare fluorescent polymers with a label on each chain. This was achieved using fluorophores with active nucleophilic moieties as initiators in a solvent-free ring opening polymerisation (ROP) reaction of lactide (LA) and glycolide (GA) monomers. We used this method to synthesise three different fluorescently labelled PLGA copolymers, by ring-opening LA and GA in the presence of 2-aminoanthracene (AA, blue), 5-aminofluorescein (AF,

green) and Rhodamine-6G (R6G, red). The newly-synthesised polymers were then used to fabricate nanoparticles *via* a solvent displacement method.

The effects of these PLGA nanoparticles on cell metabolism were evaluated through AlamarBlue assays and the intracellular location of internalised particles further investigated with wide field fluorescence microscopy in human T-helper-precursor-1 (THP-1) macrophages. The practical value of the polymers as tracers during drug delivery was demonstrated via fluorescence microscopy assays in which the anti-cancer therapeutic doxorubicin was encapsulated in the nanoparticles and the intracellular locations of both drug and delivery system in sub-cellular spaces was determined. The initial one-step synthesis used a conventional ($Sn(Oct)_2$) catalysed ring opening polymerisation route (168) and fluorophores (AA, AF and R6G) with pendant amines were used as the nucleophiles. The mechanism of this reaction occurs through anionic ROP, in which the initial dye amine attacks a carbonyl group in the LA or GA ring. This frees a nucleophilic hydroxyl group which opens further LA and GA rings, such that the reaction continues until all the LA and GA are consumed (Figure 2-1A). The resulting polymers were denoted as PLGA-AA, PLGA-5AF and PLGA-R6G (Figure 2-1B) and their structures were confirmed using H^1 NMR spectroscopy (Figures 2-S1, 2-S2 and 2-S3, respectively). The unoptimised yields of purified polymers for PLGA-AA, PLGA-5AF and

PLGA-R6G, were 60% (grey solid), 64% (deep orange solid) and 26% (light pink solid), respectively (Table 2-1). The low yield of PLGA-R6G can be explained by the low solubility in acetone, which was the solvent used to eliminate unreacted reagents. Characterisation of PLGA-5AF (1.22 Đ) and PLGA-R6G (1.41 Đ) after purification showed narrower polydispersity indices (Đ) when compared to PLGA-2AA (1.75 Đ). This may in part be attributed to the comparatively higher hydrophobicity of 2AA (LogP 3.69), such that it exhibited higher affinity for the stationary phases during gel permeation chromatography (GPC) with THF and $CHCl_{3,}$ which were used as eluants. The broader GPC traces for this polymer is shown in (Figure 2-S4).

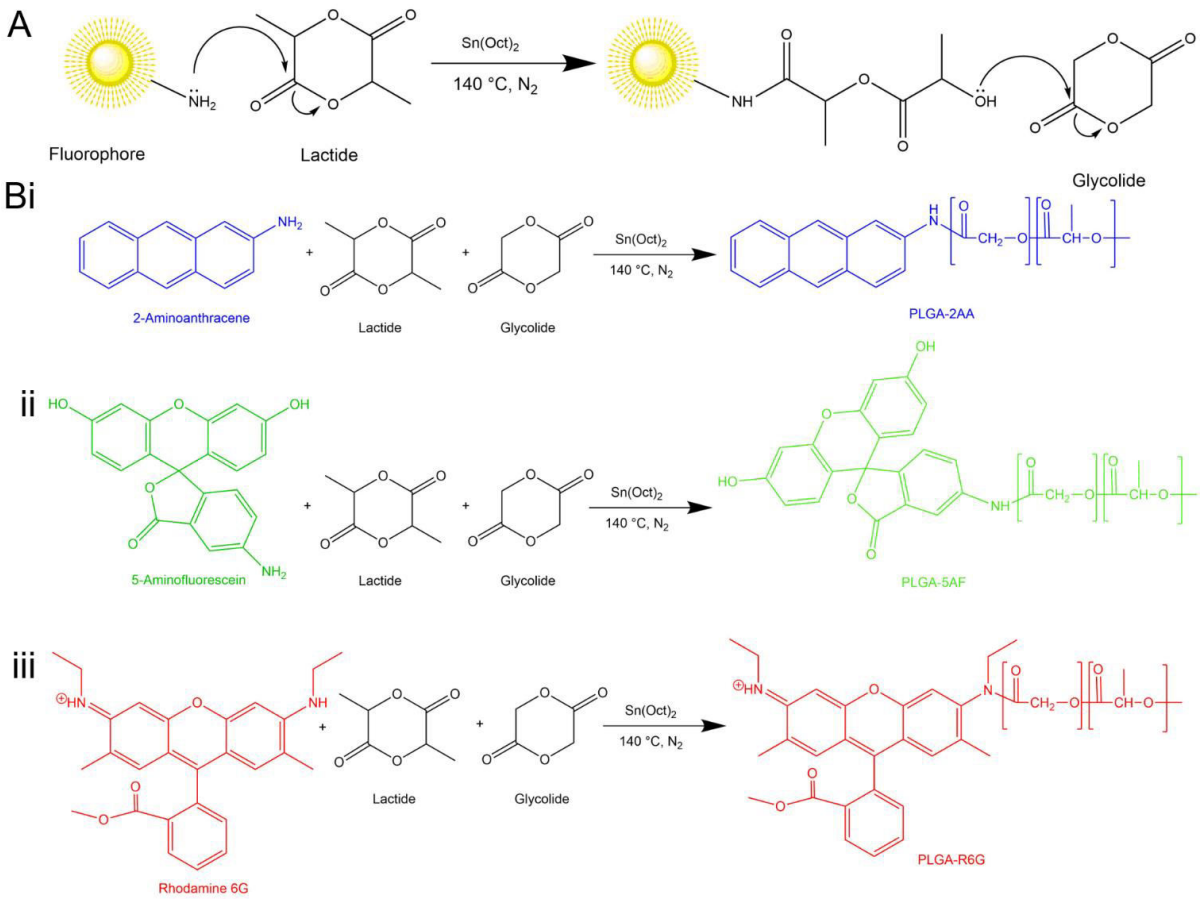


Figure 2-1. (A) Mechanism of lactide and glycolide ring opening upon nucleophilic attack by fluorophores with arylamine functionality. (B) Schematic representation of PLGA-5AF, PLGA-R6G and PLGA-2AA synthesis using ROP. All reactions were conducted at 140 °C under Nitrogen (N2), catalysed by tin (II) 2-ethylhexanoate (Sn (Oct)2).

2.3.2 NPs formation and characterisation

Following synthesis, PLGA nanoparticles were produced via a controlled flow solvent/anti-solvent nanoprecipitation methodology. Both fluorescent and unlabelled PLGA NPs had comparable hydrodynamic diameters, centred at 100 nm, and with zeta potentials of -40 mV (Table 2-S1).

Table 2-1. Labelled PLGA (Blue, green and red) synthesis, composition (monomer ratio), molecular weight (g.mol-1) and yield. NMR calculated molar mass (M Cal), and determined molar masses (Mn, Mw GPC) and polydispersity Index (Đ).

Polymer	Feed ratio (mol %)			Product ratio (mol %)			Molecular weight (g mol^{-1})			Đ	Yield (%)
	LA	GA	Dye	LA	GA	Dye	M (calc)	M_n	M_w		
PLGA-AA	59	39	2	65	33	2	11,179	7,236	12,650	1.8	60%
PLGA-AF	59	39	2	59	39	2	10,190	7,243	8805	1.2	64%
PLGA-R6G	59	39	2	55	43	2	6,365	6,284	8,828	1.4	26%

TEM imaging confirmed that the fluorescent nanoparticles were of low size dispersity and that there were no obvious differences between the polymers used to manufacture the nanoparticles (Figure 2-S5), which is in accord with previously reported literature (169). To compare the relative emission intensities of newly prepared fluorescent-dye-initiated PLGA nanoparticles versus unlabelled PLGA nanoparticles loaded with the analogous dye (5-AF), fluorescence spectroscopy was conducted. PLGA-5AF nanoparticles were found to be ~ 12.5x brighter than PLGA nanoparticles loaded with 5-AF ($p<0.0001$). Furthermore, 24 hrs after initial preparation, the fluorescence of PLGA-5AF nanoparticles had decreased by ~3 % whereas for PLGA nanoparticles loaded with 5-AF, the fluorescence intensity reduced by 45% (Figure 2-S6A). These results indicated PLGA nanoparticles

prepared using fluorophore linked PLGA are significantly brighter ($p<0.0001$) and demonstrate enhanced stability after 24 hrs of storage, thus suggesting their promise for medium and long-term experimentation.

2.3.3 NPs cellular uptake

To determine the utility of newly formed fluorescent nanoparticles, their internalisation and effects on metabolic activity were assessed in THP-1 cells, a model cell line for determining *in vitro* biocompatibility and particle uptake (170). These assays directly compared PLGA NPs (PLGA-AA, PLGA-AF and PLGA-R6G), with commercially produced unlabelled PLGA (PLGA), fluorophore loaded PLGA (AF loaded NPs) and fluorescently labelled PLGA loaded with doxorubicin hydrochloride (PLGA-AF-Dox). Cells were challenged with increasing nanoparticle concentrations (50-500 µg/mL) for 24 hrs. Fluorescently labelled PLGA NPs were well-tolerated by the cells, as more than 75% of cells were shown to be actively metabolising at 500 µg/mL (Figure 2-S6B). More importantly, no significant difference was observed in cell viability between PLGA-AA, PLGA-AF, PLGA-R6G, PLGA (commercial), AF loaded PLGA NPs and PLGA-Doxorubicin at all experimental concentrations ($p<0.01$). Therefore, a concentration of 100 µg/mL was used for subsequent experiments. To investigate the subcellular localisation of fluorescently labelled PLGA NPs (100 µg/mL), THP-1 cells were dosed with particles for 3 hrs and imaged using super-resolution

confocal microscopy. All fluorescent PLGA NPs were internalised as demonstrated by the orthogonal cross-sections (Figure 2-2Ai-Ci). As apparent from Figure 2-2A-D, dye-initiated PLGA nanoparticles (PLGA-AF) demonstrated rather different fluorescence responses, when compared to fluorophore loaded PLGA nanoparticles. Images A, B and C show the dye-initiated nanoparticles localised in bright fluorescent regions, whereas Figure 2-2Di indicated that the dye-loaded particles were less bright and more diffuse in the cells. For Figures 2-2Di and 2-2Dii the same regions of interest are shown; however, Figure 2-2Di was acquired under the same experimental laser power as Figure 2-2Bi, whereas Figure 2Dii was acquired at 8 times the laser power in order to excite the same level of fluorescence as occurred from the dye-initiated nanoparticles in Bii. In addition, the images shown in Figures 2-2Aii, 2-2Bii and 2-2Cii indicated that the dye-initiated nanoparticles were present in discrete sub-cellular vesicles. This suggested that the dyes were retained with the polymers in nanoparticles which were stable to endocytic pathways and intracellular transport processes. In contrast, close analysis of Figures 2-2Dii and 2-2Diii revealed no clear punctate regions, implying that the PLGA NPs loaded with AF released their contents into a diffuse intracellular space and that dye and nanoparticles were most probably no longer co-localised. In order to demonstrate the advantages of the single chain fluorescently labelled PLGA (PLGA-AF) for tracing the intracellular

fate of nanomaterials in a representative drug delivery experiment, the polymers were formed into nanoparticles in the presence of doxorubicin hydrochloride.

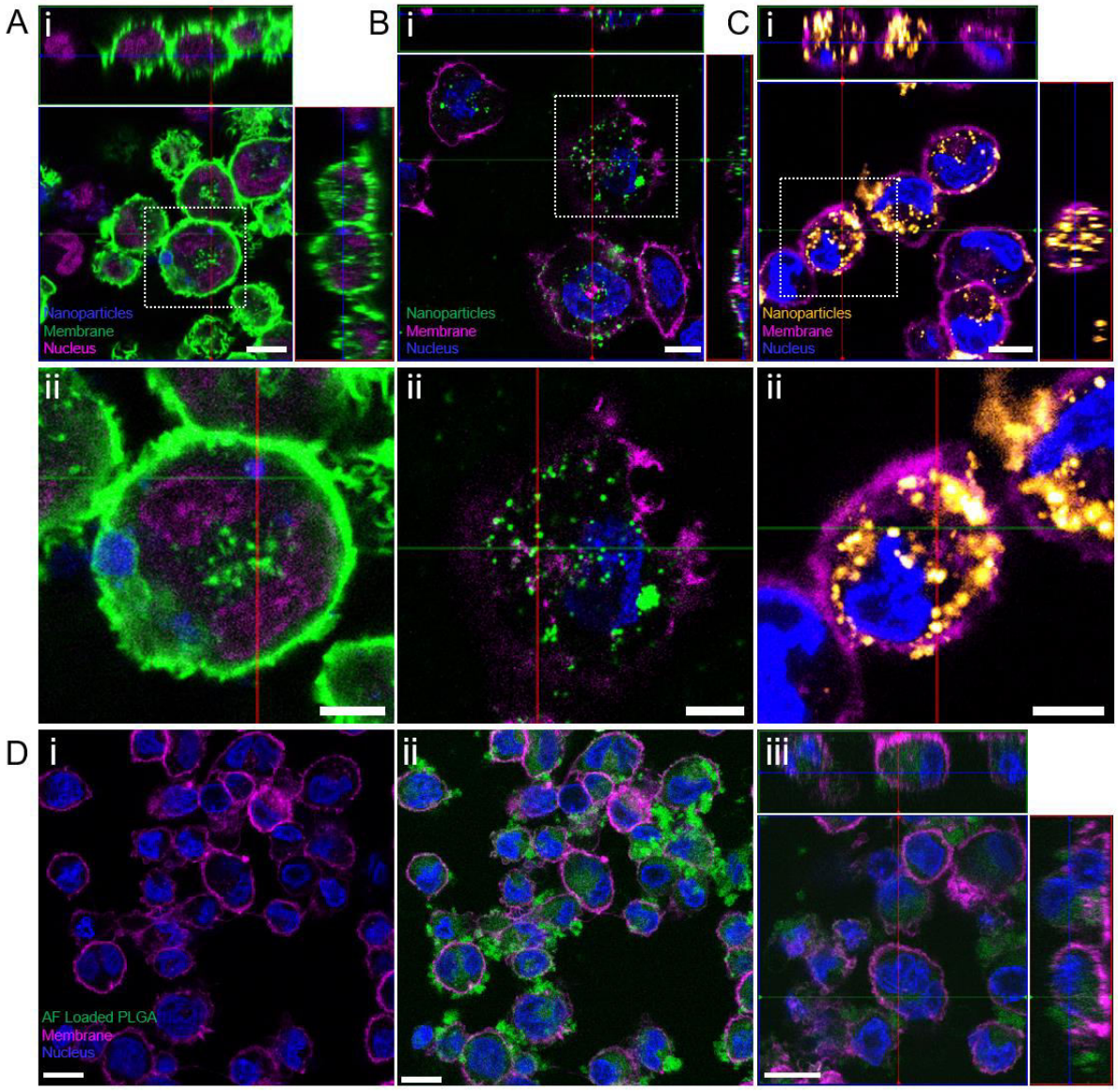


Figure 2-2. Super-resolution microscopy images of fluorescent (A) blue, (B) green and (C) red PLGA nanoparticles (100 µg/mL, 3 hrs) in activated THP-1 macrophages. Cells were fixed and stained for cytoskeleton ((A) Alexafluor 488, green and (B&C) Alexafluor 647, magenta) and nucleus ((A) Draq 5 nucleus, magenta and (B&C) Hoechst nucleus, blue). Images Aii, Bii and Cii are zoomed regions of interest, highlighted in Ai, Bi and Ci, respectively. Scale bar for Ai, Bi & Ci = 20 µm and Aii, Bii & Cii = 10 µm. (D) Fluorescence images of PLGA loaded with 5AF (100 µg/mL)) treated THP-1. Cells were fixed and stained for cytoskeleton (Alexafluor 647, magenta) and nucleus (Hoechst, blue). Image (Di) and (Dii) show the same region of interest, however, (Di) was acquired under

the same experimental laser power as (Bi), whereas Figure (Dii) was acquired at 8 times the laser power required to excite green fluorescence. (Dii) Orthogonal cross section of THP-1 cells showing internalisation of 5AF fluorophore. Scale bar = 20 μm.

This DNA intercalating anticancer drug exhibits red fluorescence (λ_{ex} 480 nm, λ_{em} 590 nm) and has been very widely used both in laboratory studies and in the clinic (171-174). We selected THP-1 cells for these experiments because they are non-proliferative, which makes them tolerant to doxorubicin and therefore a good model to study its cellular delivery. Accordingly, doxorubicin loaded PLGA-AF NPs were fabricated and dosed to activated THP-1 cells at subtoxic concentrations (100 μg/ml, 3 hrs). Figure 2-3 shows doxorubicin fluorescence was distributed in regions of interest away from PLGA-AF when imaged after 3 hrs Figure 2-4A) and after 24 hrs (Figure 2-3A). These data suggested that the drug was able to permeate away from the labelled polymers, and that the dye remained attached to the polymers over these time periods. However, the extent of any degradation of the PLGA chains during the cell assays could not be ascertained other than that no fragments were able to diffuse away at the same rate as the small molecule drug. The release of doxorubicin from PLGA-AF nanoparticles was confirmed in parallel release assays in aqueous media: after 24 hrs the fluorescence intensity of PLGA nanoparticles loaded with doxorubicin by nanoprecipitation had dropped by 44 % (Figure 2-3C). These results highlighted the

advantages of dye-initiated PLGA during the monitoring of therapeutic delivery to show the subcellular distribution of both drug and carriers *in vitro*.

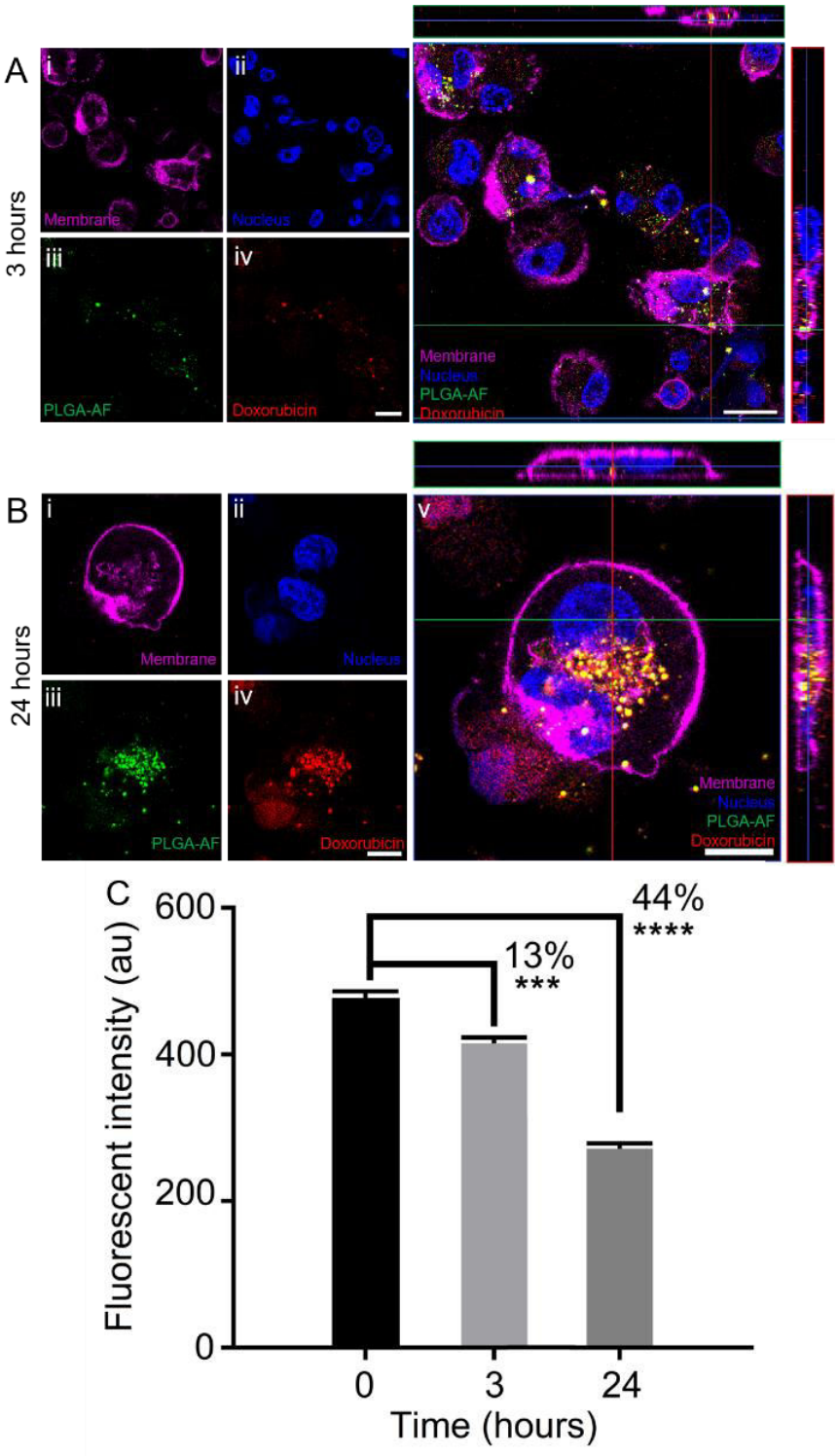


Figure 2-3. The uptake of doxorubicin loaded PLGA NPs by activated THP-1 cells. Cells were treated with RPMI complete medium containing (100 μg/mL) of doxorubicin loaded NPs for 3 hrs and imaged after (A) 3 hrs and (B) 24 hrs. Following exposure cells were fixed and stained for the cytoskeleton (magenta) and nucleus (blue). (C) Comparison of fluorescence intensity of doxorubicin in PLGA-5AF loaded nanoparticles after 0, 3 and 24 hrs. (A&B) Scale bar = 20 μm and (C) error bars represent standard deviation (n=3).

2.3.4 Caenorhabditis elegans NPs uptake

The culminating experiments aimed to demonstrate the advantages of the single-chain labelled PLGA *in vivo*. The nematode *C. elegans* was chosen as an accessible model to study *in vivo* biodistribution of the labelled nanoparticles (Figure 2-4). Synchronised cycles of *C. elegans* (L4-young adult stages) were washed with sterile deionised water prior to dosing, and ~300 nematodes were the exposed to PLGA nanoparticles at 100 μg/mL (n = 3) for 3 hrs. The nematodes were washed again before examination and collected for fluorescence microscopy imaging. The images in Figure 2-4 clearly show the internalisation of the nanoparticles and their localisation in the digestive tracts of the nematodes. Bright fluorescence was apparent in discrete regions of the nematodes and this was retained throughout the experiment without any obvious changes in the behaviour or viability of the worms. These experiments indicated good tolerability of the nanoparticles in addition to the retention of their bright fluorescence *in vivo*. Furthermore, as a final proof-of-concept, the methods described to label PLGA chains with fluorescent dyes were readily adapted to produce fluorescent

polycaprolactone (Figure 2-S7), as an example of another polymer that is generally y regarded as safe (GRAS) by FDA.

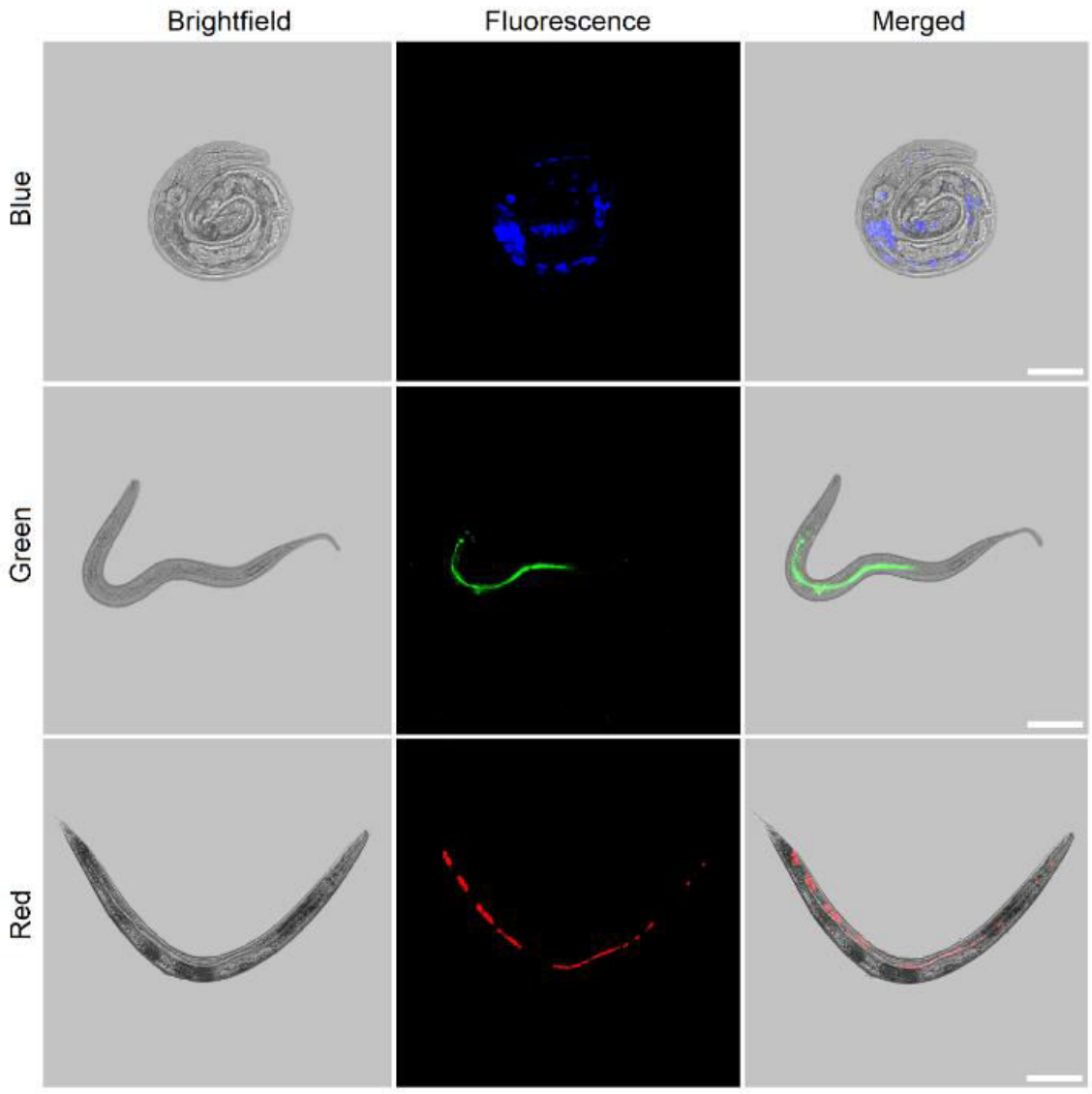


Figure 2-4. Fluorescence images of *C. elegans* challenged PLGA nanoparticles with blue, green and red fluorescence. Particles (100 µg/mL) were incubated with nematodes for 3 hrs, after which they were washed and imaged. Scale bar blue = 100µm, green = 200 µm red = 200 µm.

2.4 Conclusion

This study described the synthesis of fully fluorescently labelled PLGA using three different fluorophores via a single step ROP reaction under solvent-free conditions. The resultant PLGA polymers were able to self-assemble into well-defined nanoparticles which were extremely bright in fluorescence microscopy when compared to dye-encapsulated analogues. The nanoparticles were readily internalised by activated THP-1 macrophages and exhibited a comparable cytocompatibility profile to commercially available PLGA *in vitro*. In addition, the stability of the fluorescent dye-polymer link was demonstrated by retention of the label in punctate regions of the THP1 cells, again in contrast to PLGA which contained entrapped dye. In turn, this property was exploited in a model drug delivery experiment in which the separate intracellular locations of a released drug, doxorubicin, and the carrier polymers were shown. The preliminary in vivo study in *C. elegans* further exemplified the use of these bright and stable nanoparticles. We believe this synthetic strategy may be further used to prepare a range of intrinsically labelled biodegradable polymers which could greatly facilitate the tracking of delivery systems in sub-cellular locations in the presence of multiple therapeutic constructs. In turn, these materials will allow better characterisation of delivery

pathways and cellular transport kinetics to accelerate clinical translation.

2.5 Supporting information

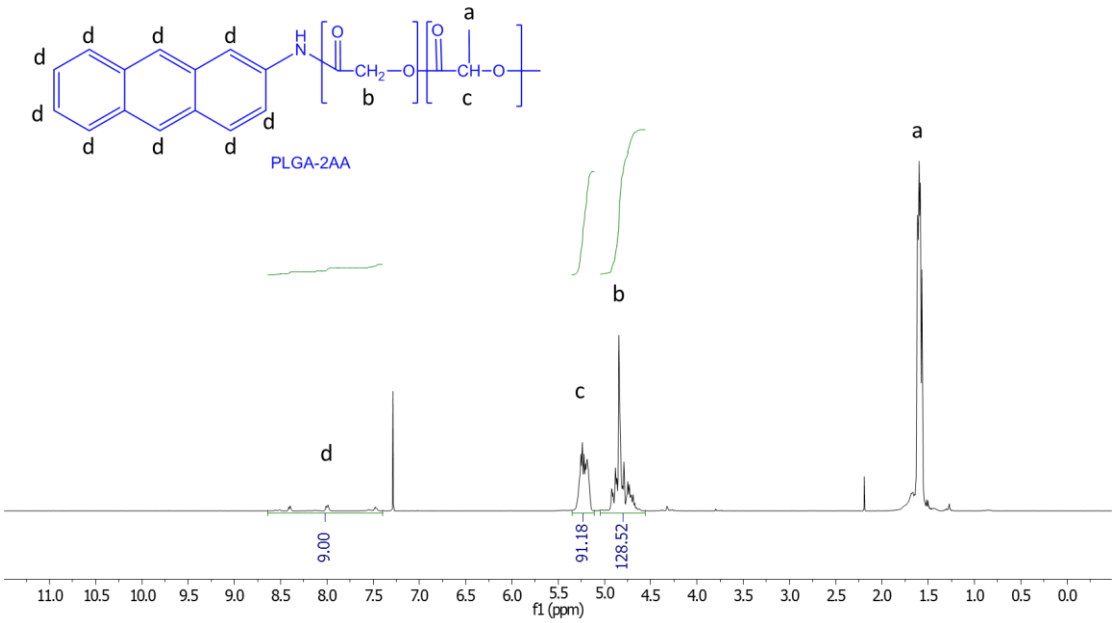


Figure 2-S1. ^{1}H NMR spectrum of PLGA-2AA in $CDCl_3$, prepared by ROP with $Sn(Oct)_2$ as catalyst and 2-AA as initiator.

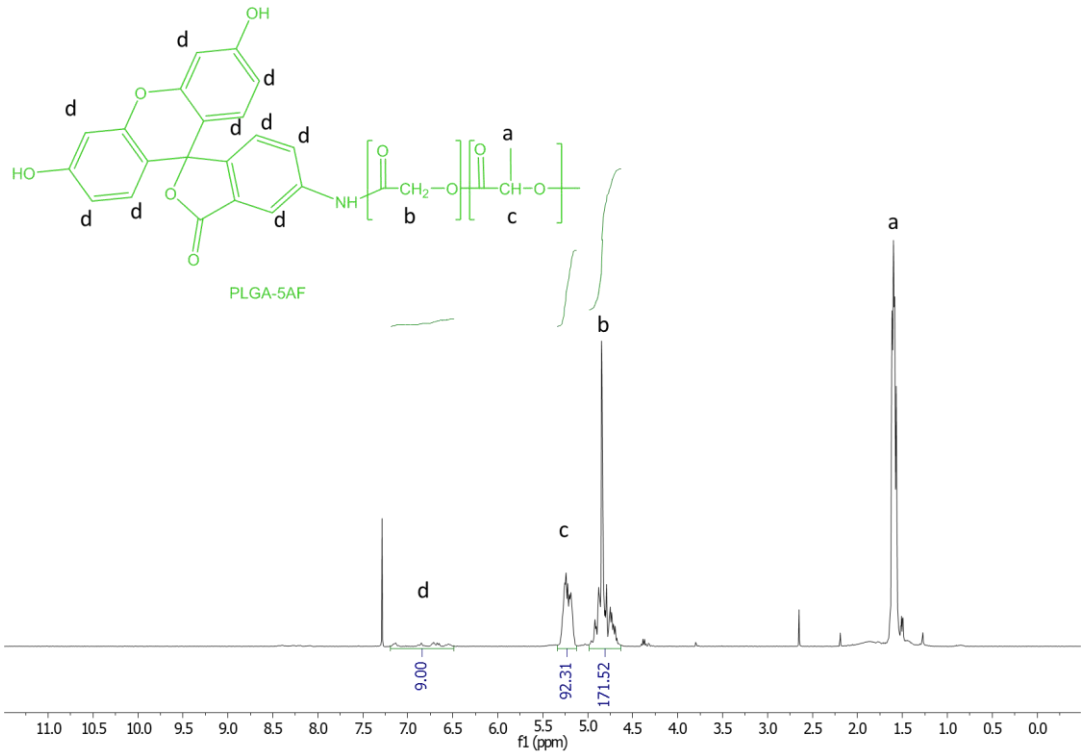


Figure 2-S2. ^{1}H NMR spectrum of PLGA-5AF in $CDCl_3$, prepared by ROP with $Sn(Oct)_2$ as catalyst and 5-AF as initiator.

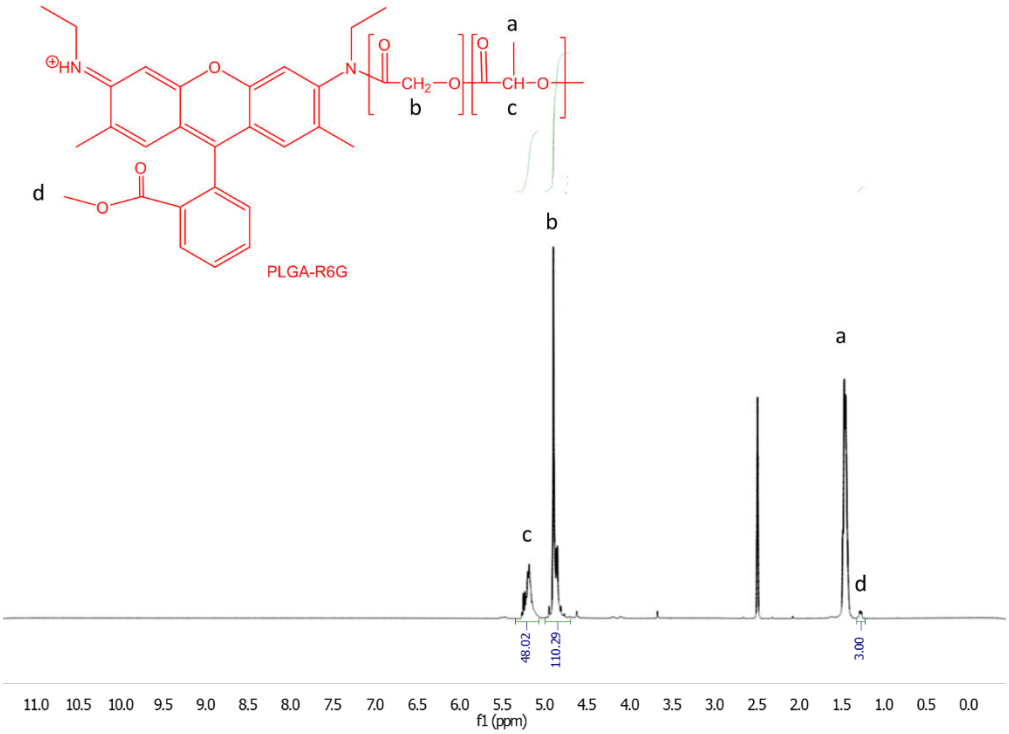


Figure 2-S3. ^{1}H NMR spectrum of PLGA-R6G in DMSO-d_6, prepared by ROP with $Sn(Oct)_2$ as catalyst and R6G as initiator.

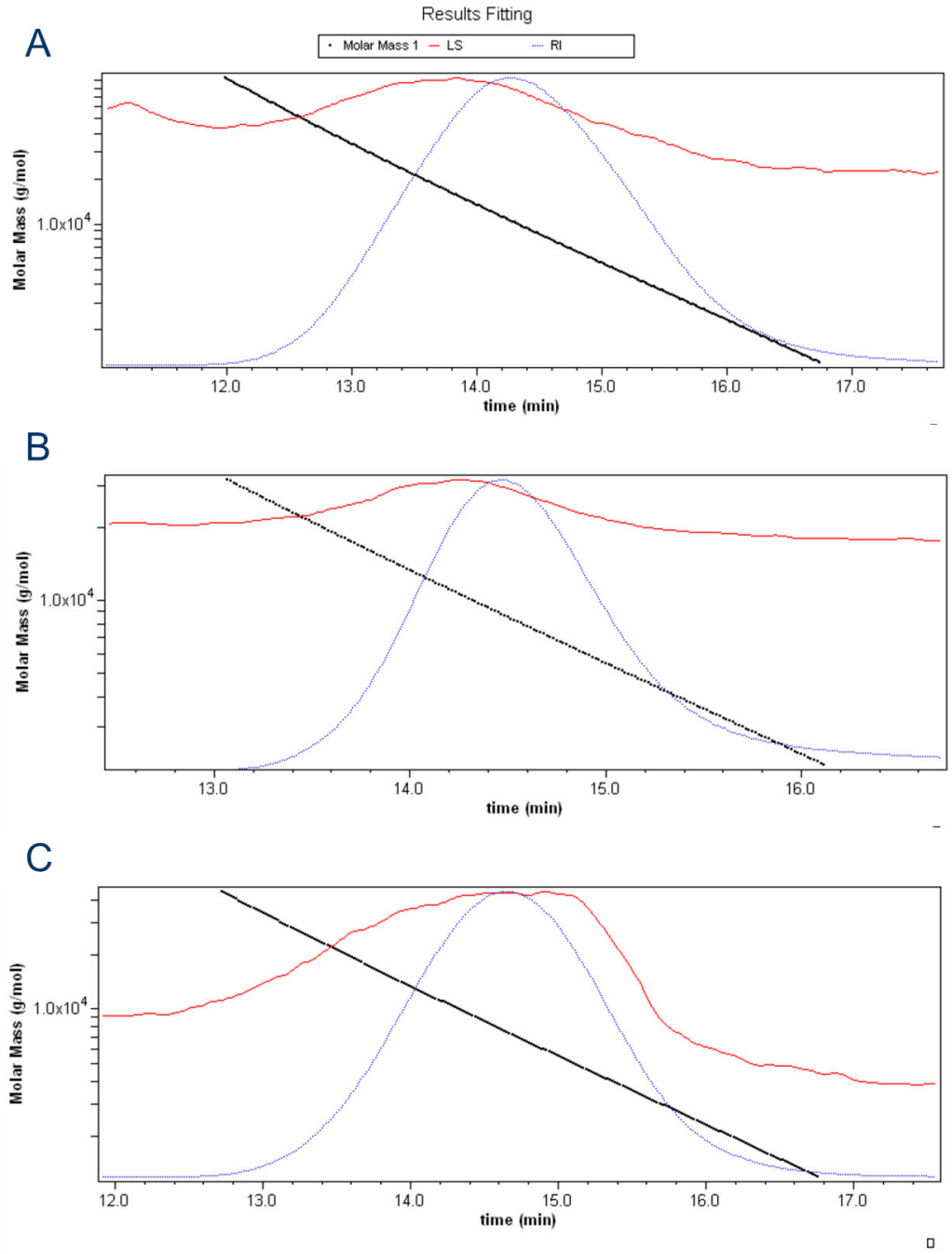


Figure 2-S4. GPC traces of (A) PLGA-AA, (B) PLGA-AF and (C) PLGA-R6G in $CHCl_3$ (poly polyester calibration).

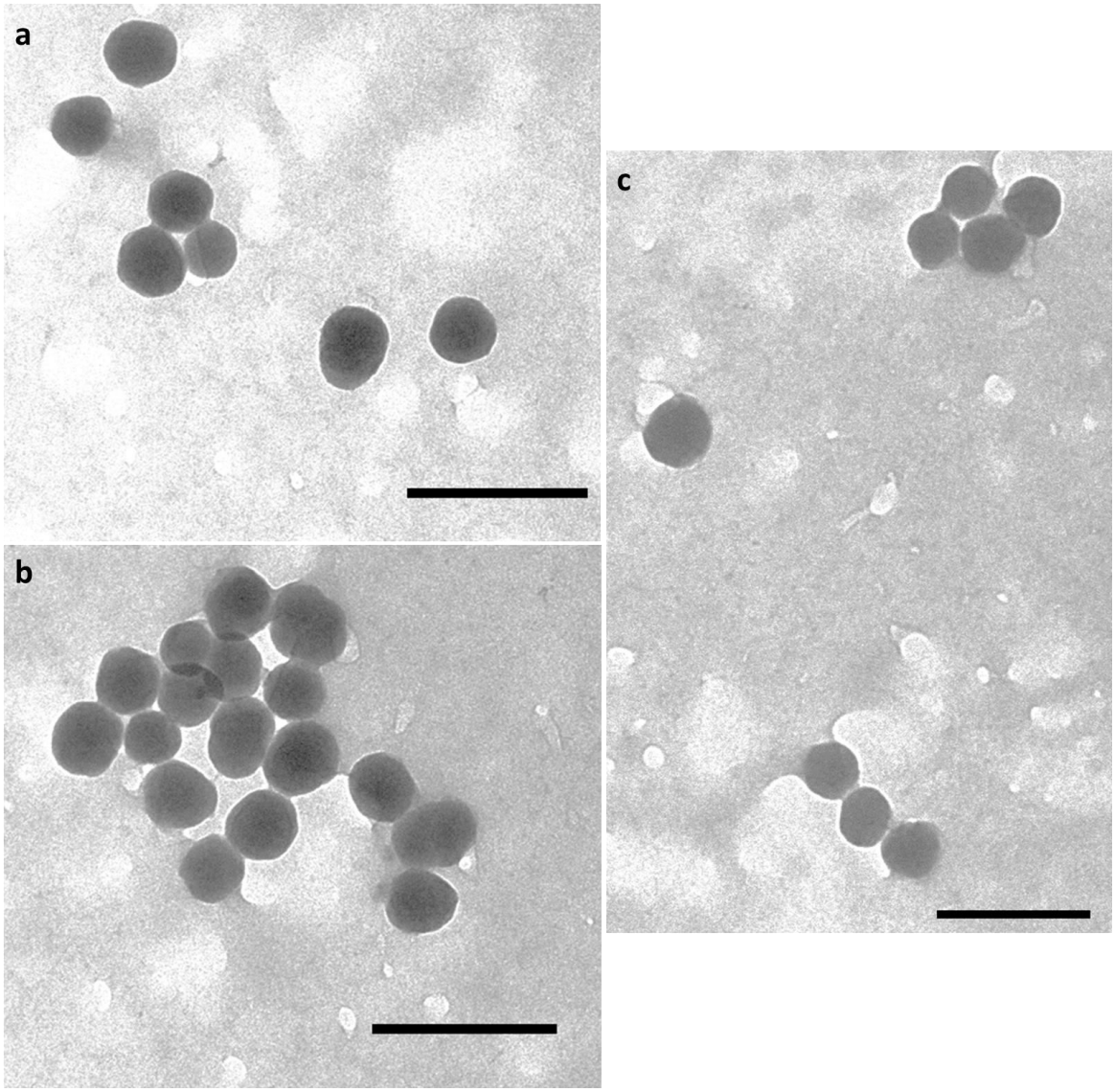


Figure 2-S5. Transmission electron micrographs of a) PLGA-2AA NPs, b) PLGA-5AF and c) PLGA-R6G.

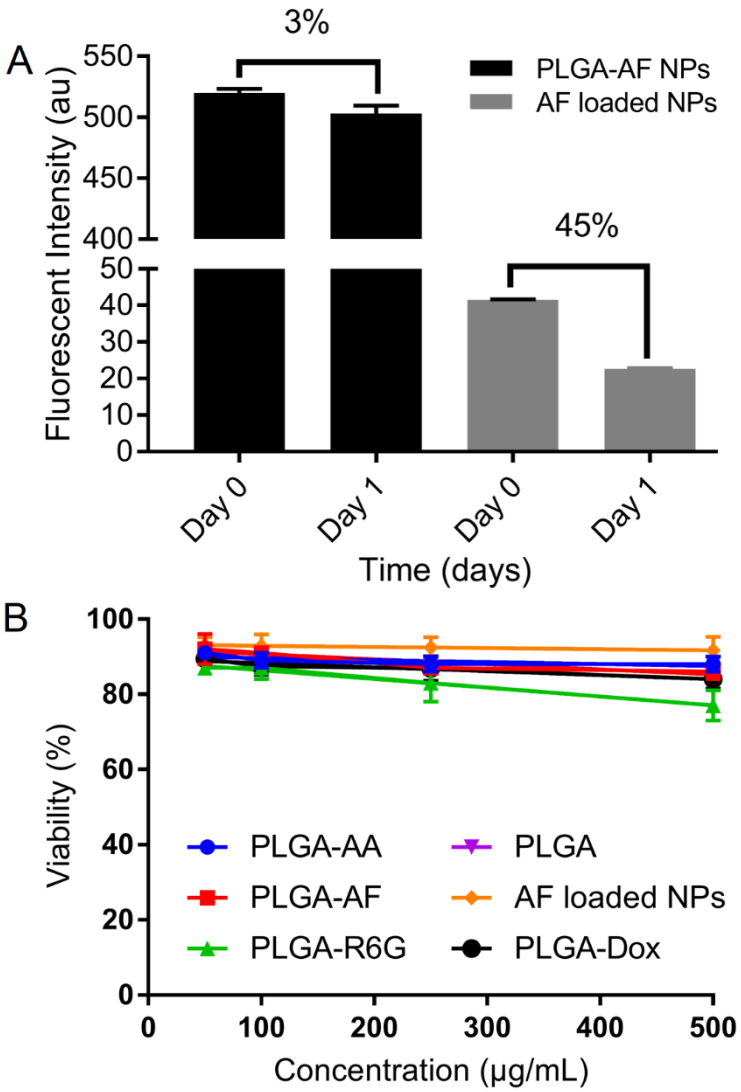


Figure 2-S6. (A) Comparison of fluorescence intensity of PLGA-5AF vs PLGA loaded with 5-AF immediately after synthesis and purification and after 24 hrs of storage. Error bars represent standard deviation (n=3). (B) Viability of activated THP-1 macrophages following exposure to PLGA NPs (50-500 µg/mL), fabricated from newly synthesised fluorescent polymers and commercially available PLGA. Cells were exposed to NPs for 24 h, cell viability was assessed *via* AlamarBlue assay. Data are expressed as the average percentage of cell viability ± SEM (n = 3).

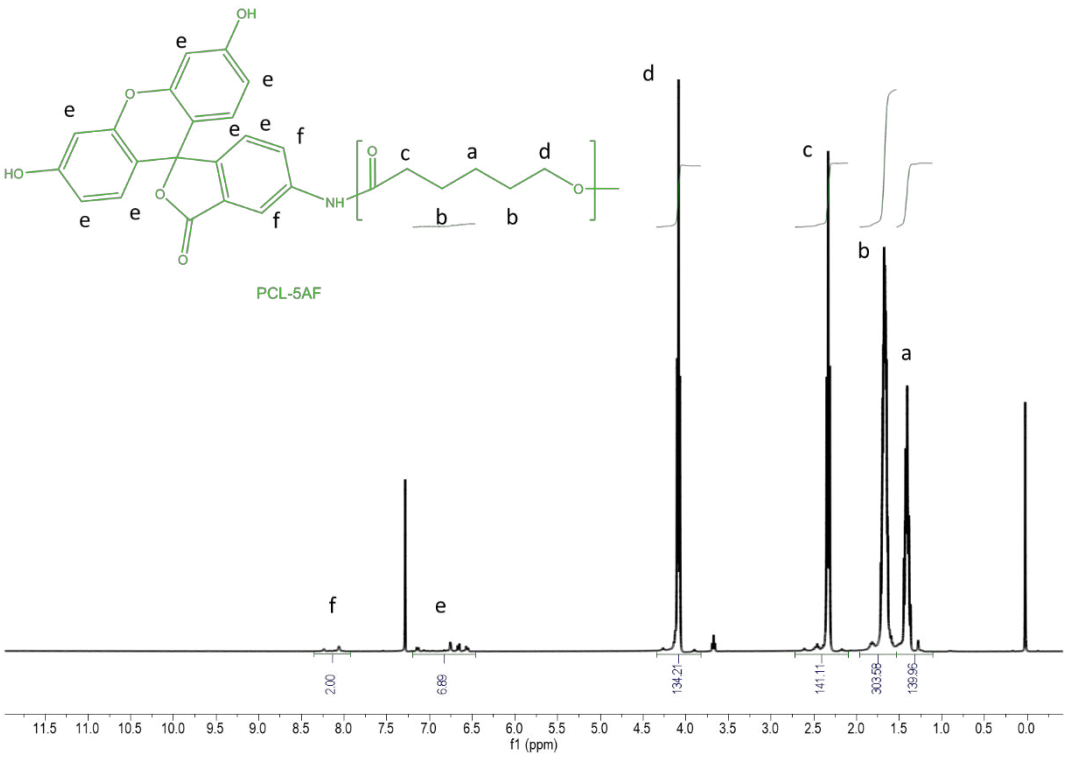


Figure 2-S7: 400 MHz ^{1}H NMR spectrum (in CDCl3) of PCL-5AF at room temperature prepared by ROP of ε-Caprolactone ring with 5-AF as initiator and $Sn(Oct)_2$ as catalyst at 130°C under a nitrogen atmosphere. δ 7.9-8.4 (ArC-*H*, 2H), 6.4-7.4 (ArC-*H*, 7H), 5.08 (t, 2H, CH_2-*CH_2*-O), 2.33 (t, 2H NCO-*CH_2*-CH_2), 1.67 (m, 4H, CO-CH_2-*CH_2*-CH_2-*CH_2*-CH_2-CH_2O), (p, 2H, CO-CH_2-CH_2-CH_2-*CH_2*-CH_2-CH_2O). NMR calculated molecular weight (M Cal)= 8,200 Da, GPC calculated number (Mn)= 6300 Da and intensity molecular weight (MW)= 7,300 Da, and polydispersity Index (PDI)= 1.16.

Table 2-S1. Size and zeta potential of the prepared NPs (n=3).

Polymer	Mean Diameter (nm) (±SD)	Zeta potential (mv) (±SD)	% Loading
PLGA-2AA	101 ± 5	-43 ± 3	N/A
PLGA-5AF	103 ± 6	-40 ± 4	N/A
PLGA-R6G	98 ± 5	-45 ± 4	N/A
PLGA	89 ± 2	-48 ± 5	N/A
AF loaded NPs	112± 6	-37± 3	3%
PLGA-Dox	108 ± 5	-35 ± 6	2%

Chapter three

Studying the impact of PLGA nanoparticles on activated THP-1 cells at the molecular level using LC-MS-based metabolomics

3.1 Introduction

In recent years, polymer therapeutics have been studied thoroughly for drug delivery, and polymeric nanoparticles (PNPs) in particular have been considered to be promising drug delivery systems to treat a variety of diseases such as cancer (175, 176). Some PNPs based drug delivery systems are in clinical use, and many more are being investigated in clinical trials for cancer treatment (177). Poly lactic-co-glycolic acid (PLGA) materials are fabricated from biodegradable/biocompatible polymers making them the most commonly used nanocarriers (178, 179). PLGA is an FDA-approved biodegradable polymer, which has been extensively employed in drug, nucleic acid (DNA and RNA) and protein delivery (180-182). However, since the properties of drug delivery particles scale non-linearly with size, and specifically PNPs have different physicochemical properties (smaller size and higher surface area) compared to more-conventionally-used PLGA implants materials, their biological effects are not fully understood and need to be furtherly studied (183).

Various *in vitro* cell assays have been employed to assess nanomaterials for their role in oxidative stress, inflammation, mitochondrial injury, DNA and cell membrane damage, usually by measuring the end-point of the NPs' triggered toxicity (184-186). Nevertheless, the information gained from such single effect assays

is far from a comprehensive description of the more subtle biological responses or highlight of the affected biochemical pathways after the exposure to NPs (187). Additionally, most of these conventional assays are colourimetric, and some nanomaterials can interfere with assay components. This can be via interaction either with an enzyme or a dye molecule (188) or through scattering or absorbing light which prevents accurate quantitation (189). Undoubtedly there is a pressing need to establish new robust methods to assess the biological effects of nanomaterials comprehensively before moving on towards clinical applications (188, 190).

The field of metabolomics aims for the qualitative and quantitative measurement of all the metabolites present in a biological system (125). Hundreds to thousands of metabolites, which are the end products of gene expression or cellular metabolic activities, can be studied using metabolomics (35), allowing the characterisation of metabolic phenotype (83). The abundant information provided by metabolomics, cell based metabolomics particularly, can, therefore, describe the molecular impact of polymeric nanomaterials on biological systems most comprehensively. Some studies have already been denoted for different metallic NPs using several cell lines (191-196). Metallic NPs are widely used for diagnostic and therapeutic applications (197), however, PNPs are still favoured for drug delivery purposes (198), that is because they are able to

control the drug release, they can be easily functionalised with targeting moieties, and most importantly can be fabricated from biocompatible biodegradable materials (36-41). Until a recent study in 2017, the toxicity of PNPs was solely assessed by conventional methods (132), Saborano et al, studied the metabolic alterations in macrophages after exposure to PLGA, silica and silk NPs, the macrophages were exposed to two doses of NPs, 10 and 500µg/ml. At low dose, PLGA NPs seemed not to affect the cellular metabolism, however, at high concentration, PLGA NPs increased glucose consumption and lactate production which indicates upregulated glycolytic activity, in addition, PLGA NPs altered the tricarboxylic acid cycle (TCA) cycle, whereas the levels of succinate and itaconate were high, these molecules were found in the pro-inflammatory type (M1) macrophages (199). Despite the fact that PLGA NPs made significant metabolic changes in the macrophages, the used concentration was very high, in order to get similar blood concentrations of NPs, approximately an IV dose of 3 grams which is very high in comparison to doses of FDA approved nanomedicines. The impact of PNPs, when administered at clinically relevant doses, is still need to be furtherly studied. The innate tendency of macrophages to phagocytose foreign particles makes these cells a good model for studying the effects of PNPs. For example, macrophages of the reticuloendothelial system take up

NPs upon IV administration, and after inhalation, alveolar macrophages respond to NPs (200).

While transcriptomic and proteomic studies could provide valuable information about cell phenotype, such studies typically do not capture potential post transcriptional or translational modifications which are critical in determining cell function. In this work, LC-MS-based metabolite profiling was selected for to assess the cellular metabolic responses in human macrophages (differentiated THP-1 cells) after treating with five types of PLGA NPs with different surface functionalities. LC-MS can detect a wider range of metabolites compared to GC-MS and NMR. In addition, LC-MS has higher sensitivity than NMR and doesn't require tedious sample derivatisation like GC-MS. Usually most NPs are subjected to opsonisation once in the bloodstream, followed by subsequent recognition and uptake by tissue resident macrophages in the organs or blood circulating monocytes of the mononuclear phagocytic system, eventually resulting in the elimination from the blood stream the model used for this work was the monocytic leukemia THP-1 cells, which are differentiated into macrophages by treatment with PMA, upon differentiation, they show enhanced adherence and phagocytosis. In addition, the major role of macrophage in the innate defense of the body, especially their strong phagocytic capacity, and their presence in many tissues and

organs make it a model of choice for many in vitro studies for toxicological impacts of NPs (201).

Pluronics™ are triblock copolymers in structure composed of central hydrophobic polypropylene glycol (PPG) block flanked by two hydrophilic PEG blocks. Three types of Pluronics™ were used to coat PLGA NPs, including F127, F68 and P85. Coating the NPs with non-ionic surfactants, such as pluronics, was reported to overcome tumer multidrug resistance mechanisms by inhibiting the excretion of NPs by efflux pumps, especially P-glycoproteins (202); leading to an enhanced sensitization of tumor cells to the used anti-cancer. In addition, Pluronics™ are considerably safe; they show low toxicity and immunogenicity (203).

In this chapter, a global metabolic profiling approach will be used to assess the biological impact of several types of PLGA NPs on human like macrophages, in order to do that, PLGA NPs with different surface chemistries will be fabricated according to published protocols, a control vs treatment study design using controls will be adopted assess the effects of these NPs and a high-throughput data analysis protocol will be established to identify the significantly altered metabolites which will be mapped to study the most important affected metabolic pathways.

3.2 Materials and methods

3.2.1 Materials

Lactide, glycolide 99%, benzyl alcohol, poly(ethylene glycol) methyl ether (Mn=5000 g/mol), 5-aminofluorescein, tin(II) 2-ethylhexanoate (Sn(Oct)2) 92.5-100.0%, deuterated chloroform $CDCl_3$, RPMI 1640 medium, heat-inactivated FBS, penicillin, streptomycin, l-glutamine, phorbol 12-myristate 13-acetate and formaldehyde were purchased from Sigma-Aldrich. Ammonium carbonate was purchased from Fluka. Isopropanol and acetonitrile were LC-MS grade and dichloromethane, methanol, diethyl ether and acetone were HPLC grade provided by Fisher Scientific.

3.2.2 Polymer synthesis

Poly (lactic-co-glycolic acid) (PLGA), PLGA-poly (ethylene glycol) (PLGA-PEG) and PLGA-5-aminofluorescein (PLGA-5AF) were synthesised by ring-opening polymerisation of lactide and glycolide shown in Figure 3-1, whereas benzyl alcohol, 5-aminofluorescein and poly (ethylene glycol) were used as initiators respectively.

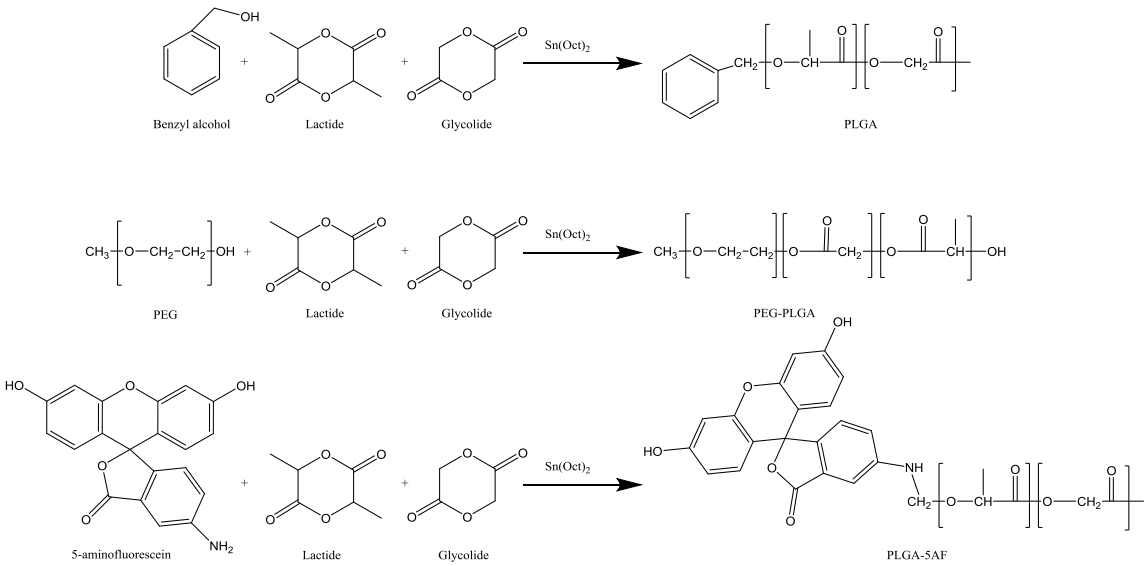


Figure 3-1: Schematic representation of PLGA, PLGA-5AF and PEG-PLGA Synthesis using ring-opening polymerisation.

PLGA synthesis

The synthesis was performed by melting 30 mmol (4.323 g, 30 eq) of D,L-lactide, 20 mmol (2.32 g, 20 eq) glycolide 130 °C under a nitrogen atmosphere. 1 mmol (104 µl, 1eq) of benzyl alcohol was added and left mixing for 1 minute after which 5% wt/wt $Sn(Oct)_2$ was added and the reaction continued for 3 hrs after which, the reaction mixture was cooled to room temperature. The synthesised polymer was dissolved in dichloromethane and precipitated in diethyl ether three times to remove unreacted monomers and other impurities. The filtered precipitate was dried under reduced pressure to generate 5.45 grams of a colourless product in 81% yield. Spectral data were in accord with prior literature (204).

^{1}H NMR (400 MHz, $CDCl_3$) δ 7.35 (ArC-H, 5H), 5.23 (m, 1H, OCO-**CH**(CH_3)-COO), 4.87 (m, 2H OCO-**CH_2**-COO), 1.59 (q, 3H, OCO-CH(C**H_3**)-COO).

PEG-PLGA synthesis

The polymer was synthesised by melting 21 mmol (3.3 g, 30 eq) of D,L-lactide, 14 mmol (1.62 g, 20 eq) glycolide and 0.695 (3.5 g, 1eq) MPEO at 130°C under a nitrogen atmosphere. Then 0.5% wt/wt $Sn(Oct)_2$ was added and the reaction continued for 3 hrs after which, the reaction mixture was cooled to room temperature. The synthesised copolymer was dissolved in dichloromethane and precipitated in ice-cold diethyl ether to remove unreacted monomers and other impurities, the filtered precipitate was dried under reduced pressure to generate 6 grams of a colourless product in 88% yield. Spectral data were in accord with prior literature (205).

^{1}H NMR (400 MHz, CDCl3) δ 5.23 (m, 1H, OCO-C**H**(CH_3)-COO), 4.87 (m, 2H OCO-C**H_2**-COO), 3.8 (m, 4H, O-C**H_2**-C**H_2**-O), 3.41 (s, 3H, OC**H_3**).

5-Aminofluorescein labelled PLGA (PLGA-5AF)

PLGA-5AF was prepared as discribed in chapter two, section 2.2.2.

3.2.3 NPs synthesis

Plain, Pluronic^{TM} coated and PEG PLGA NPs were prepared by standard nanoprecipitation with some amendments (166). A

solution of PLGA (20 mg) and PLGA-5AF (5 mg) in 10 ml of acetone was added to 10 ml of the anti-solvent (Milli-Q water) using a syringe pump (rate of addition 0.7 ml/min) to prepare PLGA NPs. By an analogous procedure, PLGA-PEG NPs were prepared using 12.5 mg of PLGA-PEG, 7.5 mg of PLGA and 5 mg of PLGA-5AF mixture. The stirring of the NP suspensions was continued at room temperature to ensure the complete evaporation of acetone. The suspensions were filtered using 0.45 µm syringe filters to ensure sterility.

Three Pluronic^{TM} poly(ethyleneglycol)-co-poly(propyleneglycol)-co-poly(ethyleneglycol) (PEG-PPG-PEG) block copolymers were used for NP coating, namely F127 (12200 g·mol^{-1}), F68 (8400 g·mol^{-1}) andP85 (4600 g·mol^{-1}). The prepared NPs were suspended in 0.1% wt/v Pluronic^{TM} water solutions for 24 hrs to ensure coating. Free Pluronics were removed by dialysing against 1liter of deionised water for 24hrs using 50 kDa membrane.

3.2.4 Cell culture, activation and treatment

THP-1 cells were cultured in T75 tissue culture flasks at 37 °C, 5% CO_2 and 95% relative humidity using RPMI media supplemented with 2 mmol/L l-glutamine, 100 µg/mL streptomycin, 100 U/mL penicillin and 10% vol/vol heat-inactivated FBS. Cell activation was done using phorbol 12-myristate 13-acetate (PMA) as previously described with some amendments (206) and THP-1 cells were then seeded in T25 flasks (6 million cells/flask) in RPMI media

containing 50 ng/ml PMA for 24 hrs under the previously described conditions. After the initial incubation, PMA containing media was replaced with fresh media containing 100 µg/ml of NPs. The cells were treated with the NPs for 24 hrs followed by metabolite extraction.

3.2.5 Metabolic activity (AlamarBlue®) assay.

The AlamarBlue® metabolic activity assay was used to assess the effects of the plain, Pluronic coated and PEG PLGA NPs on the cells. Activated cells in 24 well plates were incubated with media containing 50, 100, 250 and 500 µg/ml of NPs for 24 hrs, after which the media was removed, and the cells were washed with PBS, then the cells were incubated in fresh media containing 10% AlamarBlue for 3 hrs. 100µL of supernatants were transferred to 96 black well plates and the fluorescence was measured on Optima FLUOstar® plate reader at excitation/emission of 540/580 nm. The results are plotted as mean % viability vs control ± standard error of the mean (SEM).

3.2.6 Cellular uptake of NPs by activated THP-1 cells

Confocal microscopy

THP-1 cells were activated on 8 well chambered coverslip at 37 °C and 5% CO2 for 24 h. The media was then changed with fresh media or media containing 100 µg/mL of plain, Pluronic coated and PEGylated NPs for one hr at 37 °C and 5% CO2. Following

treatment, cells were washed twice with PBS and fixed in 4% formaldehyde (in PBS, 300 µL) for 15 min in the dark at room temperature. Subsequently, the plates were washed twice with PBS and stored with mounting media at 4 °C. Cells were imaged using a Zeiss LSM 700 Confocal Laser Scanning Microscope using the Zen program for data analyses.

Flow cytometry

THP-1 cells were activated in 24 well plates at a seeding rate of (500,000 cells/well) for 24 h at the previously described conditions. The media was then changed with fresh media or media containing 100 µg/mL of plain, pluronic coated and PEGylated NPs for three hrs. After treatment, cells were washed twice with PBS and detached using tryple express enzyme for 30 min at 37 °C and 5% CO2 with occasional gentle rocking, after which tryple express was deactivated by adding fresh media. The cells were then centrifuged and resuspended in fresh media before analysis in an FC 500 Flow Cytometer (Beckman Coulter). 10,000 live cells were gated for each analysis. Data were analysed using Weasel software (Walter and Eliza Hall Institute for Medical Research, Melbourne, Australia).

3.2.7 Metabolite extraction

After removing the media, the cells were washed briefly once with pre-warmed PBS at 37 °C. The cellular metabolism was quenched, and the metabolites were extracted simultaneously by adding

0.5 mL of ice cold methanol (−48 °C). Cell handling after quenching was performed on ice. The cells were then scraped and transferred to pre-cooled fresh tubes at 4 °C. Cell solution was vortexed vigorously for 1 h at 4 °C and centrifuged at 17000 × *g* for 10 min at 4 °C. After the centrifugation, the supernatant was removed and dried under vacuum at room temperature. The metabolite extract was reconstituted using 70 µl of pre-cooled methanol (4 °C). 10 µL aliquots were taken from all samples to make a pooled quality control (QC) in order to assess instrument performance (207).

3.2.8 Liquid chromatography-mass spectrometry (LC-MS)

LC was performed on a ZIC-pHILIC 5µm, 4.6 x 150mm column (Merck Sequant, Darmstadt, Germany), using Accela high speed system with a mobile phase consisted of A: 20 mM ammonium carbonate and B: 100% acetonitrile as previously described (134, 135). Compounds were separated by the following linear gradient: 20% A (0 min) to 95% A at 15 min to 20% A at 17 min and held to 24 min. The flow rate was 300 µl/min and the injection volume was 10 µl. Samples were maintained at 4 °C, and the column was maintained at 45 ^{0}C.

MS was performed on an Orbitrap Exactive MS (Thermo Fisher Scientific, USA) with ESI running in positive and negative ionisation modes. Briefly, spectra were acquired in full MS scan in the range of *m/z* 70-1400 and the resolution was 50,000 in both modes. The

capillary and probe temperatures were maintained at 275 and 150 °C, respectively. The instrument calibration was performed by modified Thermo calibration mixture masses with inclusion of $C_2H_6NO_2$ (*m/z* 76.0393) for positive ion electrospray ionisation and $C_3H_5O_3$ (*m/z* 89.0244) for negative ion electrospray ionisation in order to extend the calibration mass range to small metabolites.

3.2.9 Data analysis and metabolite identification

Raw LC-MS data from the control group (untreated cells), the treatments groups (cells exposed to the different NPs), and reagent blanks were acquired using Xcalibur v2.1 software (Thermo Scientific, Hemel Hemstead UK), and processed with XCMS for untargeted peak-picking (208). Peak matching and related peaks annotation were performed using mzMatch (209) and noise filtering and putative metabolite identification were then carried out using IDEOM with the default parameters (210). Metabolites that were matched with accurate masses and retention times of authentic standards were identified with Level 1 metabolite identification according to the metabolomics standards initiative (211, 212), but when standards were not available, metabolites were identified by employing predicted retention times considered as putative (Level 2 identification). The pooled QC samples were used to validate system suitability and stability (207). Multivariate data analysis was employed to assess changes in the cell metabolome between the control and each treatment group using orthogonal partial least

squares discriminant analysis (OPLS-DA) by SIMCA-P v13.0.2 (Umetrics, Umea, Sweden) (213). Mass ions with variable importance in projection scores (VIP) greater than one were selected as potential biomarkers. The results from the multivariate analysis were confirmed by carrying out one-way ANOVA using Metaboanalyst 3.0 (214) to investigate the significant differences between the control and the NPs-treated groups. The lists of significantly altered metabolites were imported to KEGG database to perform pathway analysis and to visualise the affected metabolic pathways (215).

3.3 Results and discussion

3.3.1 Polymer synthesis

Polymer synthesis and structures are shown in Figure 3-1. All the prepared polymers were synthesised by ring-opening polymerisation of lactide and glycolide using benzyl alcohol, 5-aminoflourescin and PEG as initiators to produce PLGA, fluorescently labelled PLGA-5AF and PEG-PLGA diblock copolymer respectively as appeared in H^1 NMR spectra Figures 3-S2, 3-S3 and 3-S4. The purified polymers physical state was either white powder for PLGA and PEG-PLGA or orange powder for labelled PLGA-5AF. The final yields of PLGA and PEG-PLGA were around 80%, and PLGA-5AF was lower (~50%) as a result of more extensive washing cycles needed to remove the last traces of free dye. Number

average molecular weights (Mn) for PLGA, PEG-PLGA, PLGA-5AF were 9.951×10^3, 1.146×10^4 and 8.599×10^3 g mol^{-1} as determined by gel permeation chromatography compared to polyester standards. The polydispersity index for PEG-PLGA was 1.06, however, it was higher for PLGA and PLGA-5AF, this might be attributed to the fact that the hydroxyl and amine groups of benzyl alcohol and 5-AF respectively are less nucleophilic than the hydroxyl of PEG because they are either close or directly linked to aromatic rings respectively (Figure 3-1).

3.3.2 NPs formation and characterisation

Plain and Pluronic^{TM} coated NPs were fabricated from PLGA and PLGA-5AF (4:1), and PEG-PLGA NPs were prepared from PEG-PLGA, PLGA and PLGA-5AF (5:3:2). Only 20% of PLGA-5AF was needed to make NPs fluorescent. Size and zeta potential of the prepared NPs are given in Table 3-S1.

The prepared NPs had a similar range of size around 100 nm in diameter, The high negative Zeta potential of the plain PLGA NPs is attributed to the free carboxylic acid group at the end of PLGA chains (169). However, the zeta potential of the NPs decreased significantly after the coating because these non-ionic coats shielded the negative surface charge of the NPs (216). All the used Pluronics were uncharged, however, F-127 decreased the magnitude of the negative zeta potential more than the other two because it has a higher molecular weight which makes it able to

cover the NPs surface charge more efficiently. TEM showed that all the NPs were spherical with smooth surfaces as apparent in Figure 3-S5.

3.3.3 Metabolic activity (AlamarBlue®) assay

The differentiated macrophages were grown in 24-well plates and exposed to different concentrations (50-500 µg/ml) of each type of NPs for 24 hrs, then AlamarBlue was added to the media to final 10% concentration and the plates were wrapped in aluminium foil and incubated for three hrs at 37 ^{0}C. A 100 µl sample was taken from each well and put into black 96-well plates and then the fluorescence was measured by the plate reader, each sample was done in triplicate. Figure 3-2 shows that all the synthesised NPs were well-tolerated by the cells even at the highest concentration as they caused less than 25% reduction in the number of actively metabolising cells.

3.3.4 NPs cellular uptake

Confocal microscopy revealed that all the prepared NPs were readily uptaken by the cells after one hr of exposure (Figure 3-3A). Flow cytometry results showed that all the PLGA NPs with the different surface functionalities were uptaken by at least 64-83% of the cells after one hr of exposure (Figure 3-3B).

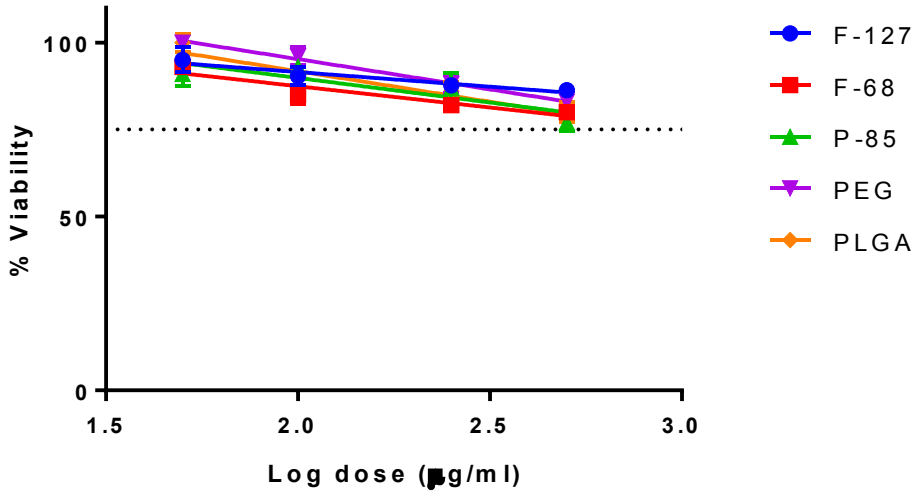


Figure 3-2 Viability of activated THP-1macrophages following exposure to Plain, F-127, F68 and P-85 coated and PEGylated PLGA NPs. Cells were exposed to NPs for 24 h, cell viability was assessed via Alamar Blue assays. Data are expressed as the average percentage of cell viability ± SEM (n = 3).

3.3.5 Multivariate analysis of LC-MS profiling data

In order to study the metabolic changes in activated THP-1 cells after 24 hrs exposure to PLGA NPs with different surface functionality, extracts from activated THP-1 cells exposed and unexposed to NPs were analysed by LC-MS. The obtained 3D data (*m/z*, retention time and peak intensity) were transformed into 2D XY output data (peak table) by mzMatch to assign each mass ion with the corresponding exact mass and retention time. OPLS-DA was implemented to visualise metabolic changes caused by the different NPs and to select potential biomarkers based on VIP values calculated based on the model. The six biological replicates for each sample group were clustered clearly in the OPLS-DA scores plots, indicating that sample clustering shows similar

biochemical composition. OPLS-DA scores plots revealed that LC-MS-based metabolic profiling was capable of investigating different molecular effects of each group of NPs on the cell metabolomes. Furthermore, Pluronic^{TM} coated PLGA NPs groups were clustered more closely to each other than the other groups (Figure 3-4A). This convergence indicates that these groups of NPs affected the cells in a similar manner which was expected as Pluronics are structurally related. However, this resulted in low model predictability (small Q2 value). To identify the most significantly changed mass ions after the exposure to each type of NPs, 2-way orthogonal comparisons based on OPLS-DA models were performed between the untreated control group and each NPs' treated group individually as shown in, Figure 3-4B.

523 metabolites have been putatively identified using IDEOM including essential and nonessential amino acids, glutathione reduced and oxidised forms, glycolysis, TCA cycle and urea cycle intermediates nucleotides and different lipid classes including phosphatidylcholines (PC), phosphatidylethanolamines (PE), phosphatidylserines (PS), phosphatidylinositols (PI) and phosphatidylglycerols (PG), Figure 3-5.

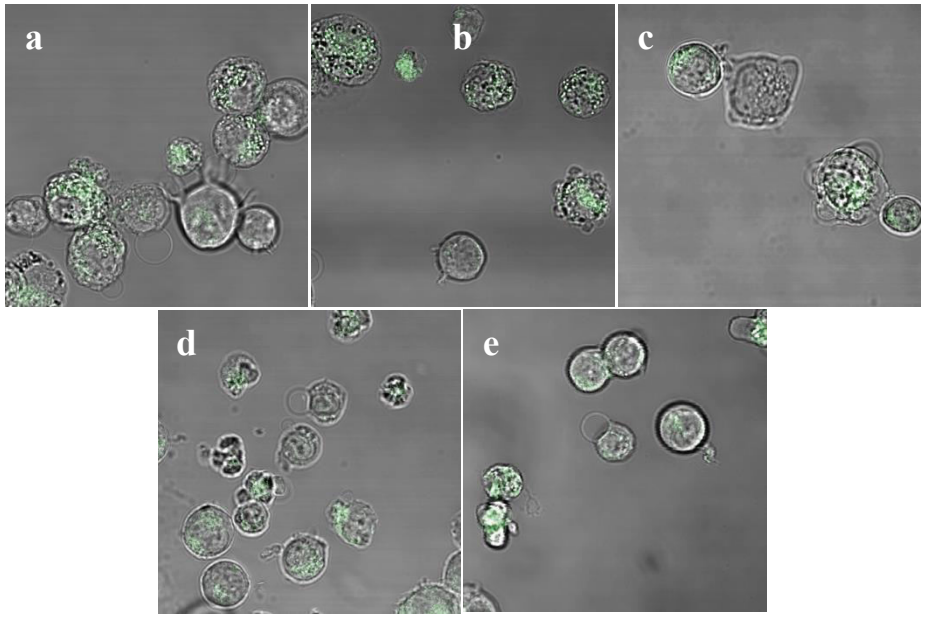
Mass ions of VIP score greater than one were selected as potential biomarkers. In addition to the multivariate analysis results, univariate ANOVA was performed to identify significantly changed compounds and mass ions with the false discovery rate ≤ 0.05

were selected as significant variables (217). The combined multi and univariate analyses revealed that 83 metabolites were altered significantly after the exposure to the five different NPs, Table 3-S3.

3.3.6 Metabolic pathway analysis

A significant number of the perturbed metabolites were linked to amino acid metabolism as shown in Figure 3-6. Amino acids are involved in many cellular metabolic pathways, providing a source purine and pyrimidine which are needed for nucleotide and nucleic acid synthesis, and a source of carbon after oxidation. Furthermore, some amino acids are precursors for other amino acids synthesis (218, 219).

A



,B

Cells up taken NPs

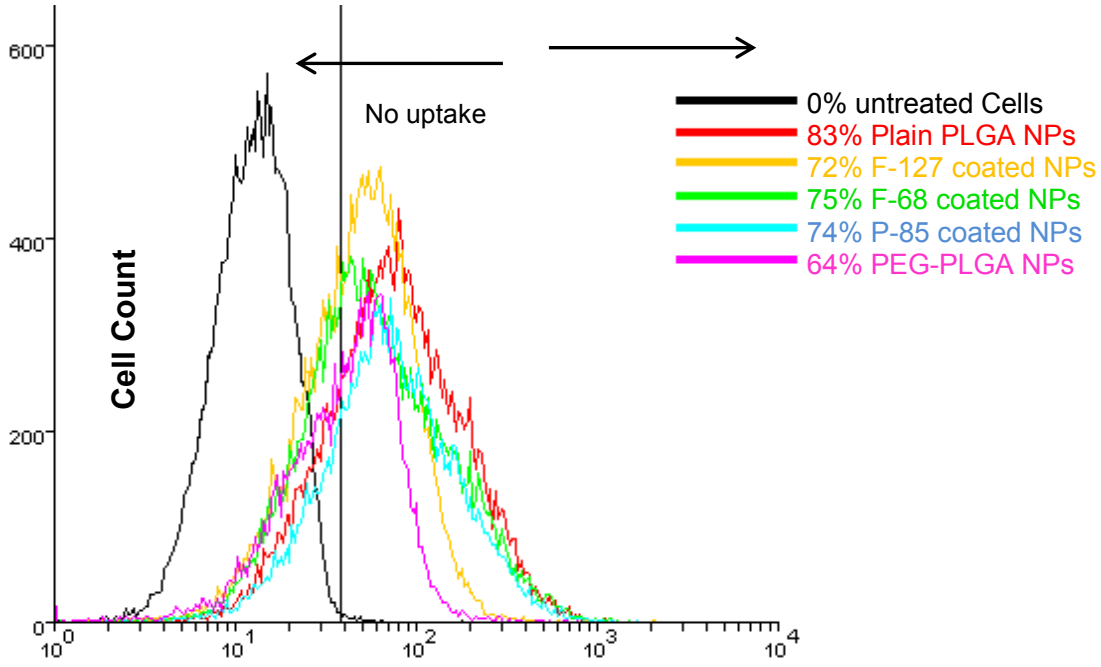
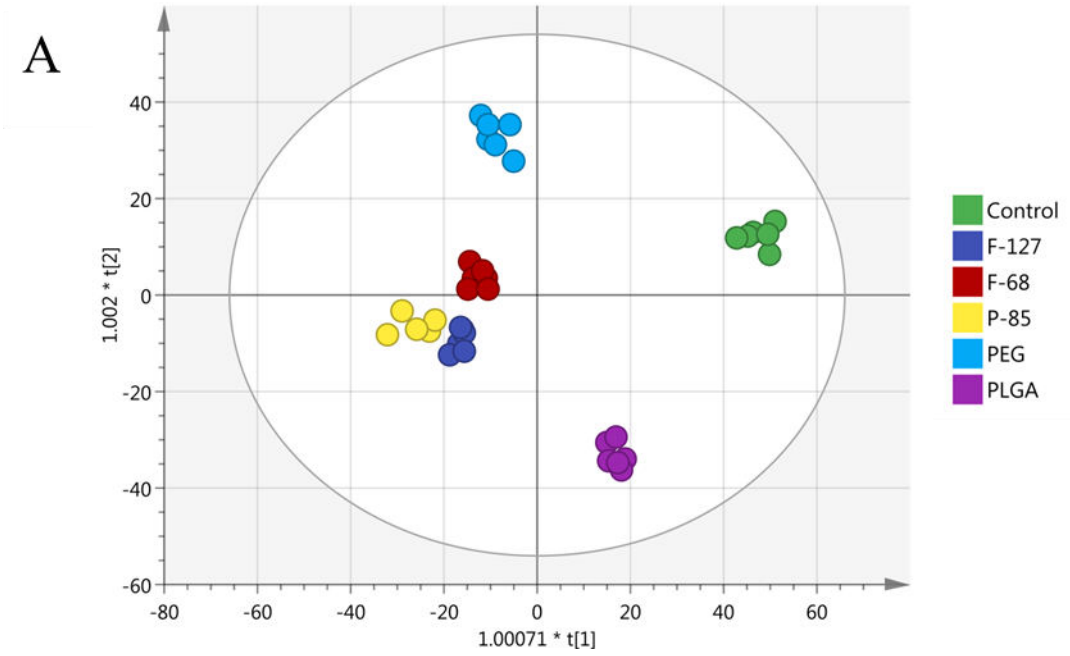


Figure 3-3: A) confocal images showing the cellular uptake of a) plain, b) F-127, c) F-68, d) P-85 coated and e) PEGylated PLGA NPs, green color represents NPs. B) a histogram showing the %cellular uptake of the NPs.



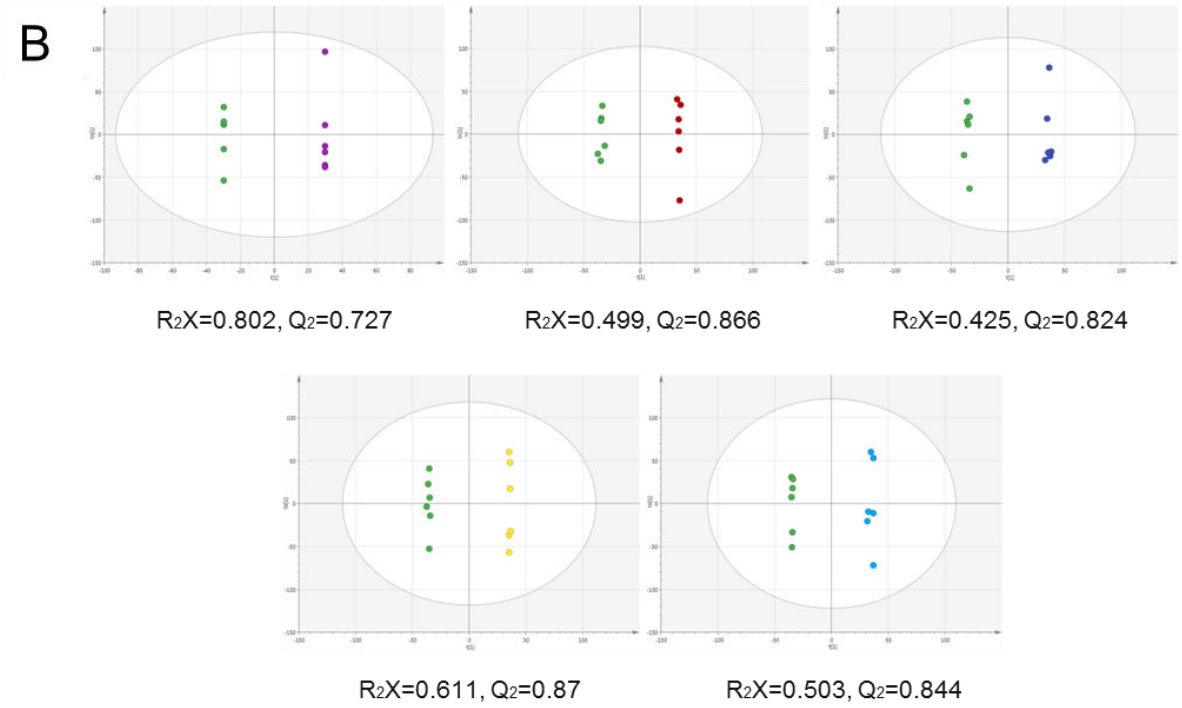


Figure 3-4: OPLS-DA scores plots of THP-1 cells samples after 24 h treatment with the different NPs and the control group without any treatment. (A) Combined control and NPs treated groups (R2X=0.685, Q2=0.359). (B) 2-way orthogonal comparisons of control group and each NPs treated group alone.

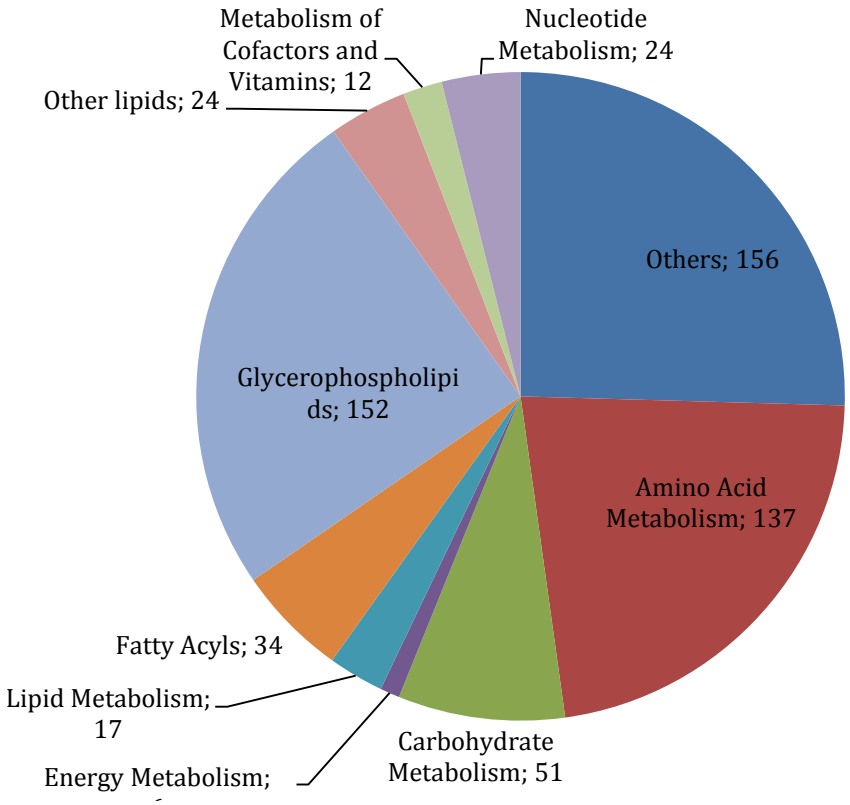


Figure 3-5 Putatively identified 613 metabolites categorised based on their biological function.

In order to fully understand the impact of the NPs on the cellular amino acid metabolism, metabolic pathways analysis was carried out using the KEGG database. KEGG is a combined database, that can provide biological interpretation of metabolomics data (215). Arginine is a semi-essential amino acid with vital intracellular roles in addition to being a building block of proteins, it is involved in urea cycle (KEGG PATHWAY: KO00220), aiding in detoxifying the ammonia resulted from amino acid deamination by converting it into urea (220), and in the production of nitric oxide (221, 222). Arginine metabolism pathway was affected significantly after the

treatment with all the same NPs, whereas the levels of N-(omega)-hydroxyarginine, N2-(D-1-carboxyethyl)-arginine, D-proline and N4-acetylaminobutanal have significantly increased. Since N-(omega)-hydroxyarginine is the first intermediate in NO synthesis through the oxidation of arginine, its accumulation indicates increased activity of nitric oxide synthase (NOS). A similar effect was seen upon treating macrophages with gold NPs (223). Figure 3-6 shows that PEG coated PLGA NPs did not increase the levels of N-(omega)-hydroxyarginine as much as plain or Pluronic^{TM} coated PLGA NPs did. N-(omega)-hydroxyarginine is known to inhibit arginase that catalyses the final step in urea cycle (Figure 3-6) (224, 225) which indicates that prolonged exposure and/or exposure to high concentrations of PLGA NPs might interfere with urea cycle, which in turn will lead to accumulation of the toxic ammonia. Similarly, arginine metabolism pathway was affected in HepG2 human liver carcinoma cells after the exposure to graphene nanosheets (190), suggesting that this effect could result from the nanomaterial physicochemical properties rather than chemistry. Additionally, the NPs that affected arginine metabolism most significantly were the plain NPs which share the hydrophobic surface properties with graphene nanosheets.

Since 3-acetaminopropanal (3-AAP) is produced from the oxidation of N-acetylspermidine and N-acetylspermine, its accumulation (Figure 3-7)along with other reactive aldehydes has been

considered as the sign of oxidative stress (226). Furthermore, 2,5,7,8-tetramethyl-2-(2'-carboxyethyl)-6-hydroxychroman (alpha-CEHC) is a major vitamin E metabolite and it is naturally occurring compound with good antioxidant activity (227). Therefore, the decrease in alpha-CEHC (Figure 3-7) could be another sign of oxidative stress. These findings suggest that plain and Pluronic^{TM} coated PLGA NPs might induce oxidative stress by enhancing the activity of NO synthase, which eventually will result in over production of NO.

To date such studies rely mainly on reporting the significantly changing metabolites, specifically the ones that are previously reported to be biomarkers for certain toxicities rather than trying to understand the mechanism of toxicities, that’s because most of time analytical scientists lead such investigations and this way of reporting the data is satisfactory for them.

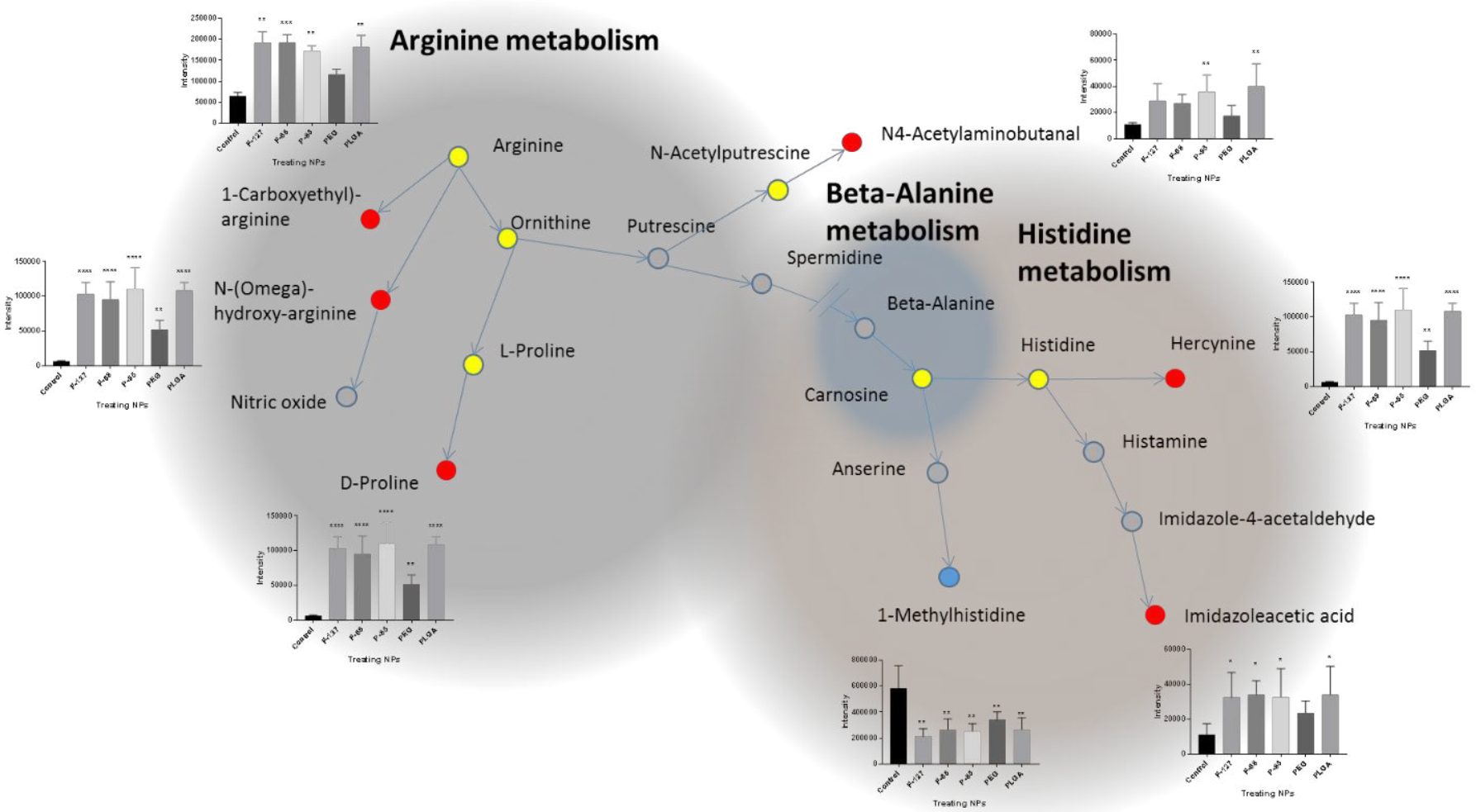


Figure 3-6: Metabolic pathways related with differential metabolites altered by plain, pluronic coated and PEG-PLGA NPs. Grey, blue and pale orange spots indicate arginine metabolism beta-alanine metabolism and histidine metabolism pathways respectively. Metabolite point colours in the figure represent changes in metabolite levels with blue indicating a decrease, yellow indicating no significant change and red denoting an increase, grey indicates that the metabolites were not detected. Data are expressed as the average peak intensity ± SEM (****p < 0.0001, ***p < 0.001, **p < 0.01, *p < 0.05. n=6.

Glycerophospholipids are considered main components of the cell membrane (228). Exposure to Pluronic^{TM} coated and PEGylated NPs resulted in decreased levels of PC and PE and such effect could indicate membrane compositional alteration and/or growth arrest as these lipids are essential components of the cell membrane (229), Figure 3-7. Similar lipid-level variations in macrophages were reported after treatment with peptide-coated silver, silk and silica NPs (132, 230) and in human keratinocytes after treatment with silver NPs (229). This could indicate that the impact of NPs on cell membrane does not result from the nature of their bulk counterparts but is caused by their unique physiochemical properties. Although PLGA NPs at 500 µg/ml concentration were reported to alter glycolysis and TCA cycle (132), however, in order to get similar plasma concentration, approximately a dose of 3 grams of NPs should by administered though IV route, which is not clinically relevant. This study showed that PLGA NPs with different surface modification at clinically relevant concentration (100µg/ml) did not induce any significant changes in energy metabolism (glycolytic activities, TCA cycle and fatty acid oxidation) or in nucleotide metabolism. This suggests that all the NPs with or without surface modification were well tolerated by the cells, which agrees with the cell viability assay.

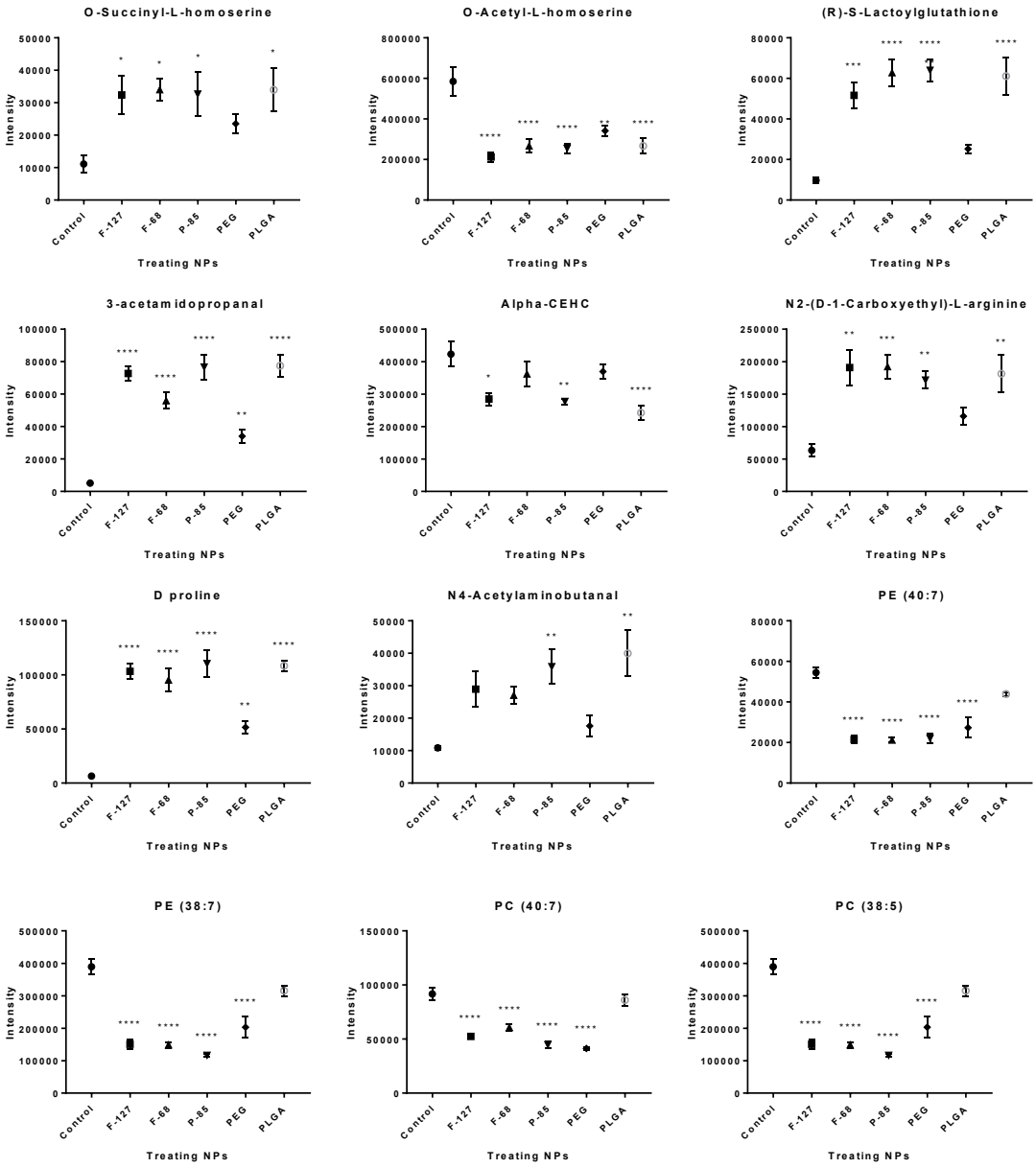


Figure 3-7: Alterations of intercellular metabolites induced by plain, pluronic coated and PEG-PLGA NPs. Data are expressed as the average peak intensity ± SEM (****p < 0.0001, ***p < 0.001, **p < 0.01, *p < 0.05; n = 6).

3.4 Conclusion

In this study, cell-based metabolomics approach was applied to investigate the biological impact of PLGA NPs with different surface functionalities on THP-1 derived macrophages using LC-MS. The metabolomics method revealed that plain PLGA NPs and surface modified ones were well tolerated by the cell, nevertheless there were several metabolic changes that are comparable to what was caused by some metal oxide NPs and other nanomaterials (190-196); exposure to plain and Pluronic^{TM} coated PLGA NPs has led to alterations in amino acid metabolism, which could tamper with urea cycle and induce signs of oxidative stress. Pluronic coated and PEGylated NPs have altered some glycerophospholipids lipids, which are core membrane component, such effects are could lead to growth arrest and membrane integrity alterations. PEGylated NPs had the least impact on the cellular metabolism in terms of metabolite levels fold changes, which agrees with the fact that PEGylation improves NPs biocompatibility (231, 232).

3.5 Supporting information

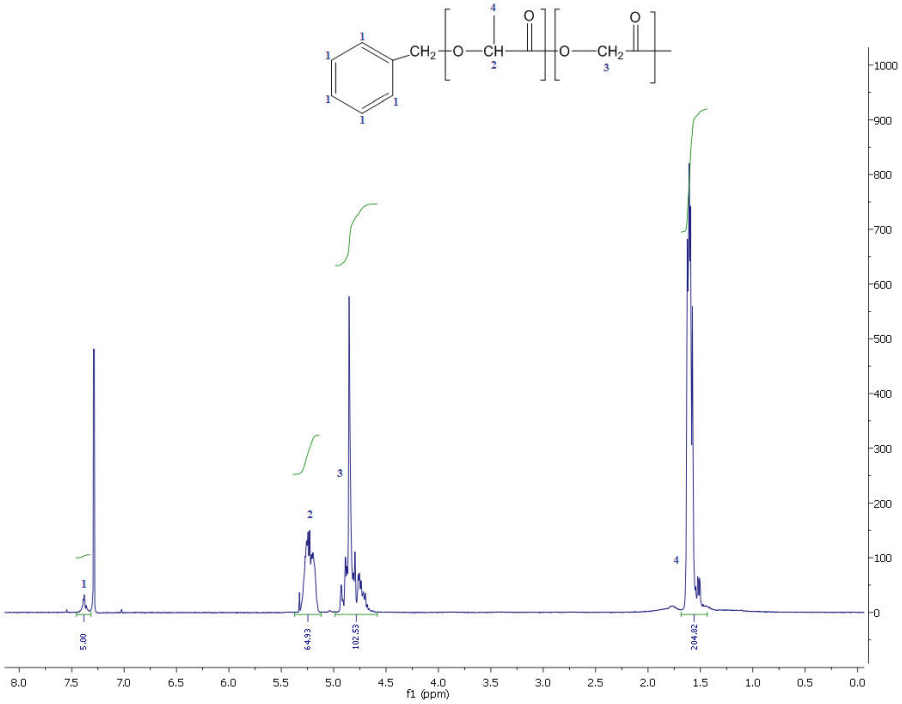


Figure 3-S1: ^{1}H NMR spectrum of PLGA in $CDCl_3$.

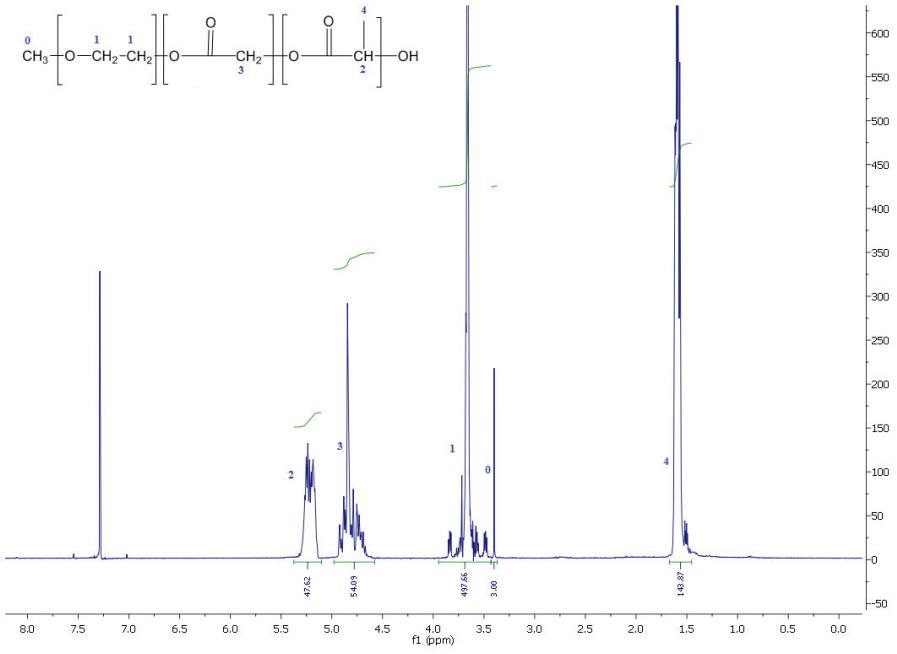


Figure 3-S2: 1H NMR spectrum of PEG-PLGA in $CDCl_3$.

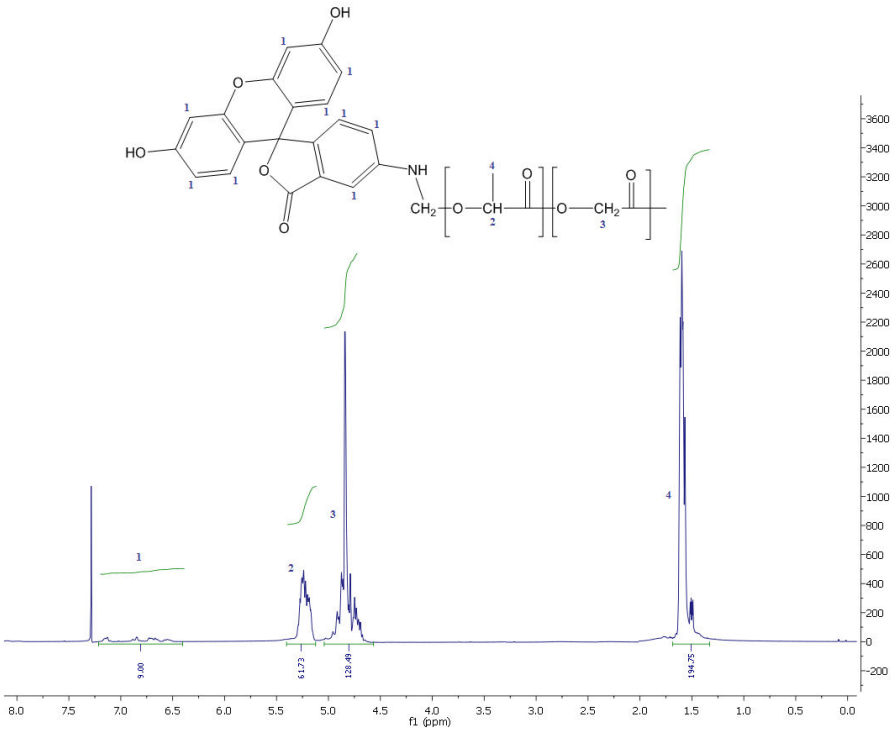


Figure 3-S3: ^{1}H NMR spectrum of PLGA-5AF in $CDCl_3$.

Table 3-S1: Size and zeta potential of the prepared NPs.

Type of NPs	Mean Diameter (nm) (±SD)	Zeta potential (mv) (±SD)
Plain PLGA NPs	101 ± 5	-43 ± 3
F-127 coated NPs	109 ± 6	-22 ± 4
F-68 coated NPs	105 ± 6	-33 ± 4
P85 coated NPs	102 ± 5	-36 ± 3
PEG-PLGA NPs	98 ± 7	-30 ± 5

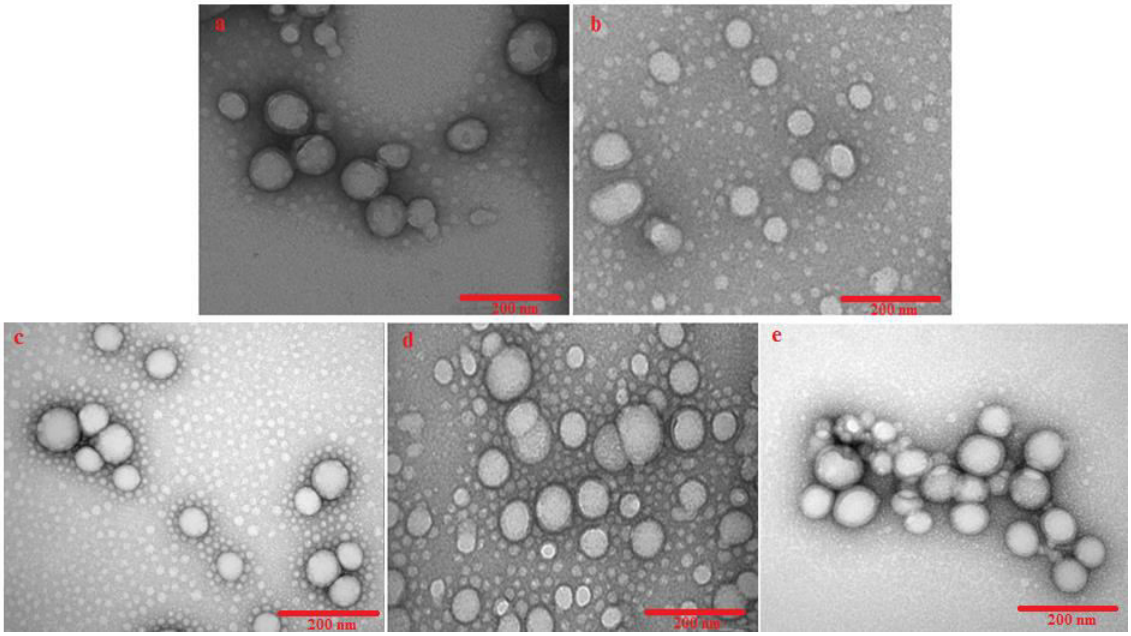


Figure 3-S4: Transmission electron micrographs of a) PLGA NPs, b) F-127 coated PLGA NPs, c) F-68 coated PLGA NPs, d) P85 coated PLGA NPs and e) PLGA PEG-PLGA NPs.

Table 33-S2: MS source parameters.

MS conditions with +/-ve switching:	
Spray Voltage (+)	4500.00
Capillary Voltage (+)	40
Tube Lens Voltage (+)	70
Skimmer Voltage (+)	20
Spray Voltage (-)	3500.00
Capillary Voltage (-)	30
Tube Lens Voltage (-)	70
Skimmer Voltage (-)	18
Capillary Temperature	275.00 ^{0}C
Sheath Gas	40.00 units
Desolvation	5.00 units
Sweep gas	1.00 units
Heater temperature	150.00 ^{0}C
Calibration:	
(+)	up to 1400 to accuracy
>1ppm	

(-)	up to 1400 to accuracy >2ppm

Table 3-S3: The metabolites that were changed significantly in THP-1 derived macrophages after exposure to the five different PLGA NPs, IDC: metabolite identification level according to the metabolomics standards initiative L1 – Level 1, L2 – Level 2. Colours in the table represent changes in metabolite levels with blue indicating a decrease and red denoting an increase.

Mass	Polarity	Mass error (PPM)	RT	FORMULA	Putative metabolite	IDC	Map	Control	F-127	F-68	P-85	PEG	PLGA
278.1518	-	-1.3771	4.18	C16H22O4	Alpha-CEHC	L2	-	1.00	0.67	0.86	0.65	0.87	0.57
723.5202	+	-0.21484	4.56	C41H74NO7P	PE(P-36:4)	L2	Lipids: Glycerophospholipids	1.00	0.45	0.51	0.36	0.53	0.80
773.6299	+	0.255985	4.87	C44H88NO7P	PC(P-36:0)	L2	Lipids: Glycerophospholipids	1.00	0.74	0.77	0.69	0.74	0.86
773.5356	+	-1.38686	4.44	C45H76NO7P	PE(P-18:7)	L2	Lipids: Glycerophospholipids	1.00	0.39	0.39	0.40	0.50	0.80
439.3064	+	-1.2289	7.29	C21H46NO6P	PC methyl(12:2)	L2	Lipids: Glycerophospholipids	1.00	0.80	1.17	0.83	1.57	0.72
749.5361	+	-1.14058	4.58	C43H76NO7P	PE(P-38:5)	L2	Lipids: Glycerophospholipids	1.00	0.44	0.46	0.40	0.57	0.82
747.5202	+	-1.21877	4.51	C43H74NO7P	PE(38:7)	L2	Lipids: Glycerophospholipids	1.00	0.39	0.38	0.30	0.52	0.81
689.4996	+	-0.87497	4.61	C37H72NO8P	PE(32:1)	L2	Lipids: Glycerophospholipids	1.00	0.59	0.57	0.50	0.56	0.88
729.5311	+	-0.25095	4.62	C40H76NO8P	PC(32:2)	L2	Lipids: Glycerophospholipids	1.00	0.63	0.83	0.64	0.69	0.89
691.5153	+	-0.74645	4.71	C37H74NO8P	PE(32:0)	L2	Lipids: Glycerophospholipids	1.00	0.69	0.85	0.64	0.70	0.88
677.4995	+	-0.3733	4.69	C36H72NO8P	PC(28:0)	L2	Lipids: Glycerophospholipids	1.00	0.64	0.81	0.56	0.76	0.87
743.547	+	-0.59104	4.67	C41H78NO8P	PE(36:2)	L2	Lipids: Glycerophospholipids	1.00	0.69	0.82	0.64	0.74	0.91
785.5935	+	0.070969	4.83	C44H84NO8P	PC(36:2)	L2	Lipids: Glycerophospholipids	1.00	0.71	0.75	0.64	0.77	0.88
146.0215	+	-0.12885	11.86	C5H6O5	Methyloxaloacetate	L2	Carbohydrate Metabolism	1.00	1.18	0.79	1.04	0.79	0.89
243.147	+	-0.02003	7.59	C12H21NO4	Tiglylcarnitine	L2	-	1.00	0.73	0.93	0.60	0.78	0.62
745.5985	+	-0.26758	4.88	C42H84NO7P	PC(P-34:0)	L2	Lipids: Glycerophospholipids	1.00	0.74	0.81	0.66	0.80	0.91
773.5938	+	-0.3789	4.86	C43H84NO8P	PE(38:1)	L2	Lipids: Glycerophospholipids	1.00	0.74	0.78	0.72	0.78	0.87
759.5777	+	-0.27196	4.88	C42H82NO8P	PC(34:1)	L2	Lipids: Glycerophospholipids	1.00	0.74	0.81	0.69	0.82	0.88
245.1627	+	-1.42099	7.45	C12H23NO4	N-(octanoyl)-L-homoserine	L2	-	1.00	0.66	0.77	0.34	0.67	0.49

731.5465	+	-1.006	4.62	C40H78NO8P	PC(32:1)	L2	Lipids: Glycerophospholipids	1.00	0.64	0.80	0.62	0.71	0.83
763.5159	+	-0.98624	4.55	C43H74NO8P	PE(38:6)	L2	Lipids: Glycerophospholipids	1.00	0.43	0.51	0.37	0.58	0.86
222.0892	-	0.030782	4.43	C12H14O4	FA (14:4)	L2	Lipids: Fatty Acyls	1.00	1.24	0.90	0.89	0.84	0.92
757.5621	+	-1.15017	4.63	C42H80NO8P	PC(34:2)	L2	Lipids: Glycerophospholipids	1.00	0.65	0.80	0.60	0.67	0.86
793.5985	+	-0.13159	4.67	C46H84NO7P	PC (38:5)	L2	Lipids: Glycerophospholipids	1.00	0.64	0.74	0.59	0.61	0.92
180.0423	-	-0.08998	7.34	C9H8O4	2-Hydroxy-3-(4-hydroxyphenyl)propenoate	L2	Amino Acid Metabolism	1.00	0.89	1.40	0.74	0.69	0.76
232.1171	+	0.015966	11.12	C8H16N4O4	(3R)-hydroxy-N-acetyl-arginine	L2	-	0.00	3022.13	3032.12	2878.31	1470.01	3452.20
161.0688	+	-1.29398	8.84	C6H11NO4	O-Acetyl-L-homoserine	L2	Amino Acid Metabolism	1.00	0.36	0.46	0.43	0.58	0.46
217.1313	+	0.095994	8.21	C10H19NO4	O-Propanoylcarnitine	L2	Lipids: Fatty Acyls	1.00	0.92	1.10	0.62	0.84	0.66
158.0579	+	0.267556	8.15	C7H10O4	2-Isopropylmaleate	L2	Amino Acid Metabolism	1.00	0.94	1.16	0.66	0.82	0.67
133.0739	+	-1.49548	7.34	C5H11NO3	N-hydroxyvaline	L2	-	1.00	0.66	1.07	0.74	0.91	0.80
703.5152	+	-0.99182	4.64	C38H74NO8P	PC(30:1)	L2	Lipids: Glycerophospholipids	1.00	0.66	0.83	0.58	0.74	0.84
813.6251	+	-0.41402	4.86	C46H88NO8P	PC(38:2)	L2	Lipids: Glycerophospholipids	1.00	0.75	0.83	0.70	0.81	0.91
791.5469	+	-1.3361	4.64	C45H78NO8P	PE(40:6)	L2	Lipids: Glycerophospholipids	1.00	0.53	0.57	0.48	0.60	0.81
781.5612	+	0.539981	4.69	C44H80NO8P	PC(36:4)	L2	Lipids: Glycerophospholipids	1.00	0.64	0.72	0.57	0.63	0.90
717.5309	+	0.733486	4.64	C39H76NO8P	PE(34:1)	L2	Lipids: Glycerophospholipids	1.00	0.70	0.82	0.61	0.70	0.92
204.1111	+	0.200347	11.05	C8H16N2O4	N6-Acetyl-N6-hydroxy-L-lysine	L2	Amino Acid Metabolism	0.00	533.28	568.61	515.36	264.55	657.86
484.2801	+	-1.51391	4.16	C22H45O9P	PG (16:0)	L2	Lipids: Glycerophospholipids	1.00	0.81	0.77	0.77	0.80	0.68
141.0191	+	0.233628	10.88	C2H8NO4P	Ethanolamine phosphate	L2	Amino Acid Metabolism	1.00	1.55	1.54	1.78	1.80	1.44
218.1266	+	0.580239	10.51	C9H18N2O4	N2-(D-1-Carboxyethyl)-L-lysine	L2	Amino Acid Metabolism	0.00	23.71	30.40	21.72	12.68	27.18
791.5828	+	0.325346	4.62	C46H82NO7P	PC(38:5)	L2	Lipids: Glycerophospholipids	1.00	0.66	0.76	0.56	0.54	0.98
115.0633	-	0.174626	5.38	C5H9NO2	3-acetamidopropanal	L2	-	1.00	14.24	10.96	15.00	6.67	15.18
771.5779	+	0.470485	4.68	C43H82NO8P	PE(38:2)	L2	Lipids: Glycerophospholipids	1.00	0.68	0.77	0.61	0.68	0.93

719.584	+	0.207208	4.87	C40H82NO7P	PC (32:2)	L2	Lipids: Glycerophospholipids	1.00	0.87	0.85	0.76	0.85	1.08
691.5517	+	1.906199	4.77	C38H78NO7P	PC (32:2)	L2	Lipids: Glycerophospholipids	1.00	0.77	0.78	0.67	0.67	1.00
379.105	+	1.018606	8.8	C13H21N3O8S	S-Lactoylglutathione	L2	Carbohydrate Metabolism	1.00	5.33	6.49	6.61	2.60	6.31
246.133	+	0.168293	10.52	C9H18N4O4	N2-(D-1-Carboxyethyl)-L-arginine	L2	Amino Acid Metabolism	1.00	3.02	3.05	2.72	1.83	2.87
787.6094	+	-0.44479	4.84	C44H86NO8P	PC(36:1)	L2	Lipids: Glycerophospholipids	1.00	0.78	0.85	0.77	0.84	0.92
223.0845	+	0.035972	7.07	C11H13NO4	N-Acetyl-L-tyrosine	L2	Amino Acid Metabolism	0.00	30.31	42.76	36.61	19.98	37.76
129.079	+	-0.28081	7.33	C6H11NO2	L-Pipecolate	L2	Amino Acid Metabolism	1.00	1.93	1.97	2.05	1.35	2.50
774.541	-	0.1744	4.03	C42H79O10P	PG(36:2)	L2	Lipids: Glycerophospholipids	1.00	1.43	1.19	1.33	0.89	1.23
831.578	+	0.196876	4.64	C48H82NO8P	PC(40:7)	L2	Lipids: Glycerophospholipids	1.00	0.64	0.73	0.61	0.53	1.01
115.0633	-	0.471352	7.33	C5H9NO2	D-Proline	L2	Amino Acid Metabolism	1.00	16.17	14.93	17.29	8.06	16.98
129.079	+	-1.07167	5.41	C6H11NO2	N4-Acetylaminobutanal	L2	Amino Acid Metabolism	1.00	2.66	2.49	3.30	1.62	3.68
807.5775	+	0.274708	4.61	C46H82NO8P	PC(38:5)	L2	Lipids: Glycerophospholipids	1.00	0.68	0.80	0.68	0.61	0.97
163.0481	-	-0.11857	8.83	C5H9NO5	3-Hydroxy-L-glutamate	L2	-	0.00	35.79	38.64	35.77	18.01	43.25
306.076	+	0.379488	11.07	C20H32N6O12S2	Glutathione disulfide	L1	Amino Acid Metabolism	1.00	1.25	1.15	1.42	0.99	1.10
705.5309	+	0.429292	4.67	C38H76NO8P	PC(30:0)	L2	Lipids: Glycerophospholipids	1.00	0.73	0.87	0.68	0.70	0.98
162.0528	-	-0.28668	7.44	C6H10O5	2-Ethylmalate	L2	Carbohydrate Metabolism	1.00	38.17	43.93	39.06	31.57	48.10
817.599	+	0.483243	4.58	C48H84NO7P	PC (40:7)	L2	Lipids: Glycerophospholipids	1.00	0.57	0.66	0.49	0.45	0.94
161.0688	-	-0.5006	10.35	C6H11NO4	N-Methyl-L-glutamate	L2	Energy Metabolism	1.00	2.47	2.68	2.10	1.53	3.12
741.5679	+	2.255547	4.68	C42H80NO7P	PC (34:3)	L2	Lipids: Glycerophospholipids	1.00	0.73	0.87	0.65	0.67	1.00
145.0375	-	1.107826	7.34	C5H7NO4	2-Oxoglutaramate	L2	Amino Acid Metabolism	1.00	1.38	1.32	1.43	1.07	1.38
809.5935	+	1.072295	4.71	C46H84NO8P	PC(38:4)	L2	Lipids: Glycerophospholipids	1.00	0.77	0.85	0.79	0.88	1.04
719.5479	+	0.319905	4.76	C39H78NO8P	PE(34:0)	L2	Lipids: Glycerophospholipids	1.00	0.79	0.90	0.74	0.75	1.04
689.5361	+	0.337488	4.73	C38H76NO7P	PC(P-30:0)	L2	Lipids: Glycerophospholipids	1.00	0.74	0.76	0.67	0.63	0.92

771.6145	+	0.260504	4.88	C44H86NO7P	PC (36:1)	L2	Lipids: Glycerophospholipids	1.00	0.77	0.83	0.66	0.82	0.92
302.2247	-	0.577009	4.46	C20H30O2	FA (20:5)	L2	Lipids: Fatty Acyls	1.00	1.61	2.25	1.99	2.18	2.05
833.5935	+	0.652803	4.65	C48H84NO8P	PC(40:6)	L2	Lipids: Glycerophospholipids	1.00	0.66	0.82	0.68	0.69	1.02
820.5254	-	0.924623	4.01	C46H77O10P	PG(40:7)	L2	Lipids: Glycerophospholipids	1.00	1.31	1.08	1.46	0.92	1.06
783.5785	+	0.655405	4.67	C44H82NO8P	PC(36:3)	L2	Lipids: Glycerophospholipids	1.00	0.69	0.82	0.70	0.65	0.94
745.5625	+	0.59015	4.74	C41H80NO8P	PE(36:1)	L2	Lipids: Glycerophospholipids	1.00	0.70	0.85	0.65	0.75	0.95
227.0907	+	0.621439	5.78	C9H13N3O4	Deoxycytidine	L2	Nucleotide Metabolism	1.00	2.70	2.16	2.56	1.26	2.76
787.6095	+	0.013965	5.98	C44H86NO8P	PC (36:1)	L2	Lipids: Glycerophospholipids	1.00	1.18	1.84	1.60	1.64	1.26
805.562	+	0.699987	4.56	C46H80NO8P	PC(38:6)	L2	Lipids: Glycerophospholipids	1.00	0.72	0.84	0.71	0.58	1.06

Chapter four

LC-MS metabolomics comparisons of cancer cell and macrophage responses to polymer-encapsulated methotrexate and free drug

4.1 Introduction

The folate antagonist methotrexate (MTX), is used widely as an antiproliferative agent in cancer treatments and as an anti-inflammatory, particularly for rheumatoid arthritis. The mechanism of action is not completely understood for MTX yet, despite the drug first being introduced ~ 70 years ago as a cancer treatment (233). MTX is known to inhibit the enzyme dihydrofolate reductase (DHFR) irreversibly (234), thus blocking the catalytic conversion of dihydrofolate to the active form tetrahydrofolate (THF). In turn, THF is essential for de novo purine, pyrimidine and neocluside thymidine synthesis which are required for DNA, RNA and thymidylates synthesis, MTX stops cell proliferation in the S phase, during which DNA replication takes place, by inhibiting nucleic acid and protein synthesis (235). High-dose MTX has been used to treat malignancies (e.g., acute lymphoblastic leukaemia (236), non-Hodgkin lymphoma (237), osteosarcoma (238), and colon cancer (239)), and to manage the symptoms of autoimmune diseases such as rheumatoid arthritis (RA) (240) at a lower dose. RA is a systemic chronic inflammatory joint disease, which is characterised by persistent synovitis, where macrophages are abundant and play a pivotal role (241). Inhibition of DHFR is not enough to manage RA; therefore, MTX is assumed to have other mechanisms including inhibition of purine metabolism by inhibiting certain enzymes that

are involved in that process. These include selective suppression of B cells, preventing T cell activation, downregulation of methyltransferase activity and inhibiting interleukin 1-beta binding to its receptor on the cell surface (242-244).

Malignant cells are highly proliferative, and DNA replication is essential for their survival, therefore these cells express high de novo nucleotide synthesis (245). MTX is capable of stopping the growth of cancer cells by inhibiting nucleobase synthesis, however, this effect of MTX can be counteracted by administration of folic acid. In contrast, although macrophages are not proliferative cells, the effects of MTX on macrophages are not modified by folic acid. These findings suggest that the mechanism of action of MTX is not limited to the inhibition of DNA replication and is cell-line dependent.

The mechanism by which MTX enters cells affects its activity, kinetics and fate. MTX is structurally similar to folic acid, it binds to folate receptors and is known to enter cells through active carrier-mediated transport (reduced folate carrier RFC) which makes it readily available in the cytoplasm (246, 247). Once MTX is free in the cytosol, folylpolyglutamate synthase catalyses conversion of MTX to MTX-polyglutamate (FPGS), rendering MTX no longer subject to the folate efflux pathway and prolonging retention inside the cells. In addition, polyglutamation increases the affinity of methotrexate for thymidylate synthetase, phosphoribosyl

aminoimidazole carboxamide formyltransferase and phosphoribosyl glycinamide formyltransferase (244, 248). The loading of MTX in nanoparticle carriers has been reported to enhance its activity in cell culture assays (49, 249), which may be related to a change in the mechanism by which MTX enters cells when encapsulated. This is because many nanoparticles enter cells by passive endocytosis, which is not a saturable process, unlike the active transport of free MTX entry by reduced folate receptors (247).

Metabolomics methods potentially allow all the end products of every cellular process to be measured, and any alterations in metabolite levels might act as signals which can describe the effects of certain stimuli on cells very comprehensively (250, 251). We therefore chose LC-MS based metabolite profiling to investigate the effects of free MTX and MTX loaded NPs on selected cancer cells and macrophages. The resultant global metabolic profile data provide an explanation for the differences in cellular processing between fast proliferative cancer cells and non-proliferative human-like macrophages when challenged with MTX in free drug form and when encapsulated in polymeric nanoparticles.

4.2 Materials and methods

4.2.1 Materials

RPMI 1640 medium, heat-inactivated FBS, penicillin, streptomycin, L-glutamine, phorbol 12-myristate 13-acetate and formaldehyde were purchased from Sigma-Aldrich. Ammonium carbonate was purchased from Fluka. Isopropanol and acetonitrile were LC-MS grade and dichloromethane, methanol, diethyl ether and acetone were HPLC grade provided by Fisher Scientific. Fisher Scientific provided Trypan blue 0.4% and all HPLC/LC-MS grade solvents.

4.2.2 Cell culture

THP-1 (human monocyte from acute monocytic leukaemia, ATCC® TIB-202™) and A549 (human adenocarcinoma alveolar basal epithelial, ATCC® CCL-185™) cells were cultured in RPMI and DMEM media respectively, supplemented with 10% FBS, 2 mM L-glutamine, 100 µg/mL streptomycin and 100 U/mL penicillin, in a humidified atmosphere containing 5% CO_2. The cells were used at passage number between 5-15.

4.2.3 Metabolic activity (AlamarBlue®) assay.

In 250 µl of fully supplemented medium, THP-1 and A549 cells were seeded on 48-well plates at density of 250 x 10^3 cell/cm^2 and 25 x 10^3 cell/cm^2 respectively. After 24 hrs, the cells were washed with PBS and treated with fee MTX and MTX loaded PLGA NPs, for

24 hrs. Thereafter, the cells were washed with PBS and the culture media were replaced with fresh fully supplemented media containing 10% AlamarBlue® reagent for 4 hrs. Finally, 100 µL were taken from each well and transferred to 96 black well plates and the fluorescence was measured on a TECAN plate reader at excitation/emission of 540/580 nm. The results are plotted as mean % viability vs control ± standard error of the mean (SEM).

4.2.4 Cellular uptake study

Nanoparticles were prepared using fluorescein amine labelled PLGA (chapter 2) to follow the cellular uptake. For confocal microscopy, THP-1 and A549 cells were seeded into 8-well chamber slides (obtained from Ibidi) at a seeding density of 3 x 10^5 cell/cm^2 and 1x 10^4 cell/cm^2 respectively in 300 µl of fully supplemented medium. After 24 hrs, the cells were treated with MTX loaded PLGA NPs for 3 hrs. Then, the cells were washed with PBS three times, fixed with 4% paraformaldehyde for 15 minutes, stained with Hoechst (20 µM in PBS for 10 minutes) for the nucleus, stained with phalloidin Alexafluor 647 for cytoskeleton and covered with mounting medium.

4.2.5 Metabolomic analysis

MTX treatment and metabolite extraction

THP-1 and A549 cells were seeded on T25 flasks (6 replicate for each condition) at a density of 2 x 10^5 cell/cm^2 and 25 x 10^3

cell/cm^2 in 50ng/ml fully supplemented RPMI 1640 media and DMEM media respectively. After 24 hrs, the cells were treated with free MTX, MTX loaded PLGA NPs and blank PLGA NPs for 24 hrs. Then, after removing the medium, the cells were washed briefly once with pre-warmed PBS at 37 °C. The cellular metabolism was quenched, and the metabolites were extracted simultaneously by adding 0.5 mL of methanol (−48 °C), and cell handling after quenching was performed on ice. The cells were then scraped and transferred to precooled fresh tubes at 4 °C. Cell solution was vortexed vigorously for 1 h at 4 °C and centrifuged at 17000 × *g* for 10 min at 4 °C. After the centrifugation, the supernatant was removed and dried under vacuum at room temperature. The metabolite extract was reconstituted using 70 µl of pre-cooled methanol (4 °C). 10 µL aliquots were taken from each sample to make a pooled QC in order to assess instrument performance (207).

Liquid chromatography-mass spectrometry (LC-MS)

LC was performed on a ZIC-pHILIC 5µm, 4.6 x 150mm column from Merck Sequant (Watford, UK), using Accela LC system with a mobile phase consisted of A: 20 mM ammonium carbonate and B: 100% acetonitrile as previously described in (134, 135). Compounds were separated by the following linear gradient: 20% A (0 min) to 95% A at 15 min to 20% A at 17 min and held to 24

min. A flow rate was 300 µl/min and an injection volume was 10 µl. Samples were maintained at 4 °C, and the column was maintained at 45 °C.

MS was performed on an Orbitrap Exactive MS (Thermo Fisher Scientific, Hemel Hempstead, UK) with ESI running in positive and negative ionisation modes. Briefly, spectra were acquired in full MS scan in the range of *m/z* 70-1400 and the resolution was 50,000 in both modes. The capillary and probe temperatures were maintained at 275 and 150 °C, respectively. The instrument calibration was performed by modified Thermo calibration mixture masses with inclusion of $C_2H_6NO_2$ (*m/z* 76.0393) for positive ion electrospray ionisation and $C_3H_5O_3$ (*m/z* 89.0244) for negative ion electrospray ionisation in order to extend the calibration mass range to small metabolites.

Data analysis and metabolite identification

Raw LC-MS data from the control group (untreated cells), the treatments groups (cells exposed to the different NPs), and reagent blanks were acquired using Xcalibur v2.1 software (Thermo Scientific, Hemel Hemstead UK), and processed with XCMS for untargeted peak-picking (208). Peak matching and related peaks annotation were performed using mzMatch (209) and noise filtering and putative metabolite identification were then carried out using IDEOM with the default parameters (210). Metabolites that were

matched with accurate masses and retention times of authentic standards were identified with Level 1 metabolite identification according to the metabolomics standards initiative (211, 212), but when standards were not available, metabolites were identified by employing predicted retention times considered as putative (Level 2 identification). Pooled QC samples were used to validate system suitability and stability (207). Multivariate data analysis was employed to assess changes in the cell metabolome between the control and each treatment group using orthogonal partial least squares discriminant analysis (OPLS-DA) using SIMCA-P v13.0.2 (Umetrics, Umea, Sweden) (213). In addition to the multivariate analysis, univariate one-way ANOVA was carried out using Metaboanalyst 3.0 (214). Mass ions with false discovery rate (FDR) less than 5 % and variable importance in projection scores (VIP) greater than one were selected as potential biomarkers. The lists of significantly altered metabolites were imported to Metaboanalyst 3.0 to visualise the affected metabolic pathways (215).

4.3 Results and discussion

A global LC-MS metabolic profiling approach was employed to study the effects of MTX and nanoparticles (NPs) with entrapped MTX on THP-1 derived macrophages and A549 cells respectively. Subtoxic concentrations of MTX (2μg/ml) and MTX loaded NPs with

equivalent amount of MTX, 92µg/ml), Figures 4-S1 and 4-S2. The NPs were readily uptaken by the cells, Figure 4-S3.

Using highly sensitive Orbitrap coupled LC-MS, a total of 408 and 773 different metabolites were identified in THP-1 and A549 cells respectively. These included amino acids, lipids, carbohydrates, nucleotides, cofactors and energy metabolism metabolites.

Metabolic alterations were assessed primarily by OPLS-DA where a clear separation between the tested groups was observed, and the two cell lines showed different responses to free MTX, MTX loaded NPs and unloaded 'blank' PLGA NPs. The OPLS-DA plot for THP-1 cells (Figure 4-1A) shows that the cells were sensitive to the treatment groups with NPs more than to free MTX, whereas MTX loaded NPs and blank PLGA NPs treated groups clustered close to each other. This implies that both MTX loaded and blank NPs affected the cells in a similar manner, even though MTX is a potent drug. This can be interpreted as a consequence of the phagocytic nature of THP-1 cells. The presence of NPs, which were of similar dimensions and charges to viral particles, might be expected to have activated strongly any phagocytosis processes and their accompanying metabolic changes (132) in ways that may have been analogous to those in processing exogenous small molecule components.

As expected, the proliferative A549 cells were more sensitive to MTX, where MTX treated groups were not separable (see Figure 4-

1B), despite the fact that one group was treated with free MTX and the other was exposed to MTX loaded PLGA NPs. This indicated that MTX loaded NPs caused similar metabolic alterations in A549 cells to those caused by free MTX.

Two-stage statistical analysis combining multivariate and univariate analysis was adopted to study further the key metabolites upon the different treatments to both cell lines. Metabolites responsible for the separation in the OPLS-DA models having VIP values greater than 1 were selected as changing metabolites. In addition, one way ANOVA was employed to enhance the statistical power of this study and the metabolites with FDR of <0.05 were further studied. Non-proliferative activated THP-1 macrophages were expected to tolerate MTX well because THP-1 cells lose their proliferative ability once activated into macrophages, and MTX exerts its effect during the S phase in cellular proliferation (252). Surprisingly free MTX resulted in a decrease in TCA cycle (2-oxoglutarate, citrate and cis-aconitate) and glycolytic activities (phosphoenolpyruvate, 3-phospho-D-glycerate and D-gluconic acid), as shown in Table 4-1. Energy metabolism has a main role in macrophage polarisation, which results in either M1 macrophages that encourage inflammation, or in M2 macrophages that suppress inflammation.

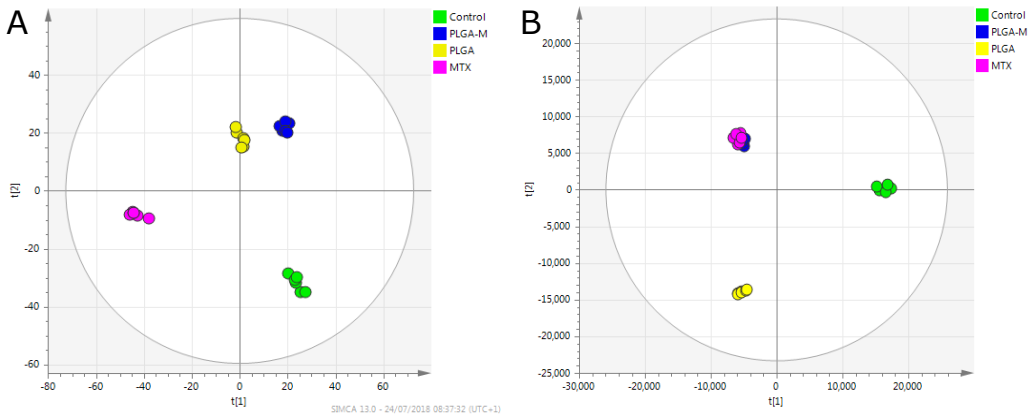


Figure 4-1: (A) OPLS-DA scores plots of THP-1 cells samples (R2X=0.616, R2Y=0.99 Q2=0.68, CV-ANOVA p-value 0.0083). (B) A549 cells samples (R2X=0.84, R2Y=0.98, Q2=0.82, CV-ANOVA p-value $1.7e^{-6}$) after 24 hrs treatment with free MTX, MTX loaded PLGA NPs and blank PLGA NPs. (the control group without any treatment).

It is well known that M1 polarisation depends on glycolysis and M2 polarisation relies on fatty acid oxidation (FAO) (253, 254). The drop in glycolysis and the absence of any signs of FAO hyperactivity (no significant decrease in carnitine or increase in acylcarnitine) suggest that the macrophage were not extensively polarised in these assays. In addition, downregulation of the TCA cycle results in depletion of ATP, which is essential for macrophage activation. These results suggest that impairing cellular energy production could be an important mechanism by which MTX controls the symptoms of RA by preventing macrophages polarisation to the inflammatory type M1. The pentose phosphate pathway is the main source of NADPH in the cell, and cellular redox homeostasis is maintained via NADPH which is used to recycle glutathione from its oxidised form.

Table 4-1: The most biologically relevant metabolites that were changed significantly in THP-1 and A549 cells after the treatment with free MTX and MTX loaded NPs, IDC: metabolite identification level according to the metabolomics standards initiative L1 – Level 1, L2 – Level 2. Colours in the table represent changes in metabolite levels, with blue indicating a decrease and red denoting and increase.

THP-1 cells

Mass	RT	FORMULA	Putative metabolite	IDC	MTX NPs	Free MTX
			Redox homeostasis			
307.0838	9.80	C10H17N3O6S	Glutathione	L1	1.01	0.65
612.1523	11.00	C20H32N6O12S2	Glutathione disulfide	L1	0.80	0.97
			Energy metabolism			
146.0215	10.32	C5H6O5	2-Oxoglutarate	L2	0.71	0.59
192.0270	11.72	C6H8O7	Citrate	L2	0.70	0.43
174.0164	11.29	C6H6O6	cis-Aconitate	L2	0.71	0.39
167.9823	11.42	C3H5O6P	Phosphoenolpyruvate	L1	1.02	0.43
			Nucleotide Metabolism			
286.0567	10.72	C7H15N2O8P	GAR	L2	17.12	8.20
308.0411	9.41	C9H13N2O8P	dUMP	L1	1017	705
228.0747	7.84	C9H12N2O5	Deoxyuridine	L2	7.88	9.20

A549 Cells

Mass	RT	FORMULA	Putative metabolite	IDC	MTX NPs	Free MTX
			Redox homeostasis and apoptotic markers			
307.0837	9.77	C10H17N3O6S	Glutathione	L1	0.72	0.74
306.0759	10.83	C20H32N6O12S2	Glutathione disulfide	L1	0.93	0.84
183.0661	10.15	C5H14NO4P	Choline phosphate	L1	0.64	0.84
103.0997	10.43	C5H13NO	Choline	L2	0.47	0.59
			Energy metabolism			
260.0297	10.46	C6H13O9P	Fructose 6-phosphate	L1	0.66	0.64
359.2670	5.51	C19H37NO5	2-Hydroxylauroylcarnitine	L2	2.29	2.03
259.1784	5.72	C13H25NO4	Hexanoylcarnitine	L2	2.09	2.17
397.3190	5.19	C23H43NO4	Hexadecenoylcarnitine	L2	1.96	2.32
425.3503	5.08	C25H47NO4	Elaidiccarnitine	L2	1.69	1.82
387.2983	5.49	C21H41NO5	Hydroxymyristoylcarnitine	L2	1.66	1.87
371.3034	5.28	C21H41NO4	Tetradecanoylcarnitine	L2	1.60	1.79
			Nucleotide Metabolism			
136.0384	8.89	C5H4N4O	Hypoxanthine	L1	0.81	1.42
267.0967	8.22	C10H13N5O4	Adenosine	L1	0.74	1.74
135.0545	8.64	C5H5N5	Adenine	L1	0.79	1.10
347.0630	9.46	C10H14N5O7P	AMP	L1	0.64	0.65
286.0565	10.56	C7H15N2O8P	GAR	L2	11.46	9.78

The results showed that administration of free MTX decreased the intracellular glutathione levels, this could be attributed to the drop in glucose metabolism, characterised by the depletion of gluconic

acid. Unexpectedly MTX loaded NPs did not affect the glycolytic activity, nor were the glutathione levels decreased.

Another distinct fingerprint difference between the two types of macrophages (M1 and M2) is arginine metabolism, whereby the first type converts arginine to nitric oxide, which endows macrophages with cytostatic or cytotoxic activity against microorganisms, and the second type converts arginine to ornithine which is an anabolic promoter of cell proliferation. Cells treated with free MTX showed higher levels of ornithine, potentially indicating an enhanced polarisation to an M2 anti-inflammatory macrophage phenotype. Metabolic profiling results also showed that free MTX had a greater impact on the metabolism of THP-1 cells in comparison to NPs loaded with MTX. In this case MTX suppressed glycolytic activity, disturbed redox homeostasis, decreased TCA cycle activity and altered nucleotide metabolism (see Table 4-1), while MTX loaded NPs changed only TCA cycle activity and nucleotide metabolism. The variations in effects on the cell lines likely arose due to the differences between the concentrations of MTX in the cytoplasm. In the case of the drug alone, MTX would have been rapidly available following internalisation, whereas the NPs loaded MTX would have been trapped in phagosomes and inaccessible during the initial stages in the cytoplasm, which is where all glycolytic activities take place. Over time, the phagosomes in macrophages fuse with lysosomes to

produce phagolysosomes which are rich in hydrolytic enzymes and reactive oxygen species. MTX in free drug form is susceptible to oxidative degradation (255) whereas MTX entrapped in a nanoparticle core would have been less accessible to oxidants. In addition, drug release kinetics have a grate impact on its activity, for instance, the release of physically entrapped drug inside carriers as best described as a burst release followed by slower release depending on drug diffusion or carrier degradation. In the present work, MTX release from PLGA NPs depends on both mechanisms, nevertheless, the burst release from MTX loaded PLGA NPs makes some of the MTX available in the free form which might makes the comparison between the two cases hard. Further effects on cell processes were apparent in terms of nucleotide metabolism, which was altered both by free MTX and MTX loaded NPs. Thymidine synthesis, which starts by reduction of uridine to deoxyuridine, followed by phosphorylation to produce dUMP and methylation by thymidylate synthase to produce thymidine monophosphate was reduced. This occurred via suppression of thymidylate synthase by MTX, and as a result, the levels of deoxyuridine and dUMP were higher in MTX and MTX loaded NPs treated groups in comparison to the control groups. Secondly, de novo purine synthesis was also suppressed by both treatments, in particular, the third step where the enzyme phosphoribosylglycinamide formyltransferase (GART) catalyses the

formation of 5'-phosphoribosyl-N-formylglycinamide (FGAR) from 5'-phosphoribosyl-glycinamide (GAR) resulting in accumulation of GAR, (see Figure 4-2).

A549 cells showed early signs of apoptosis upon treatment with free MTX and MTX loaded NPs. The levels of choline, phosphocholine, and glutathione were lower compared to the untreated groups. Similar changes have been reported in apoptotic cells (256-258), accompanied by increased fatty acid oxidation (FAO). The levels of several acylcarnitines i.e. hexadecanoyl-carnitine, O-hexanoyl-carnitine, palmitoyl-carnitine and 2-hydroxylauroylcarnitine, were higher in the MTX treated groups (see Table 4-1). A shift toward FAO can occur during energy crisis, when cells cannot produce enough ATP from glucose metabolism, or to survive oxidative stress (259). Cancer cells generally prefer glucose metabolism to harness energy rapidly, in a process known as the Warburg Effect (260) but also recycle glutathione from its oxidised form in order to retain cellular redox homeostasis. Free MTX and MTX loaded NPs treated groups showed a decrease in glutathione, suggestive of oxidative stress mechanisms. Indeed, MTX has previously been reported to exert a cytotoxic effect by inducing oxidative stress (261) and this could explain the upregulation of FAO observed. In contrast to the effects in THP-1 cells, treating the cancer cells with MTX-loaded NPs induced more metabolic changes than when free MTX was administered. A549

cells treated with MTX-loaded NPs showed depletion in hypoxanthine, adenine, adenosine and AMP, which are four consecutive metabolites in the purine metabolism pathway. In addition, an increased GAR level indicated suppression in purine metabolism. On the other hand, free MTX resulted in depletion of AMP only, and an increase in GAR. The degree of purine synthesis inhibition could thus be considered as a measure for the potency of MTX inside the cells. The increased activity of the MTX-loaded NPs could, as noted earlier, be attributed to the fact that the NPs entered the cells via passive endocytosis, allowing higher uptake compared to the RFC-mediated transport of MTX alone (49).

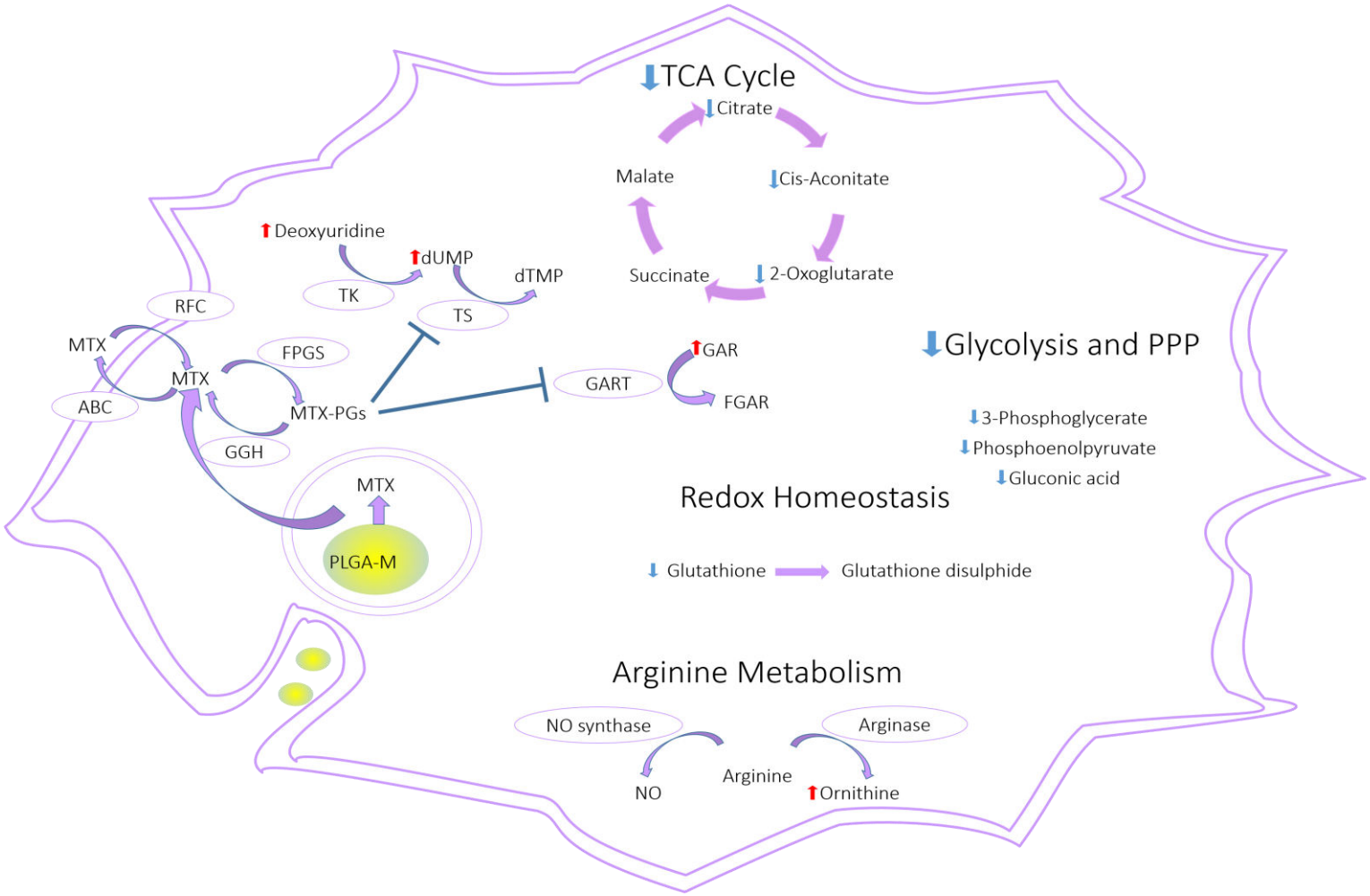


Figure 4-2: Overview of the affected pathways in the THP-1 cells after treatment with the free MTX and MTX loaded NPs. Red arrow = increased, blue arrow = decreased, Methotrexate enters the cell mainly via reduced folate carrier (RFC). Folylpolyglutamyl synthetase (FPGS) catalyses the polyglutamation of MTX to produce MTX polyglutamates (MTX-PGs). MTX-PGs are better retained intracellularly than MTX because they are not susceptible to the ATP-binding cassette (ABC) that is responsible for MTX efflux. MTX-PGs have higher affinity than MTX to thymidylate synthetase (TS) and phosphoribosylglycinamide formyltransferase (GART). Deoxyuridine-5-monophosphate (dUMP), deoxythymidine monophosphate (dTMP), 5'-phosphoribosyl-glycinamide (GAR), 5'-phosphoribosyl-N-formylglycinamide (FGAR) and nitric oxide (NO)

4.4 Conclusion

In this study, THP-1 derived macrophages and A549 lung carcinoma cells were exposed to subtoxic concentrations of free MTX and MTX loaded NPs, and global metabolic profiling was performed. The results showed that free MTX had higher impacts on the metabolome than MTX-loaded NPs in THP-1 derived macrophages. In these cells, MTX induced oxidative stress, a drop in glycolytic activity, reduction in the TCA cycle, and inhibition of nucleotide metabolism. In contrast, the effects of MTX-loaded NPs were limited to alteration of nucleotide metabolism and inhibition of TCA cycle. In comparison, A549 cancer cells were more susceptible to MTX-loaded NPs than to the free drug, in terms of purine synthesis suppression, which we suggest was linked to the different entry mechanisms for nanoparticles compared to free MTX, and lack of efflux pumps for the NPs. We believe the presented work shows that metabolomics is a valuable analytical technique that can be used to understand mechanisms of action of drugs and formulations in various clinically important cell lines.

4.5 Supporting information

Table 4-S1: Size and zeta potential of the blank and MTX loaded NPs.

Type of NPs	Mean Diameter (nm)	Zeta potential (mv)
Blank NPs	120 ± 1.4	-46.7 ± 2.5
MTX NPs	129 ± 2.0	-27.1 ± 3.3

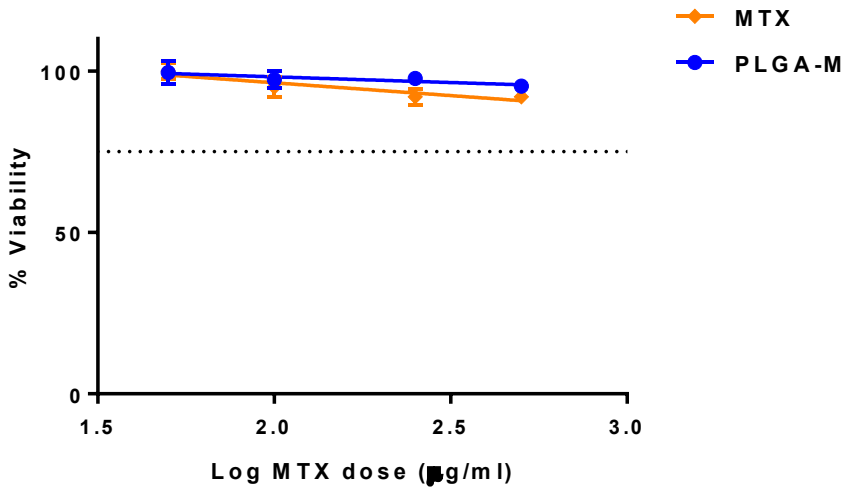


Figure 4-S1: Viability of activated THP-1 macrophages following exposure to free and polymer encapculated methotrexate for 24 hrs.

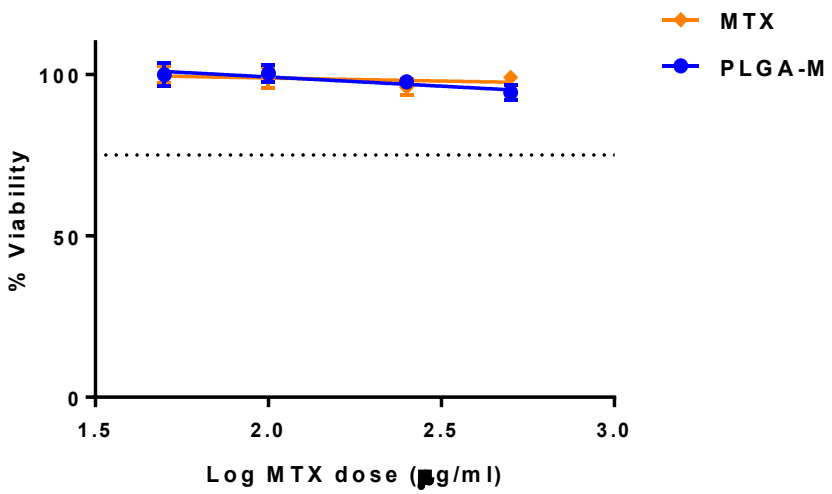


Figure 4-S2: Viability of A549 cells following exposure to free and polymer encapculated methotrexate for 24 hrs.

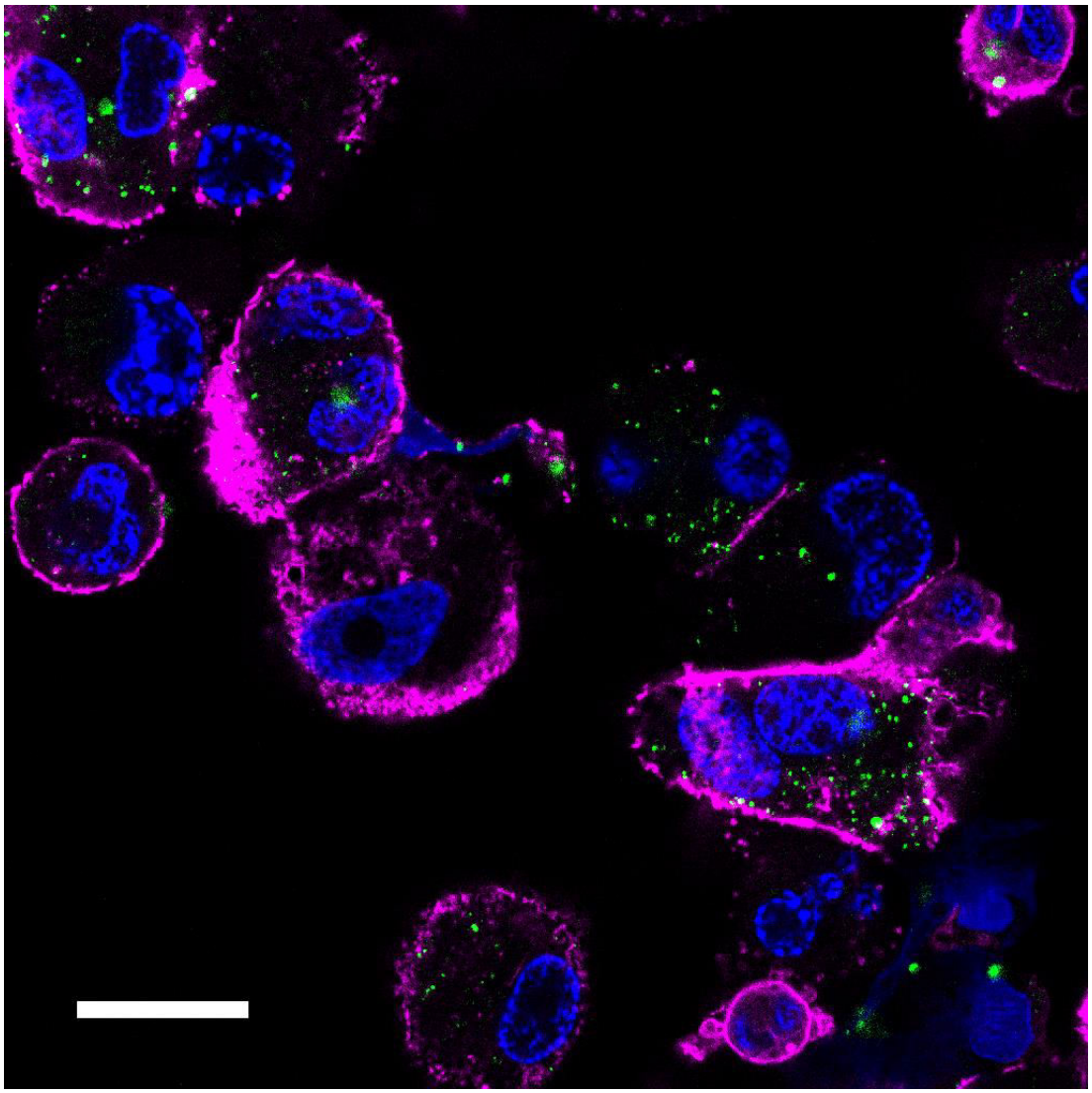


Figure 4-S4-3: Super-resolution microscopy images of methotrexate loaded PLGA nanoparticles (green) (92 µg/mL, 3 hrs) in A) THP-1 derived macrophages and B) A549 cells. Cells were fixed and stained for cytoskeleton (Alexafluor 647, magenta) and nucleus (Hoechst nucleus, blue). Scale bar = 20 µm.

Table 4-S1: The metabolites that were changed significantly in THP-1 derived macrophages after the treatment with free and polymer-encapsulated methotrexate, IDC: metabolite identification level according to the metabolomics standards initiative L1 – Level 1, L2 – Level 2. Colours in the table represent changes in metabolite levels with blue indicating a decrease and red denoting an increase.

Mass	Polarity	Mass error (ppm)	RT	FORMULA	Putative metabolite	IDC	Map	Control	MTX	MTX NPS
109.0198	+	0.467	11.13	C2H7NO2S	Hypotaurine	L2	Amino Acid Metabolism	1.00	0.67	0.86
118.0267	-	0.806	10.12	C4H6O4	Succinate	L1	Carbohydrate Metabolism	1.00	1.27	1.43
125.0589	+	-0.37	11.71	C5H7N3O	5-Methylcytosine	L2	Nucleotide Metabolism	1.00	1.05	1.13
131.0946	+	-0.44	9.31	C6H13NO2	Leucine	L1	Amino Acid Metabolism	1.00	0.77	0.81
132.0534	+	-0.75	8.85	C4H8N2O3	N-Carbamoylsarcosine	L2	Amino Acid Metabolism	1.00	1.58	1.26
132.0899	+	-0.26	16.12	C5H12N2O2	Ornithine	L1	Amino Acid Metabolism	1.00	1.59	1.05
136.0384	+	-0.93	8.98	C5H4N4O	Hypoxanthine	L1	Nucleotide Metabolism	1.00	2.65	0.62
141.0191	-	0.373	10.88	C2H8NO4P	Ethanolamine phosphate	L1	Amino Acid Metabolism	1.00	0.95	1.25
145.0851	+	-0.45	11.32	C5H11N3O2	4-Guanidinobutanoate	L2	Amino Acid Metabolism	1.00	0.81	1.00
146.0691	+	-0.67	10.94	C5H10N2O3	Glutamine	L1	Amino Acid Metabolism	1.00	0.95	0.94
148.0372	-	0.589	10.1	C5H8O5	2-Hydroxyglutarate	L1	Amino Acid Metabolism	1.00	0.61	0.82
149.051	+	-0.8	9.43	C5H11NO2S	Methionine	L1	Amino Acid Metabolism	1.00	0.82	0.86
155.0695	+	-0.23	11.18	C6H9N3O2	Histidine	L2	Amino Acid Metabolism	1.00	0.84	0.85
158.0439	-	-0.12	10.86	C4H6N4O3	Allantoin	L1	Nucleotide Metabolism	1.00	0.87	0.85
159.126	+	0.076	5.65	C8H17NO2	FA amino(8:0)	L2	Lipids: Fatty Acyls	1.00	1.54	1.29
161.0687	+	-0.65	9.04	C6H11NO4	O-Acetyl-L-homoserine	L2	Amino Acid Metabolism	1.00	0.46	0.73
163.0481	-	0.456	8.67	C5H9NO5	L-erythro-4-Hydroxyglutamate	L2	Amino Acid Metabolism	0.00	0.00	11.79
165.079	+	-0.29	8.64	C9H11NO2	Phenylalanine	L2	Amino Acid Metabolism	1.00	0.83	0.78
169.0044	-	0.063	10.91	C3H7NO5S	L-Cysteate	L1	Amino Acid Metabolism	1.00	0.73	0.82
174.0791	+	-1.34	7.25	C10H10N2O	Indole-3-acetamide	L2	Amino Acid Metabolism	1.00	0.32	0.52

175.0633	+	-0.47	4.49	C10H9NO2	5-Hydroxyindoleacetaldehyde	L2	Amino Acid Metabolism	1.00	0.90	0.58
175.0957	+	-0.53	11.4	C6H13N3O3	Citrulline	L1	Amino Acid Metabolism	1.00	0.88	0.94
181.074	+	0.473	10.21	C9H11NO3	Tyrosine	L1	Amino Acid Metabolism	1.00	0.88	0.82
188.1273	+	-0.33	18.52	C7H16N4O2	Homoarginine	L2	Amino Acid Metabolism	1.00	1.19	0.93
189.1	-	0.228	5.43	C8H15NO4	2 -(Butylamido)-4-hydroxybutanoic acid	L2	-	1.00	1.11	81.74
203.1157	+	-0.56	8.95	C9H17NO4	O-Acetylcarnitine	L1	Amino Acid Metabolism	1.00	0.40	0.44
208.0848	+	-0.5	9.22	C10H12N2O3	Kynurenine	L1	Amino Acid Metabolism	1.00	0.86	0.81
215.0559	-	0.649	11.08	C5H14NO6P	sn-glycero-3-Phosphoethanolamine	L2	Lipid Metabolism	1.00	0.70	0.81
231.1471	+	-0.47	7.92	C11H21NO4	O-Butanoylcarnitine	L1	Lipids: Fatty Acyls	1.00	0.55	0.69
257.103	+	0.06	10.51	C8H20NO6P	sn-glycero-3-Phosphocholine	L1	Lipid Metabolism	1.00	0.87	0.79
259.1784	+	-0.56	7.29	C13H25NO4	O-hexanoyl-R-carnitine	L2	Lipids: Fatty Acyls	1.00	0.47	0.45
264.1045	+	-0.4	18.46	C12H16N4OS	Thiamin	L2	Metabolism of Cofactors and Vitamins	1.00	0.92	0.79
278.1519	-	0.989	4.26	C16H22O4	Alpha-CEHC	L2	-	1.00	0.77	0.86
299.2824	+	-0.67	6.21	C18H37NO2	FA (16:2)	L2	Lipids: Fatty Acyls	1.00	0.94	1.19
324.0361	-	1.312	10.05	C9H13N2O9P	UMP	L1	Nucleotide Metabolism	1.00	1.07	1.11
384.1217	+	-0.2	10.15	C14H20N6O5S	Adenosyl-L-homocysteine	L2	Amino Acid Metabolism	1.00	1.16	1.29
425.3505	+	-0.37	5.14	C25H47NO4	Elaidiccarnitine	L2	-	1.00	0.49	0.49
427.3662	+	-0.32	5.11	C25H49NO4	Stearoylcarnitine	L2	-	1.00	0.51	0.61
479.3011	+	-0.39	5.04	C23H46NO7P	PE (18:1)	L2	Lipids: Glycerophospholipids	1.00	1.30	1.11
523.291	-	1.192	4.39	C24H46NO9P	PS (18:1)	L2	Lipids: Glycerophospholipids	1.00	1.41	1.06
593.575	-	1.884	4.57	C38H75NO3	SP (20:0)	L2	Lipids: Sphingolipids	1.00	1.87	1.46
619.59	+	-0.32	4.53	C40H77NO3	Cer(d-40:2)	L2	Lipids: Sphingolipids	1.00	1.26	1.04
673.5045	+	0.019	4.56	C37H72NO7P	PE(P-32:1)	L2	Lipids: Glycerophospholipids	1.00	0.77	0.98
729.5309	+	0.136	4.73	C40H76NO8P	PC(32:2)	L2	Lipids: Glycerophospholipids	1.00	0.78	1.00
733.5628	+	0.978	4.72	C40H80NO8P	PC(32:0)	L2	Lipids: Glycerophospholipids	1.00	0.93	1.19
759.5774	+	-0.58	4.7	C42H82NO8P	PC(34:1)	L2	Lipids: Glycerophospholipids	1.00	0.85	1.03

776.5571	-	1.592	4.22	C42H81O10P	PG(36:1)	L2	Lipids: Glycerophospholipids	1.00	0.70	1.18
787.609	+	-0.23	4.7	C44H86NO8P	PC(36:1)	L2	Lipids: Glycerophospholipids	1.00	0.85	0.99
820.5258	-	1.093	4.07	C46H77O10P	PG(40:7)	L2	Lipids: Glycerophospholipids	1.00	0.78	0.83
879.5838	+	-0.06	4.17	C45H86NO13P	PI (36:0)	L2	Lipids: Glycerophospholipids	1.00	1.02	0.87
883.535	+	-1.65	4.07	C50H78NO10P	PS(44:10)	L2	Lipids: Glycerophospholipids	1.00	0.90	1.00

Table 4-S2: The metabolites that were changed significantly in A549 cells after the treatment with free and polymer-encapsulated methotrexate, IDC: metabolite identification level according to the metabolomics standards initiative L1 – Level 1, L2 – Level 2. Colours in the table represent changes in metabolite levels with blue indicating a decrease and red denoting an increase.

Mass	Polarity	Mass error (ppm)	RT	FORMULA	Putative metabolite	IDC	Map	Control	MTX	MTX NPs
89.0477	+	-1.619	11.19	C3H7NO2	Alanine	L1	Amino Acid Metabolism	1	1.06	1.03
103.0633	+	-2.095	11.18	C4H9NO2	4-Aminobutanoate	L2	Amino Acid Metabolism	1	0.68	0.62
105.0426	+	-1.48	6.03	C3H7NO3	2-Amino-3-hydroxypropanoic acid	L2	Lipids: Fatty Acyls	1	1.16	1.03
105.079	+	-1.534	15.28	C4H11NO2	Diethanolamine	L2	Lipid Metabolism	1	0.27	0.19
109.0198	+	-1.41	11.04	C2H7NO2S	Hypotaurine	L2	Amino Acid Metabolism	1	0.9	0.97
113.0589	+	-1.32	8.59	C4H7N3O	Creatinine	L2	Amino Acid Metabolism	1	1.14	1.11
117.0538	+	-1.97	11.64	C3H7N3O2	Guanidinoacetate	L1	Amino Acid Metabolism	1	1.13	1.03
127.0382	+	-1.162	9.12	C4H5N3O2	5-Amino-4-imidazole carboxylate	L2	Nucleotide Metabolism	0	94.12	103.21
129.079	+	-1.539	7.22	C6H11NO2	N4-Acetylaminobutanal	L2	Amino Acid Metabolism	1	0.79	0.77
131.0583	+	-1.449	10.75	C5H9NO3	L-Glutamate 5-semialdehyde	L2	Amino Acid Metabolism	1	0.71	0.69
131.0583	+	-1.424	5.57	C5H9NO3	N-Acetyl-beta-alanine	L2	Amino Acid Metabolism	1	1.12	1.23
131.0695	+	-1.542	10.94	C4H9N3O2	Creatine	L1	Amino Acid Metabolism	1	1.01	0.9
132.0899	+	-1.856	16.19	C5H12N2O2	L-Ornithine	L1	Amino Acid Metabolism	1	1.46	1.28
145.0739	+	-1.792	5.64	C6H11NO3	4-Acetamidobutanoate	L2	Amino Acid Metabolism	1	0.44	0.37
145.0851	+	-2.031	11.25	C5H11N3O2	4-Guanidinobutanoate	L2	Amino Acid Metabolism	1	1.02	0.92

146.0691	+	-2.163	10.85	C5H10N2O3	Glutamine	L1	Amino Acid Metabolism	1	2.06	2.22
146.1054	+	-2.359	17.25	C6H14N2O2	Lysine	L2	Amino Acid Metabolism	1	1.39	1.25
147.0531	+	-1.988	9.99	C5H9NO4	Glutamate	L2	Amino Acid Metabolism	1	1.77	1.54
161.0688	+	-1.865	8.95	C6H11NO4	O-Acetyl-L-homoserine	L2	Amino Acid Metabolism	1	0.27	0.21
169.0504	+	-2.021	9.73	C4H12NO4P	Phosphodimethylethanolamine	L2	Lipid Metabolism	1	0.79	0.71
174.1117	+	-1.571	18.34	C6H14N4O2	Arginine	L1	Amino Acid Metabolism	1	1.41	1.21
175.0634	+	-1.673	4.37	C10H9NO2	5-Hydroxyindoleacetaldehyde	L2	Amino Acid Metabolism	1	1.74	1.66
179.0795	+	-1.268	10.39	C6H13NO5	Glucosamine	L2	Carbohydrate Metabolism	1	1.46	1.49
181.074	+	-1.151	10.19	C9H11NO3	Tyrosine	L1	Amino Acid Metabolism	1	1.38	1.24
183.0661	+	-1.574	10.15	C5H14NO4P	Choline phosphate	L1	Lipid Metabolism	1	0.84	0.64
193.0741	+	-0.91	5.04	C10H11NO3	Phenylacetylglycine	L2	Amino Acid Metabolism	1	1.36	1.31
203.1157	+	-1.933	8.85	C9H17NO4	O-Acetylcarnitine	L1	Amino Acid Metabolism	1	0.68	0.72
204.0899	+	-1.895	9.68	C11H12N2O2	Tryptophan	L1	Amino Acid Metabolism	1	0.86	0.78
211.0357	+	-2.163	10	C4H10N3O5P	Phosphocreatine	L2	Amino Acid Metabolism	1	0.89	0.68
217.1313	+	-2.242	8.28	C10H19NO4	O-Propanoylcarnitine	L2	Lipids: Fatty Acyls	1	0.72	0.6
257.1028	+	-2.086	10.43	C8H20NO6P	sn-glycero-3-Phosphocholine	L1	Lipid Metabolism	1	0.66	0.5
262.0888	+	-2.115	7.43	C12H14N4OS	Thiamine aldehyde	L2	Metabolism of Cofactors and Vitamins	1	2.17	2.11
264.1044	+	-2.209	18.82	C12H16N4OS	Thiamin	L2	Metabolism of Cofactors and Vitamins	1	0.86	0.98
297.0895	+	-2.202	7.24	C11H15N5O3S	5'-Methylthioadenosine	L1	Amino Acid Metabolism	1	1.24	1.14
304.2401	-	-2.723	4.12	C20H32O2	FA (20:4)	L2	Lipids: Fatty Acyls	1	2.26	1.07
307.0837	+	-2.296	9.77	C10H17N3O6S	Glutathione	L2	Amino Acid Metabolism	1	0.74	0.72
371.3034	+	-2.105	5.28	C21H41NO4	Tetradecanoylcarnitine	L2	-	1	1.79	1.6
397.319	+	-1.963	5.19	C23H43NO4	Hexadec-2-enoylcarnitine	L2	-	1	2.32	1.96
399.3347	+	-2.01	5.15	C23H45NO4	O-Palmitoyl-R-carnitine	L2	Lipids: Fatty Acyls	1	2.14	1.84
425.3503	+	-1.936	5.08	C25H47NO4	Elaidiccarnitine	L2	-	1	1.82	1.69
437.2903	-	-2.645	4.99	C21H44NO6P	PE (16:1)	L2	Lipids: Glycerophospholipids	1	1.57	1.24
467.301	+	-1.636	5.31	C22H46NO7P	PC (14:0)	L2	Lipids: Glycerophospholipids	1	2.07	1.57
479.301	+	-1.707	4.97	C23H46NO7P	PE (18:1)	L2	Lipids: Glycerophospholipids	1	1.7	1.32
481.3531	+	-1.439	5.23	C24H52NO6P	PC (16:2)	L2	Lipids: Glycerophospholipids	1	1.55	1.1

493.3165	+	-1.818	5.23	C24H48NO7P	PC (16:1)	L2	Lipids: Glycerophospholipids	1	2.13	1.51
495.3322	+	-1.689	5.18	C24H50NO7P	PC (16:0)	L2	Lipids: Glycerophospholipids	1	2.05	1.48
507.3687	+	-1.439	5.13	C26H54NO6P	PC (18:1)	L2	Lipids: Glycerophospholipids	1	1.55	1.09
519.3328	+	-0.408	5.15	C26H50NO7P	PC (18:2)	L2	Lipids: Glycerophospholipids	1	2.95	2.17
537.5117	-	-2.498	4.5	C34H67NO3	SP (16:0)	L2	Lipids: Sphingolipids	1	1.47	1.54
721.5042	+	-1.725	4.43	C41H72NO7P	PE(P-36:4)	L2	Lipids: Glycerophospholipids	1	1.3	1.29
723.5199	+	-1.616	4.44	C41H74NO7P	PE(P-36:4)	L2	Lipids: Glycerophospholipids	1	1.36	1.29
743.5464	+	-1.349	4.51	C41H78NO8P	PE(36:2)	L2	Lipids: Glycerophospholipids	1	1.46	1.26
747.5199	+	-1.714	4.42	C43H74NO7P	PE (38:7)	L2	Lipids: Glycerophospholipids	1	1.3	1.25
765.5308	+	-1.376	4.43	C43H76NO8P	PE(38:5)	L2	Lipids: Glycerophospholipids	1	1.32	1.36
767.5464	+	-1.525	4.44	C43H78NO8P	PE(38:4)	L2	Lipids: Glycerophospholipids	1	1.33	1.34
771.6139	+	-1.712	4.66	C44H86NO7P	PC (36:1)	L2	Lipids: Glycerophospholipids	1	1.24	0.98
787.5359	-	-2.214	4.09	C42H78NO10P	PS(36:2)	L2	Lipids: Glycerophospholipids	1	0.96	0.9
787.6085	+	-2.266	4.73	C44H86NO8P	PC(36:1)	L2	Lipids: Glycerophospholipids	1	1.29	1.09
807.5776	+	-1.793	4.57	C46H82NO8P	PC(38:5)	L2	Lipids: Glycerophospholipids	1	1.38	1.27
809.5936	+	-1.318	4.58	C46H84NO8P	PC(38:4)	L2	Lipids: Glycerophospholipids	1	1.33	1.18
883.536	+	-2.269	3.95	C50H78NO10P	PS(44:10)	L2	Lipids: Glycerophospholipids	1	1.32	1.19

Chapter five

Investigating the molecular effects of hyperbranched polycation-DNA complexes on lung cancer cells using LC-MS-based metabolite profiling

5.1 Introduction

Gene therapy is a promising approach for addressing both hereditary and acquired diseases. However, the clinical applications of this approach are still limited because of the difficulties in delivery of therapeutic nucleic acids (262-265). Viral vectors, although they are efficient, have serious safety issues and technical drawbacks, which have focused more attention to non-viral carriers (263, 266-268). In this context, cationic polymers have emerged as attractive gene delivery systems; they are easy to functionalise and cheap to scale up, however many of them are cytotoxic (269-273).

Over the last two decades, a large number of cationic polymers have been designed and investigated to develop efficient gene vectors with special emphasis on toxicity issue (274-276). However, the toxicity of these polymers has been routinely evaluated in *in vitro* cell culture based on simple cell viability assays, such as MTT and LDH (113, 114). These methods, although they are fast and appropriate for routine toxicity assessment, have several limitations and do not provide sufficient information on potential mechanisms of cell toxicity to inform the design of new polymeric materials (119). Also, these assays give indications of the crude toxicity of materials but not the safety of these materials at subtoxic

concentrations. In some cases, mechanistic studies have been applied to understand the toxic effects of cationic polymers and their complexes with nucleic acids (277-279), however, these studies have generally relied on limited conventional toxicity assays which are expensive and time-consuming. Hence, there is a practical incentive to establish comprehensive and reliable toxicity assessment methods that can be applied to evaluate safety of drug delivery materials in general (280). In this regard, metabolomics can be considered as a promising tool that could fulfil the requirements for in depth nanotoxicology investigations. This approach traces the changes in metabolites levels present in biological samples in response to external stimuli and can afford deep understanding of the molecular mechanisms of toxicity (280, 281). Metabolomics provides qualitative and quantitative measurements of small biomolecules like sugars, amino acids, nucleotides, etc., which are the end products of genetic translation processes. The very large number of detected metabolites in these types of analysis provides a comprehensive view about the intracellular functions and can create a chemical map of the affected pathways in the cells, which reflects the impact of a xenobiotic, such as an applied cationic polymer, and its potential toxicity (282, 283).

Polylysine, PEI and their derivatives are among the most studied cationic polymers for gene delivery. Apart from the variation in their transfection efficiency, several studies indicated that they share some similar manifestations of cytotoxicity (277, 278). They interact with, and induce plasma membrane damage in, the early stage of exposure, and can provoke programmed cellular death (apoptosis) through destabilisation of mitochondrial membranes and release of cytochrome C, as a late stage of toxicity (284). Furthermore, it has been reported that the cytotoxicity of these polycations is highly related to their architectures (279, 285). Considering that the branched forms of polylysine and PEI showed a better transfection efficiency in comparison with the linear forms, they would be interesting candidates for metabolomics studies. Also, thermally polymerised hyperbranched polymers have attracted our interest for their advantages over dendritic polymers in terms of applicability and feasibility for manufacturing and scale up, and because the impact of these polymers and their polyplexes at the cellular and molecular level is not fully understood (24, 285). In the present work, a global metabolic profiling approach was employed to study the effect of hyperbranched polylysine (hb-polyK), hyperbranched polylysine-co-histidine (hb-polyKH2) and branched polyethyleneimine (PEI) polyplexes with plasmid DNA on two

lung carcinoma cell lines (A549 and H1299). These two cell lines were chosen as they are initial targets for local administration and inhalation in cancer therapy. In addition, these cell lines showed unexpected variations in their responses to gene delivery complexes in terms of uptake and transfection (24), thus an evaluation of their metabolomics profiles was expected to enhance our understanding of the intracellular behaviour of the polyplexes and their potential toxicity at sub-toxic concentrations.

5.2 Materials and methods

5.2.1 Materials

Hyperbranched polylysine, hyperbranched polylysine-co-histidine, and their FITC-labelled forms were prepared and characterised as described previously (24). Branched polyethyleneimine (25 kDa), methylthiazolyldiphenyl-tetrazolium bromide (MTT), annexin V-FITC/PI apoptosis detection kit, N-acetylcysteine (NAC) and all buffers were purchased from Sigma-Aldrich. Cytotoxicity Detection Kit^{PLUS} (for LDH) was obtained from Roche. Luciferase reporter plasmid (gWiz-Luc) from Aldevron and Luciferase assay kit were purchased from Promega Corporation. Label IT® Cy^{TM}3 Labeling Kit was abtained from Mirus. All routine cell culture

materials were purchased from Sigma-Aldrich. Fisher Scientific provided Trypan blue 0.4% and all HPLC/LC-MS grade solvents.

5.2.2 Preparation of polyplexes

The complexes of the polymers with plasmid DNA were prepared in 10 mM HEPES buffer of pH 7.4. Aliquots of similar volumes and required concentrations, to prepare the desired N/P ratios, of polymers and plasmid DNA solutions were mixed and vortexed for 10 sec. Then, the polyplexes were left for 30 min before used in the experiments. The N/P ratios, the charge ratio, were calculated based on the results of fluorescamine assay and all the physicochemical characterisations were as previously described (24).

5.2.3 Cell culture

A549 (human adenocarcinomic alveolar basal epithelial, ATCC® CCL-185™) and H1299 (human non-small cell lung carcinoma, ATCC® CRL-5803™) cells were cultured in DMEM and RPMI media respectively, supplemented with 10% FBS and 1% L-glutamic acid, in a humidified atmosphere containing 5% CO_2. The cells were used at passage number between 30-40.

5.2.4 Metabolic activity (MTT) assay.

In 100 µl of fully supplemented medium, A549 and H1299 cells were seeded on 96-well plates at density of 25 x 10^3 cell/cm^2. After 24 hrs, the cells were washed with PBS and treated with polyplexes (at different N/P ratios) suspended in 100 µl of FBS free medium to a concentration of plasmid of 2 µg/ml for 4 hrs. Then, the culture media were replaced with fresh fully supplemented media and the cells were incubated for additional 24 hrs. 25 µl/well of MTT reagent (5mg/ml in PBS) was directly added to the cells and incubated for 3 hrs. Thereafter, the cells were washed with PBS, 150 µl of DMSO was added and the metabolic activity was determined by measuring the absorbance at 570 nm using cells treated with FBS free media and Triton 0.2% as a positive and negative control respectively. The following equation was used to calculate the percentage of metabolic activity:

Metabolic activity (%)= S-T / C-T x 100

Where S is the absorbance obtained with the tested samples, T is the absorbance observed with Triton, and C is the absorbance observed with the FBS free media treated cells.

5.2.5 Lactate dehydrogenase (LDH) detection assay

On 96-well plates, A549 and H1299 cells were seeded at density of 25 x 10^3 cell/cm^2 and cultured in 100 µl of media

for 24 hrs. Then, the cells were washed, treated with polyplexes at different N/P ratios (final concentration of plasmid DNA was 2 µg/ml in FBS-free media) and incubated for 4 hrs. After that, 50 µl aliquots of the treatment media were taken, mixed with 50 µl LDH reagent and allowed the reaction to conduct at room temperature for 20-30 minutes before adding the stop solution, 5 µl. The released LDH was detected by measuring the absorbance at 490 nm using cells treated with Triton 0.2% and FBS free medium as controls. The percentage of released LDH was calculated using the following equation:

Released LDH (%)= S-C / T-C x 100

Where S is the absorbance obtained with the tested samples, T is the absorbance observed with Triton, and C is the absorbance observed with the FBS free media treated cells.

5.2.6 Annexin-V/PI apoptosis assay

On 24-well plates, A549 and H1299 cells were seeded at density of 25 x 10^3 cell/cm^2 and cultured in 500 µl of fully supplemented medium for 24 hrs. Then, the cells were washed, incubated for 4 hrs in FBS-free medium with the polyplexes at N/P ratios of 10 and concentration equivalent to 2 µg/ml of plasmid DNA. After the incubation period, the treatment medium was replaced with fully supplemented

medium and the cells were incubated for further 24 hrs. Thereafter, the culture medium was collected into labelled FACS tubes on ice (4 °C), the cells were detached (using trypsin/EDTA solution for 5 min) and collected together with their corresponding culture medium. The cells were centrifuged, re-suspended in 100 µL of 1X annexin V binding buffer, treated with 2.5 µL annexin-V FITC and 1 µL of 100 µg/mL PI solutions (from ThermoFisher), and incubated in the dark for 15 min. Then, the samples were diluted with 1X binding buffer to 500 µl and analysed using a Beckman Coulter FC-500 flow cytometer. The data were processed using Kaluza 1.5 software.

5.2.7 *In vitro* Transfection study

Both cell lines were seeded on 24-well plates at a density of 25 x 10^3 cell/cm^2 and incubated in 500 µl of fully supplemented medium for 24 hrs. Then, the cells were washed with PBS, covered with 500 µl of FBS-free media, and treated with gWiz-Luc polyplexes of N/P ratio of 10 at concentration of 2 µg/ml of plasmid. After 4 hrs, the transfection medium was replaced with fully supplemented medium and the cells incubated for further 24 hrs. After that, the cell washed with PBS and the expression of luciferase was detected by luciferase assay kit. The effect of NAC on the

transfection efficiency was studied by adding NAC at a concentration of 5 mM into the culture medium before for 1 hr and after the treatment with the polyplexes for 24 hrs with keep the period of treatment with polyplexes free from NAC.

5.2.8 Cellular uptake study

Polyplexes were prepared using FITC-labelled polymers and Cy3-labelled plasmid DNA for study the cellular uptake and internalisation. For confocal microscopy, A549 and H1299 cells were seeded into 8-well chamber slides (obtained from Ibidi) at a seeding density of 1 x 10^4 cell/cm^2 in 300 µl of fully supplemented medium. After 24 hrs, the cells were washed with PBS, covered with 300 µl of FBS-free media, and treated with labelled polyplexes of N/P ratio of 10 at concentration of 2 µg/ml of DNA for 4 hrs. Then, the cells were washed with PBS three times, fixed with 4% paraformaldehyde for 15 minutes, stained with DRAQ5 (20 µM in PBS for 5 minutes), and covered with mounting medium. In the case of flow cytometry, the cells were prepared in conditions similar to the transfection experiment. After incubation of cells with labelled polyplexes for 4 hrs, the cells were washed with PBS three times and detached from the plates using trypsin solution for 5 minutes at 37C. Then, the cells were collected, centrifuged, and re-suspended in 0.3ml of PBS in FACS tubes. Thereafter,

the samples mixed with 150 µl of 0.4% trypan blue and measured using Astrios flow cytometer from Beckman Coulter Life Sciences.

5.2.9 Metabolomic analysis

Incubation of polyplexes with cells and metabolite extraction

The assay times and cell treatments with the polyplexes were based on those shown to be efficient for transgene expression in our previous experiments with polymer/DNA complexes in A54 and H1299 cells. Both cell lines were seeded on T25 flasks (6 replicate for each condition) at a density of 25 x 10^3 cell/cm^2 and incubated in 5 ml of fully supplemented medium for 24 hrs. Then, the cells were washed with PBS, covered with 5 ml of serum free medium, and treated with polyplexes of N/P ratio of 10 at a concentration of 2 µg/ml of plasmid DNA. After 4 hrs, aliquots were taken from the transfection medium and the medium replaced with fully supplemented medium. The cells were incubated for a further 24 hrs and aliquots from the medium were taken. Then, after removing the medium, the cells were washed briefly once with pre-warmed PBS at 37 °C. The cellular metabolism was quenched, and the metabolites were extracted simultaneously by adding 0.5 mL of methanol (−48 °C), cell handling after quenching was performed on ice. The cells were then scraped and

transferred to precooled fresh tubes at 4 °C. Cell solution was vortexed vigorously for 1 h at 4 °C and centrifuged at 17000 × *g* for 10 min at 4 °C. After the centrifugation, the supernatant was removed and dried under vacuum at room temperature. The metabolite extract was reconstituted using 70 µl of pre-cooled methanol (4 °C). 10 µL aliquots were taken from each sample to make a pooled QC in order to assess instrument performance (207).

Liquid chromatography-mass spectrometry (LC-MS)

LC was performed on a ZIC-pHILIC 5µm, 4.6 x 150mm column from Merck Sequant (Watford, UK), using Accela LC system with a mobile phase consisted of A: 20 mM ammonium carbonate and B: 100% acetonitrile as previously described in (134, 135). Compounds were separated by the following linear gradient: 20% A (0 min) to 95% A at 15 min to 20% A at 17 min and held to 24 min. A flow rate was 300 µl/min and an injection volume was 10 µl. Samples were maintained at 4 °C, and the column was maintained at 45 °C.

MS was performed on an Orbitrap Exactive MS (Thermo Fisher Scientific, Hemel Hempstead, UK) with ESI running in positive and negative ionisation modes. Briefly, spectra were acquired in full MS scan in the range of *m/z* 70-1400 and the resolution was 50,000 in both modes. The capillary and probe

temperatures were maintained at 275 and 150 °C, respectively. The instrument calibration was performed by modified Thermo calibration mixture masses with inclusion of $C_2H_6NO_2$ (*m/z* 76.0393) for positive ion electrospray ionisation and $C_3H_5O_3$ (*m/z* 89.0244) for negative ion electrospray ionisation in order to extend the calibration mass range to small metabolites.

Data analysis and metabolite identification

Raw LC–MS data from the control group (untreated cells), the treatments groups (cells exposed to the different NPs), and reagent blanks were acquired using Xcalibur v2.1 software (Thermo Scientific, Hemel Hemstead UK), and processed with XCMS for untargeted peak-picking (208). Peak matching and related peaks annotation were performed using mzMatch (209) and noise filtering and putative metabolite identification were then carried out using IDEOM with the default parameters (210). Metabolites that were matched with accurate masses and retention times of authentic standards were identified with Level 1 metabolite identification according to the metabolomics standards initiative (211, 212), but when standards were not available, metabolites were identified by employing predicted retention times considered as putative (Level 2 identification). Pooled QC samples were injected

randomly in between every 5-6 samples to validate system suitability and stability (207). Multivariate data analysis was employed to assess changes in the cell metabolome between the control and each treatment group using orthogonal partial least squares discriminant analysis (OPLS-DA) using SIMCA-P v13.0.2 (Umetrics, Umea, Sweden) (213). In addition to the multivariate analysis, univariate one-way ANOVA was carried out using Metaboanalyst 3.0 (214). Mass ions with false discovery rate (FDR) less than 5 % and variable importance in projection scores (VIP) greater than one were selected as potential biomarkers. The lists of significantly altered metabolites were imported to Metaboanalyst 3.0 to visualise the affected metabolic pathways (215).

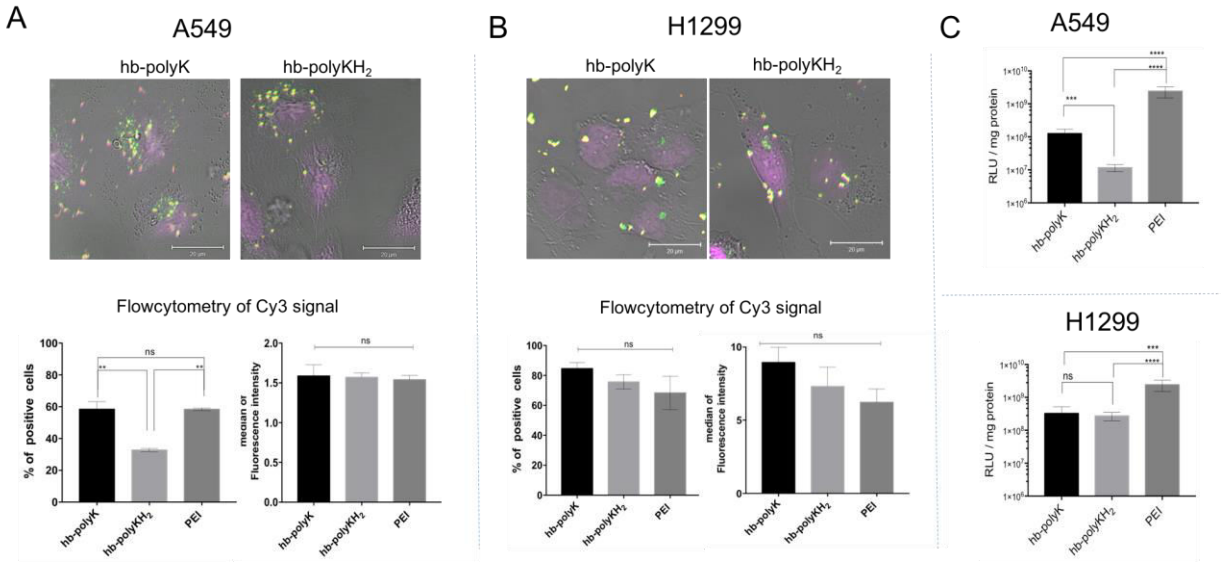


Figure 5-1: The uptake data in A549 cells (A) and in H1299 cells (B); presented by confocal images (more images in Figure 5-S2) and flowcytometry data, where the flowcytometry reported as a percentage of positive cells and median of the

florescence intensity of signal of Cy3 labelled plasmid. (C) The transfection efficiency of the polyplexes with gWiz-Luc in A549 cells and in H1299 cells. The results represent mean and SD values (n= 4). The significance represents the difference in comparison with the controls, where ns=insignificant, *= significant ($p < 0.05$), **= very significant ($p < 0.01$), ***= extremely significant ($p < 0.001$) and ****= extremely significant ($p < 0.0001$).

5.3 Results and discussion

In this study, a metabolomics approach was adopted as a comprehensive and reliable method to assess the impact of the polyplexes of hb-polyK, hb-polyKH_2 and PEI, and their potential toxicity at sub-toxic concentration, on A549 and H1299 cell lines. We chose chromatographic separation of metabolites followed by mass spectrometric analysis, as this is the most frequently used approach in metabolomics, especially via GC-MS and LC-MS systems. NMR spectroscopic analysis has also been widely used in metabolomics as it is quantitative, reproducible, selective and more importantly does not need complicated sample preparation (133, 286). However, current levels of sensitivity remain a limitation in comparison to mass spectrometric techniques. In addition, MS metabolic approaches have the advantage of high throughput and wide metabolite coverage (287). For example, GS-MS has high resolution and is able to retain small molecules that elute

with the solvent front in LC approaches, nevertheless sample derivatisation is needed for GS-MS and it is only applicable for thermally stable stationary phases and samples. Although LC-MS approach is less reproducible than GS-MS and NMR (288), its high sensitivity and the wide range of compounds that can be analysed by LC-MS in addition to the non-destructive soft ionisation techniques in both polarities has made LC-MS one of the most attractive approaches for metabolic profiling in recent years, hence our adoption of this method.

The polyplexes were prepared at N/P ratio of 10, where they showed the best transfection efficiency as previously described (24). The size and zeta potential measurements indicated that the polymers efficiently condensed plasmid DNA into positively charged nanoparticles of around 150 nm in diameter and the AFM images confirmed the results (Figure 5-S1). Regarding the uptake, confocal microscopy images showed that the polyplexes were efficiently internalised in both cell lines. Flow cytometry revealed that there was no statistically significant difference between the uptakes of all polyplexes in H1299 cells. Also, the extent of internalisation of hb-polyK and PEI polyplexes in A549 cells was similar, but the histidine-containing polymer hb-polyKH_2 complexes with DNA were present in significantly fewer A549 cells. However, the median of fluorescence intensity was comparable for all the

polyplexes in A549 cells (Figures 5-1A and 5-1B). Conversely, the transfection experiments revealed that PEI achieved the best transfection efficiency in both cell lines in comparison with hb-polyK and hb-polyKH_2. Also, in A549 cells, hb-polyK showed greater transfection efficiency than hb-polyKH_2, while in H1299 the difference between them was not statistically significant (Figure 5-1C). Considering the results of the uptake studies, it can be suggested that the variation of transfection, at least in case of PEI, may have been related to the different intracellular processing of these polymers and their polyplexes. Accordingly, we aimed to investigate the metabolomics profiles for these polyplexes in the selected cell lines, as a means to understand better the pathways by which the cells processed the polyplexes during the transfection experiments.

In metabolomics studies, it is important to work at the sub-toxic level as the differences in viability between the control and treated cells would affect the reliability of the results. Therefore, MTT and LDH assays were used to investigate any toxicity resulting from the polyplexes (Figure 5-2). These data show that the polyplexes of all the polymers were well tolerated by both cell lines at the selected concentration and N/P ratio. Signs of toxicity were seen, especial for PEI, at high N/P ratios (>20). It was previously reported that these

polymers could provoke apoptosis as a late stage of toxicity (277, 289); therefore the cells were further assessed using Annexin-V/PI apoptosis assays to check if there were any apoptotic features on treatment with the polyplexes at the concentrations used in this study. The results (Figure 5-S3) did not show any significant shift in the cells toward apoptosis and/or necrosis and confirmed that the selected concentrations of polyplexes were suitable for metabolomics study. The N/P ratio used in this study is the charge ratio and reflects the effective concentration of each polymer which achieved the best DNA condensation and delivery in previous work (24), the 2 µg/ml of plasmid DNA, used to treat the cells at N/P ratio of 10, was corresponding to 0.012, 0.016 and 0.002 mg/ml of hb-polyK, hb-polyKH_2 and PEI respectively. As expected, PEI was a more potent transfection agent than hb-polyK and hb-polyKH_2, but it was also more cytotoxic.

A total of 482 and 421 metabolites were putatively identified in A549 and H1299 cells respectively, including amino acids, carbohydrates, nucleotides and lipids (Figure 5-3A). In order to study the metabolic changes in A549 and H1299 cells after treatment with polyplexes of hb-polyK, hb-polyKH_2 and PEI, extracts from treated and control cells from both cell lines were analysed by LC-MS.

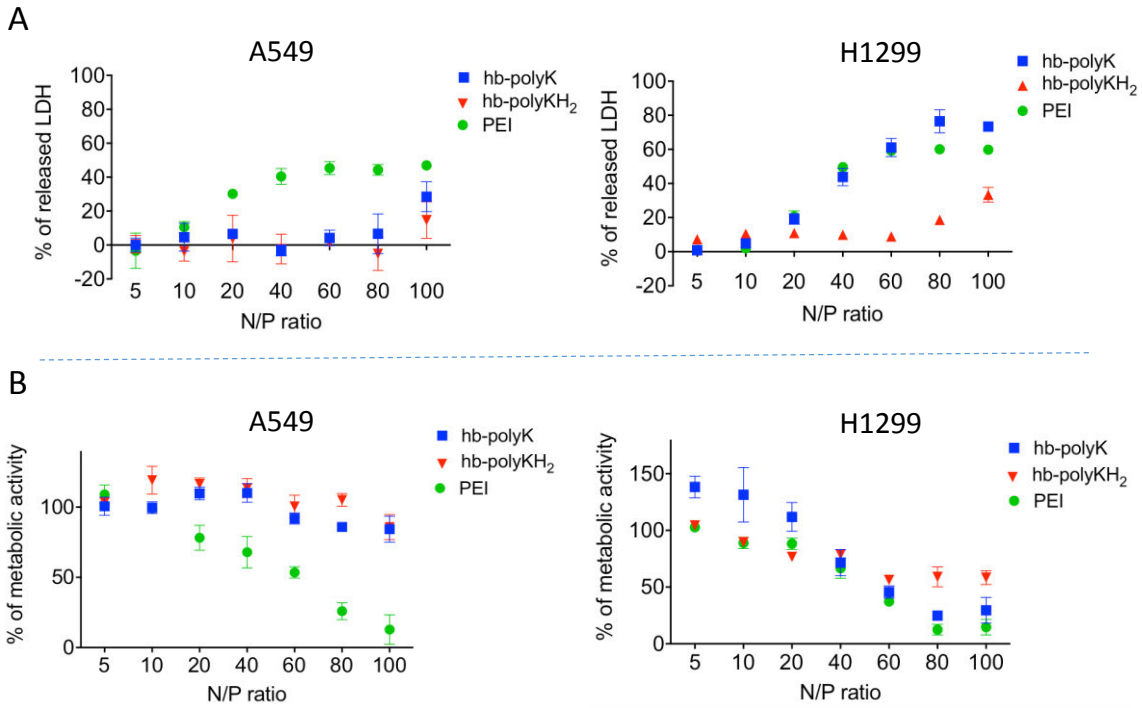


Figure 5-2: (A) LDH and (B) MTT assay of hb-polyK, hb-polyKH2 and PEI polyplexes at different N/P ratios in A549 and H1299 cell lines. The polyplexes were prepared in HEPES (10mM, pH 7.4), diluted with FBS-free medium, and applied on the cells at a final concentration of 2 µg/ml of siRNA for 4 hrs. The results are shown as mean and SE values of triplicate experiments (n=4).

The six biological replicates for each sample group were clustered clearly in the OPLS-DA scores plots (Figure 5-3B), indicating reproducible data sets. OPLS-DA scores plots also showed distinct separations between the different sample groups revealing that LC-MS-based metabolic profiling was capable of investigating different molecular effects of each group of polyplexes on the cell metabolomes. Mass ions of VIP score greater than 1 were selected as potential biomarkers. In addition to the multivariate analysis results, univariate ANOVA was performed to identify significantly changed compounds;

mass ions with the false discovery rate ≤ 0.05 were selected as significant variables (217). Combining multi and univariate analyses revealed that 98 and 86 metabolites were altered significantly in A549 and H1299 cells respectively after the exposure to the different polyplexes, Tables 5-S1 and 5-S2.

Disturbed metabolic pathways

The metabolomics approach revealed that the polyplexes affected several pathways in A549 and H1299 cells, including amino acids and nucleotides metabolism, citric acid cycle, and redox state; as shown in Figure 5-3C. Although we cannot rule out effects of the delivered plasmid on all the metabolic changes detected, we specifically focused on metabolites previously linked to toxicity mechanisms of polymers as reported in the literature (277, 284). Accordingly, we show the significantly changed and biologically relevant metabolites summarised in Table 5-1.

First of all, the fold changes in metabolite levels (as presented in the 'heat map' of Table 1) show that hb-polyKH_2 had the least impact on cellular metabolism, which in turn may indicate reduced toxicity of this polymer in comparison to PEI and hb-polyK. Although the metabolic changes could, in principle, be connected to the lower uptake of hb-polyKH_2 in A549 cells, they were more likely attributed to the different intracellular behaviour of this polymer in H1299 cells, as the

cellular uptake results were comparable for all polyplexes. This is possibly due to the low ability of hb-polyKH_2 to interact and permeabilise the cellular membrane as it is less flexible and has lower charge density in comparison with hb-polyK and PEI, an effect which is more pronounced in the H1299 cell line, as reported in our previous study (24). The reduced membrane disruption activity of the hb-polyKH2 can be noted in the LDH assay as well (Figure 5-2). In this regard, several studies have suggested that there is a correlation between the toxicity of cationic polymers and their transfection efficiency, particularly PEI. These studies have considered the ability of cationic polymers to interact, destabilise, and permeabilise the biological membrane as a mechanism for transfection and toxicity as well.

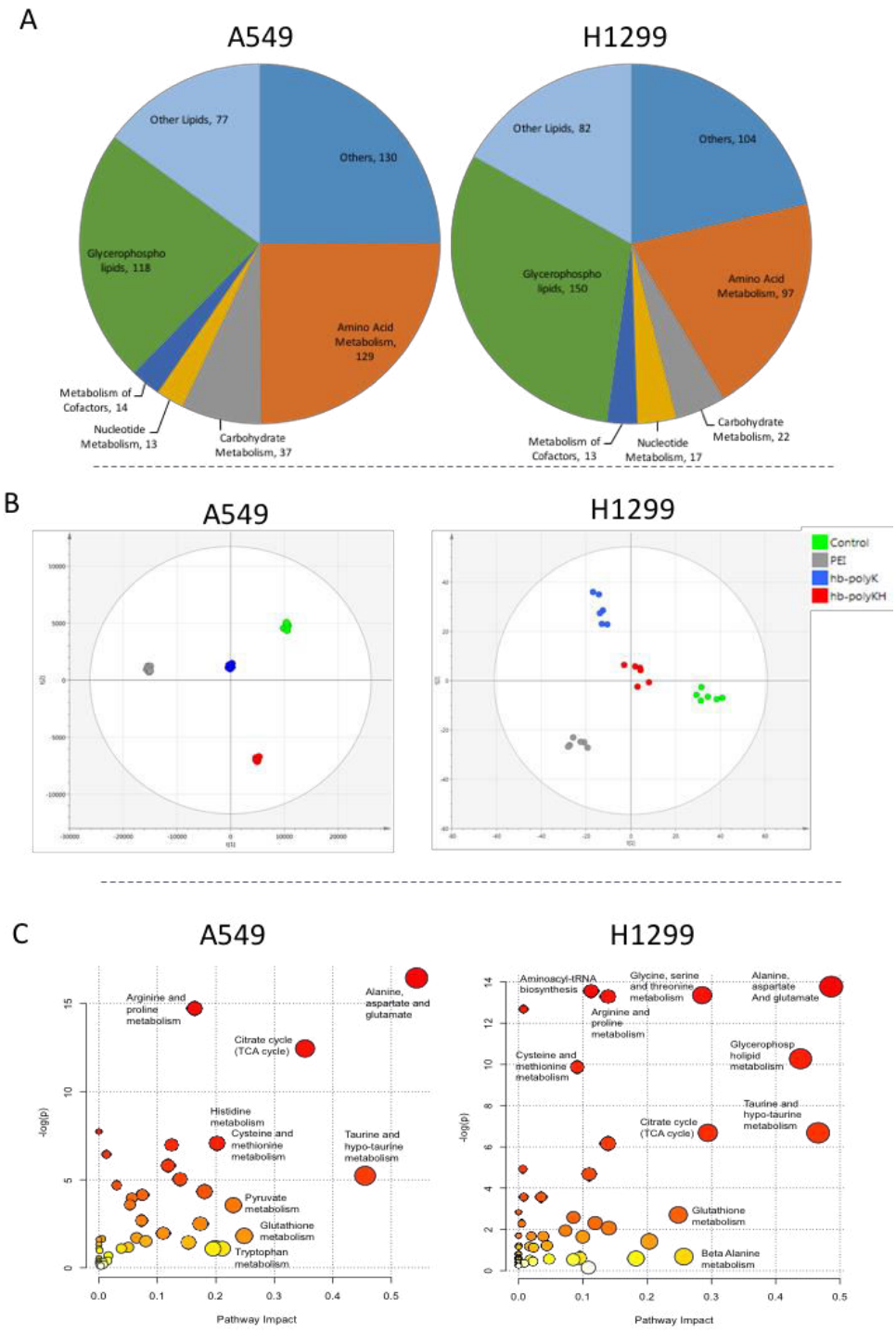


Figure 5-3: (A) Classification of the identified metabolites according to their biological role. (B) OPLS-DA scores plots of A549 cells samples (R2X=0.89, R2Y=0.99, Q2=0.72, CV ANOVA p value=$3.1e^{-4}$) and H1299 cells samples (R2X=0.71, R2Y=0.83 Q2=0.56 p value=$9.4e^{-3}$) after four hrs treatment with polyplexes of hb-polyK, hb-polyKH2 and PEI (the control group with FBS-free medium), and then 20 hrs of incubation without fully supplemented medium. (C) Summary of pathway analysis with MetaboAnalyst 4.0. The node colour is based on its p-value and the node radius is determined based on their pathway impact values.

Table 5-1: The most biologically relevant metabolites that were changed significantly in THP-1 and A549 cells after the treatment with free MTX and MTX loaded NPs, IDC: metabolite identification level according to the metabolomics standards initiative L1 – Level 1, L2 – Level 2. Colours in the table represent changes in metabolite levels with blue indicating a decrease and red denoting an increase.

Mass	RT	FORMULA	Putative metabolite	IDC	A549			H1299		
					PEI	hb-polyK	hb-polyKH$_2$	PEI	hb-polyK	hb-polyKH$_2$
TCA cycle										
146.0215	10.29	C5H6O5	2-Oxoglutarate	L1	0.42	0.68	0.88	0.43	0.45	0.61
192.0270	11.56	C6H8O7	Citrate	L2	0.60	0.60	0.93	0.76	0.60	0.97
134.0216	10.44	C4H6O5	(S)-Malate	L1	0.69	0.92	1.00	0.63	0.53	0.79
174.0164	11.55	C6H6O6	cis-Aconitate	L2	0.63	0.70	1.08	0.67	0.52	0.83
118.0267	10.35	C4H6O4	Succinate	L1	0.72	1.13	1.10	1.30	0.81	0.98
Glycolysis										
88.0161	7.30	C3H4O3	Pyruvate	L1	0.30	0.57	0.63	0.49	0.86	0.78
167.9823	11.28	C3H5O6P	Phosphoenolpyruvate	L1	0.63	0.73	1.05	0	0	0
185.9928	11.01	C3H7O7P	3-Phospho-D-glycerate	L2	0.39	0.59	1.05	0.67	0.87	0.90
Carnitine shuttle										
425.3505	5.23	C25H47NO4	Elaidiccarnitine	L2	1.36	1.09	1.34	3.99	3.41	1.62
427.3662	5.18	C25H49NO4	Stearoylcarnitine	L2	1.38	1.40	1.03	3.83	5.58	2.07
399.3349	5.3	C23H45NO4	Palmitoylcarnitine	L2	0	0	0	3.25	3.05	1.67
161.1052	9.84	C7H15NO3	L-Carnitine	L1	0.63	0.94	1.01	0.68	0.66	0.73
Redox homeostasis and apoptosis										
147.0532	7.44	C5H9NO4	O-Acetyl-L-serine	L2	0.47	0.84	1.16	0	0	0
161.0688	7.41	C6H11NO4	O-Acetyl-L-homoserine	L2	0.41	0.73	0.90	0.50	0.44	0.70
219.0742	9.4	C8H13NO6	O-Succinyl-L-homoserine	L2	0.27	0.54	0.59	0.55	0.38	0.66
183.0661	10.09	C5H14NO4P	Choline phosphate	L1	0.77	0.93	0.97	0.64	0.85	0.87
103.0997	10.23	C5H13NO	Choline	L2	0.74	0.83	0.76	2.88	1.77	1.81

125.0147	10.70	C2H7NO3S	Taurine	L1	0.62	0.87	0.88	0.39	0.49	0.63
307.0838	9.82	C10H17N3O6S	Glutathione	L1	0.65	0.79	1.04	0.55	0.64	0.81
147.0532	5.54	C11H12N2O2	L-Glutamate	L1	0.53	0.86	0.89	0.60	0.39	0.65
Kynurenine metabolism										
204.0899	9.56	C10H12N2O3	L-Tryptophan	L1	0.50	0.73	0.83	2.03	1.25	1.27
208.0848	9.05	C11H12N2O4	L-Kynurenine	L1	8.25	7.76	0.74	1.32	0.91	1.04
236.0797	8.38	C8H7NO3	L-Formylkynurenine	L2	76.38	48.13	0.00	0	0	0
165.0426	4.89	C7H7NO2	Formylanthranilate	L2	54.71	33.75	1.18	0	0	0
137.0476	7.35	C7H7NO2	Anthranilate	L2	6.11	6.55	1.54	0	0	0

It has been suggested that the interactions with cellular membranes can enhance the uptake, endosomal escape and nuclear entry of polyplexes but also induce apoptotic events; mainly by interacting with mitochondrial membrane (290-292). The early findings of metabolomics are in agreement with this suggestion, in that PEI, which achieved the best transfection, had the highest impact on the cellular metabolism. Furthermore, the metabolomics data suggest that the PEI and hb-polyK polyplexes altered the cellular energy metabolism of A549 and H1299 cells through glycolysis and the tricarboxylic acid (TCA) cycle. Usually, cancer cells predominantly use glycolysis for energy production rather than TCA cycle, a phenomenon known as the Warburg Effect (293). The metabolic changes, observed in this study, indicate that PEI and hb-polyK polyplexes inhibited glycolysis; the levels of three main glycolysis metabolites (pyruvate, phosphoenolpyruvate and 3-phospho-D-glycerate in A549 cells and only pyruvate and 3-phospho-D-glycerate in H1299 cells) were decreased. Similarly, PEI and hb-polyK polyplexes showed a down-regulated TCA cycle activity in both cell lines, which was manifest as a decrease in four main TCA cycle intermediates: 2-oxoglutarate, citrate, malate and cis-aconitate as shown in Table 1. PEI and hb-polyK have been reported previously to cause mitochondrial impairment by

either directly interacting with the mitochondrial membrane or by inducing oxidative stress (289, 294); in addition, it is known that mitochondrial impairment can result in TCA cycle dysfunction (295). The inhibition of glycolysis could have been a consequence of ATP decreases resulting from TCA dysfunction because the early steps of glycolysis are ATP dependent. PEI and hb-polyK have been reported previously (284) to interfere with cell membrane permeability/integrity and to induce LDH release outside the cell. This might be a detrimental factor because LDH is essential for glycolysis (294), however, in this study, concentrations of the polyplexes applied were below those causing a significant release of LDH, Figure 5-2.

Interestingly, energy metabolism of H1299 cells was shifted towards fatty acid oxidation, whereas a decrease in carnitine and increase in several acylcarnitines were noticed (296), as shown in Table 5-1. Upregulated fatty acid oxidation results in the accumulation of acetyl CoA, especially when the TCA cycle is malfunctioning because there is not enough oxaloacetate to convert acetyl CoA to citrate. This will lead to increased production of acetoacetate and decreased intracellular pH, until ketoacidosis is reached (297), which might explain the higher susceptibility of H1299 cells towards the polyplexes in our study in comparison to A549 cells.

Cellular redox homeostasis is directly linked to energy metabolism, where glycolysis and TCA cycle are two of the main sources of nicotinamide adenine dinucleotide reduced form (NADH). NADH is utilised inside the mitochondria to produce nicotinamide adenine dinucleotide phosphate (NADPH) (298), which can restore any oxidised glutathione (GSSG) to its reduced state (GSH) through the action of glutathione reductase as the electron donor (299), thus affecting the redox homeostasis directly (300). The observed changes in metabolites also indicated that the amino acid metabolism and redox state of A549 and H1299 cells were altered. In particular, cysteine metabolism was one of the perturbed pathways reported by these experiments. Cysteine, alongside glutamic acid and glycine, is used to form GSH, which plays a key role in cellular redox balance. PEI and hb-polyK polyplexes resulted in a decrease in GSH and at least two of three cysteine precursors in both cell lines (Table 5-1). These changes might indicate that the cells altered their synthesis pathways for GSH from amino acids due to a defect in GSH recycling from its oxidised form (301). A summarised metabolic pathway diagram of disturbed pathways in A549 and H1299 cells after the treatment with the different polyplexes is shown in Figure 5-4, revealing alterations in

energy metabolism and their consequences on redox homeostasis.

Several studies have reported oxidative stress in cells following treatment with similar materials (294, 302, 303). For example, Moghimi et al. found that intracellular ROS was increased on treatment with branched PEI, suggesting that the mitochondrial destruction and glycolytic collapse caused by PEI treatment led to the impaired ability of cells to maintain the level of GSH and in turn the oxidative haemostasis. This study also reported that the presence of N-acetylcysteine (NAC), a precursor of GSH, improved the transfection of PEI polyplexes significantly (279). Therefore, in order to investigate the effect of oxidative stress on the transfection efficiency of the polyplexes, further transfection experiments were performed in the presence of NAC. However, as shown in Figure 5-5, the transfection efficiency for all the polyplexes and in both cell lines was significantly decreased in the presence of NAC, these data implied that oxidative stress improved the transfection efficiency, in contrast with the results reported by Moghimi et al. However, it should be noted that in the prior study, the enhancement of transfection was in part due to an increase in cell viability in the presence of NAC due to a decrease in the toxic effect of ROS (279).

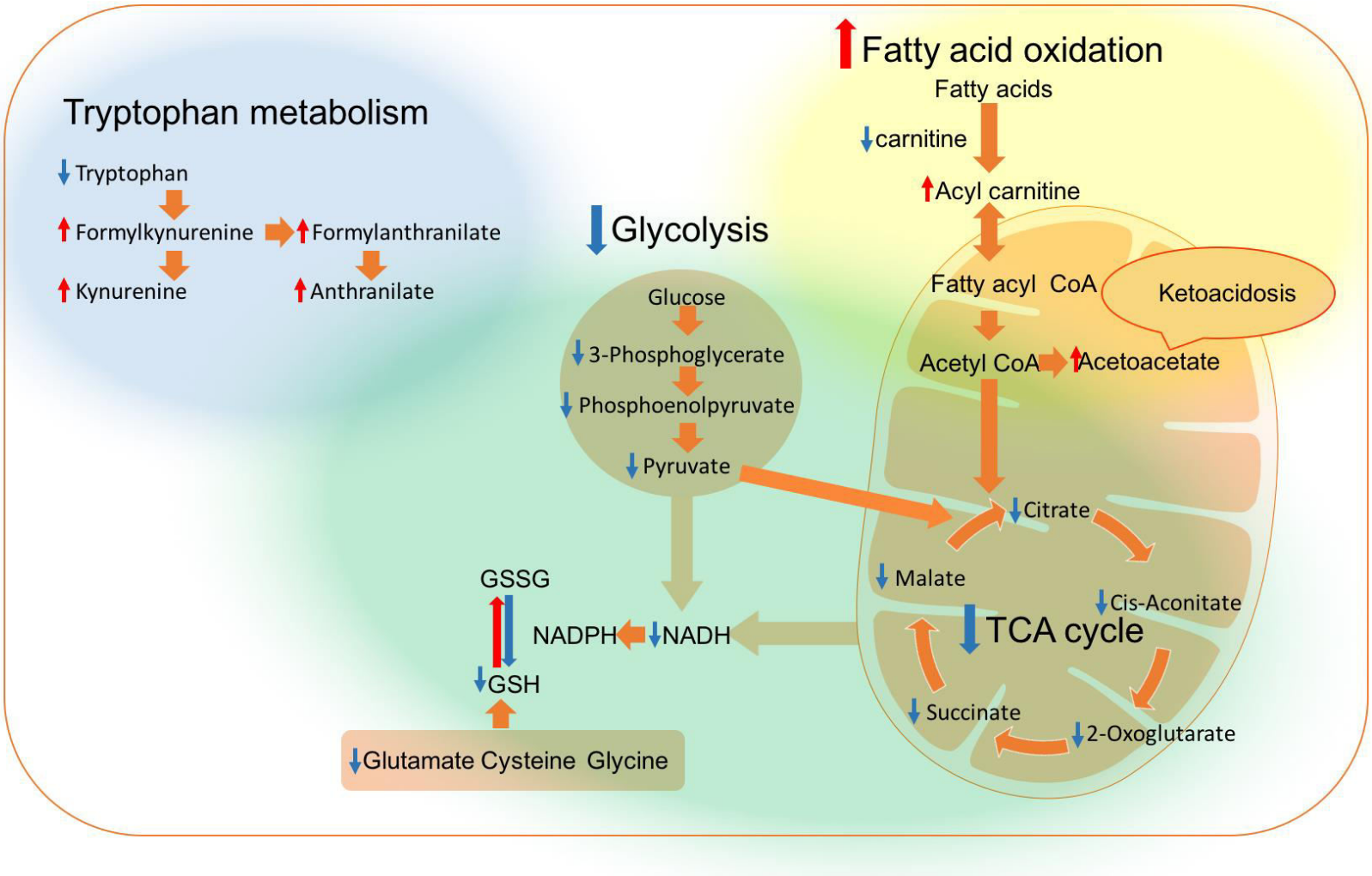


Figure 5-4: Overview of the affected pathways in the A549 and H1299 cells after treatment with the polyplexes. Red arrow = increased, blue arrow = decreased, blue region = altered pathways in A549 cells only, yellow region = altered pathways in H1299 cells only, and the green region = altered pathways in both cell lines.

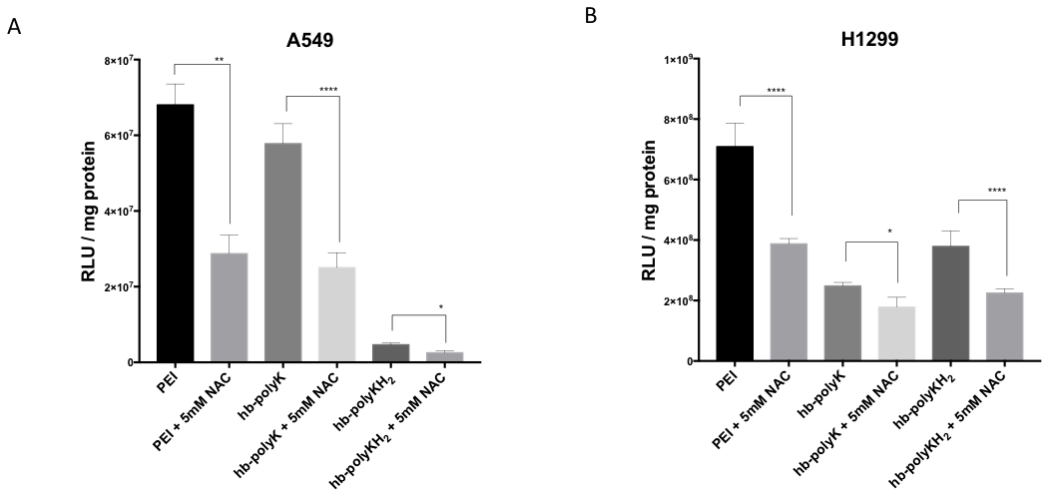


Figure 5-5: The transfection efficiency of polyplexes in the presence of 5 mM NAC in A549 and H1299. The results represent mean and SD value (n= 4). The significance represents the difference in comparison with the controls, where *= significant ($p < 0.05$), **= very significant ($p < 0.01$), and ****= extremely significant ($p < 0.0001$).

In our work, sub-toxic concentrations of polyplexes/polymers were used and thus no improvement in cell viability would be expected in the presence of NAC. In addition, the transfection data in our case were normalised based on total protein measurement of the cells, which cancelled any differences related to the number of cells. Although a high level of ROS is toxic for cells, a sub-toxic level can act as a key modulator for the expression of several transcription factors, growth factors and cytokines (304), which in turn can either directly or indirectly affect transfection and transgene expression. Collectively our results alongside those from Moghimi et al. suggest that NAC either (a) improves the transfection when toxic levels of polyplexes (i.e. ROS) are used by improving cell viability or (b) decreases the transfection efficiency when sub-

toxic concentrations of polyplexes are used, probably by counteracting the effects of sub-toxic levels of ROS.

It has been reported also that the reduction of choline, taurine and GSH metabolites is associated with apoptosis (305, 306). In this study, the levels of choline, taurine and GSH were significantly decreased in A549 cells upon treatment with PEI polyplexes, whereas all the other polyplexes caused decreases in GSH and taurine in H1299 cells. Choline increased in H1299 cells, due most probably to the increase in lipid metabolism in this cell line. These metabolites suggest that the polyplexes may promote apoptosis, which is in line with the reported toxicity for PEI and hb-polyK polyplexes (277, 289). Interestingly, the changes in levels of choline, taurine and GSH metabolites were the least in A549 cells for hb-polyK and hb-polyKH_2 polyplexes, indicating that this effect was more tolerated in A549 cells. This agrees with the results of metabolic activity assays of the cells (MTT), which showed that increasing the N/P ratio increased the toxicity of PEI polyplexes only in A549 but increased the toxicity of all the polyplexes in H1299 cells (Figure 5-2).

Tryptophan metabolism was affected in A549 cells by the polyplexes. The level of tryptophan decreased overall, while four intermediates of the kynurenine pathway, L-formylkynurenine, formylanthranilate, L-kynurenine and

anthranilate were increased. This implied that the tryptophan metabolism via indoleamine 2,3 dioxygenase (IDO), a first and rate-limiting step in the tryptophan catabolism along the kynurenine pathway, had been upregulated, most likely by pro-inflammatory cytokines including TNF α and interferon γ (307). This pathway is involved in different immune/inflammatory activities that are associated with several pathological conditions such as infection (308, 309), which may have been in indicator that this effect had been caused in part by the delivered plasmid. However, Matz et al. reported a similar inflammatory response upon transfection with PEI polyplexes and found that this effect was unrelated to the origin of promoter in the plasmid, whether cytomegalovirus or elongation factor-1 alpha (310). Interestingly, this inflammatory response was not detected in H1299 cells, an effect which can be correlated with the greater transgene expression observed in this cell line for all polyplexes in comparison with A549 cells (Figure 5-1C).

5.4 Conclusion

In this study, branched polycationic polymers (hyperbranched polylysine (hb-polyK), hyperbranched polylysine-co-histidine (hb-polyKH_2) and branched polyethyleneimine (PEI), were used polyplexes with DNA were administered to A549 and

H1299 cells and global metabolic profiling was performed. Subtoxic concentrations of the polyplexes were used, as determined by MTT and LDH assays. Metabolic profiling revealed that PEI and hb-polyK polyplexes down regulated metabolites associated with glycolysis and the TCA cycle and induced oxidative stress in A549 cells. The suggested markers for apoptosis were reported only with PEI polyplexes in this cell line. On the other hand, analogous metabolic profiling in H1299 cells showed that PEI and hb-polyK polyplexes down regulated metabolites associated with glycolysis and the TCA cycle, and all the polyplexes shifted the energy metabolism toward fatty acid oxidation and induced markers of oxidative stress and apoptosis. The lower extent of changes in metabolites suggest that the hb-polyKH_2 polyplexes were the most tolerated polyplexes in this study, which might be due to the reduced ability of hb-polyKH_2 to interact and destabilise the cellular membrane, particularly in H1299 cells. The results also indicated that there was a correlation between the toxicity of these polyplexes and their transfection efficiency.

Finally, this study suggests that the metabolomics approach is a powerful safety assessment tool, as these assays were able to detect potential toxicity markers at sub-toxic concentrations where the traditional methods are insensitive. Also, this method provided insight into the molecular

mechanism of toxicity and therapeutic effect alike, which might accelerate design of more efficient and applicable delivery systems. Although metabolomics studies of delivery systems are still in their infancy, we believe this approach is highly promising and, in the future, can enhance our understanding of the efficacy and safety of drug delivery materials.

5.5 Supporting information

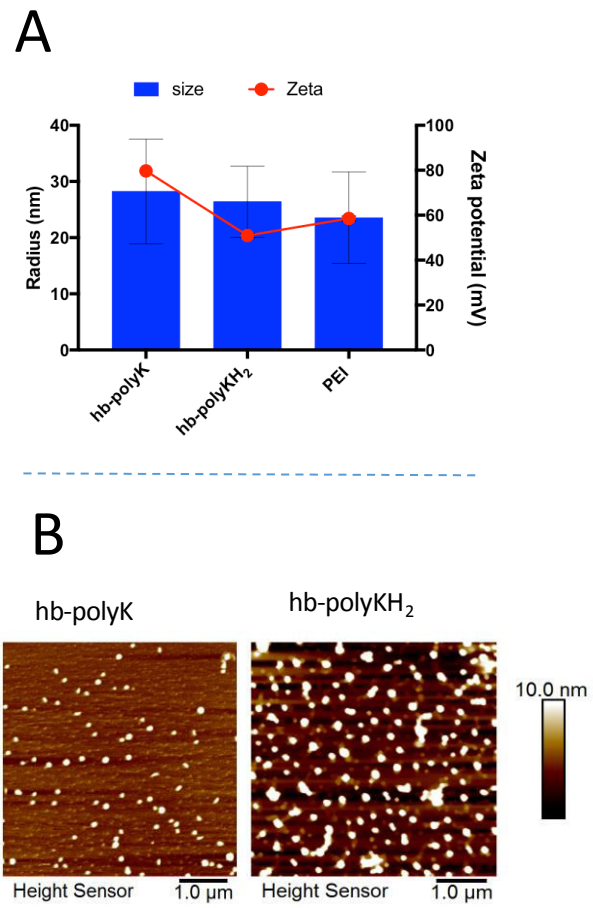


Figure 5-S1: The physicochemical characterisation of the polyplexes prepared in HEPES buffer (0.1 mM, pH 7.4) at N/P of 10, the size and zeta potential measurements (A) and the AFM images (B).

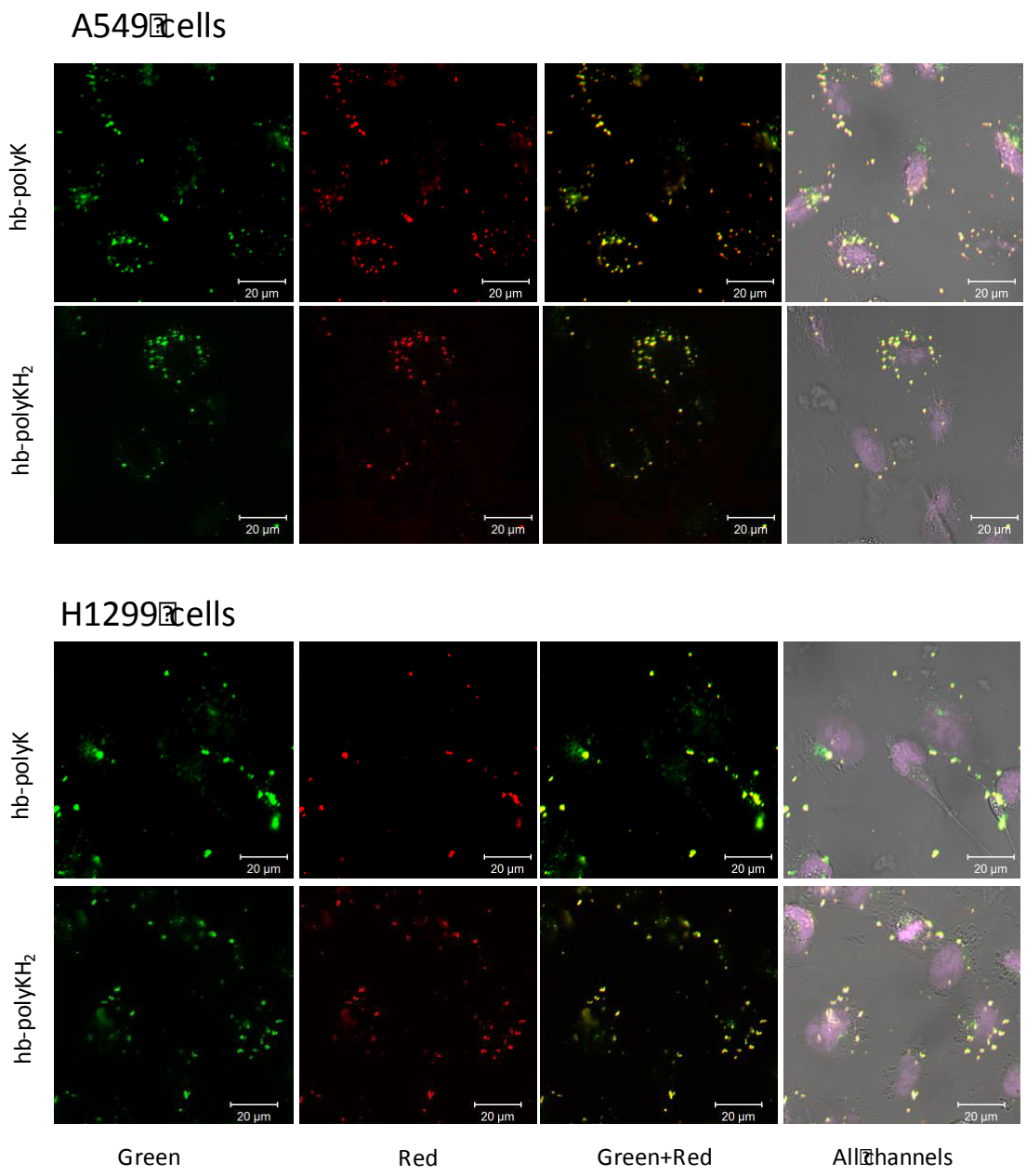


Figure 5-S52: Confocal images show the uptake of hb-polyK and histidine containing hb-polyKH_2 complexes in A549 and H1299 cells. Areas in green are FITC-labelled polymers, area in red are Cy3-labelled plasmid, regions in yellow are assigned to overlaid Cy3-labelled plasmid and FITC-labelled polymers, and areas in purple correspond to DRAQ5 stained nuclei.

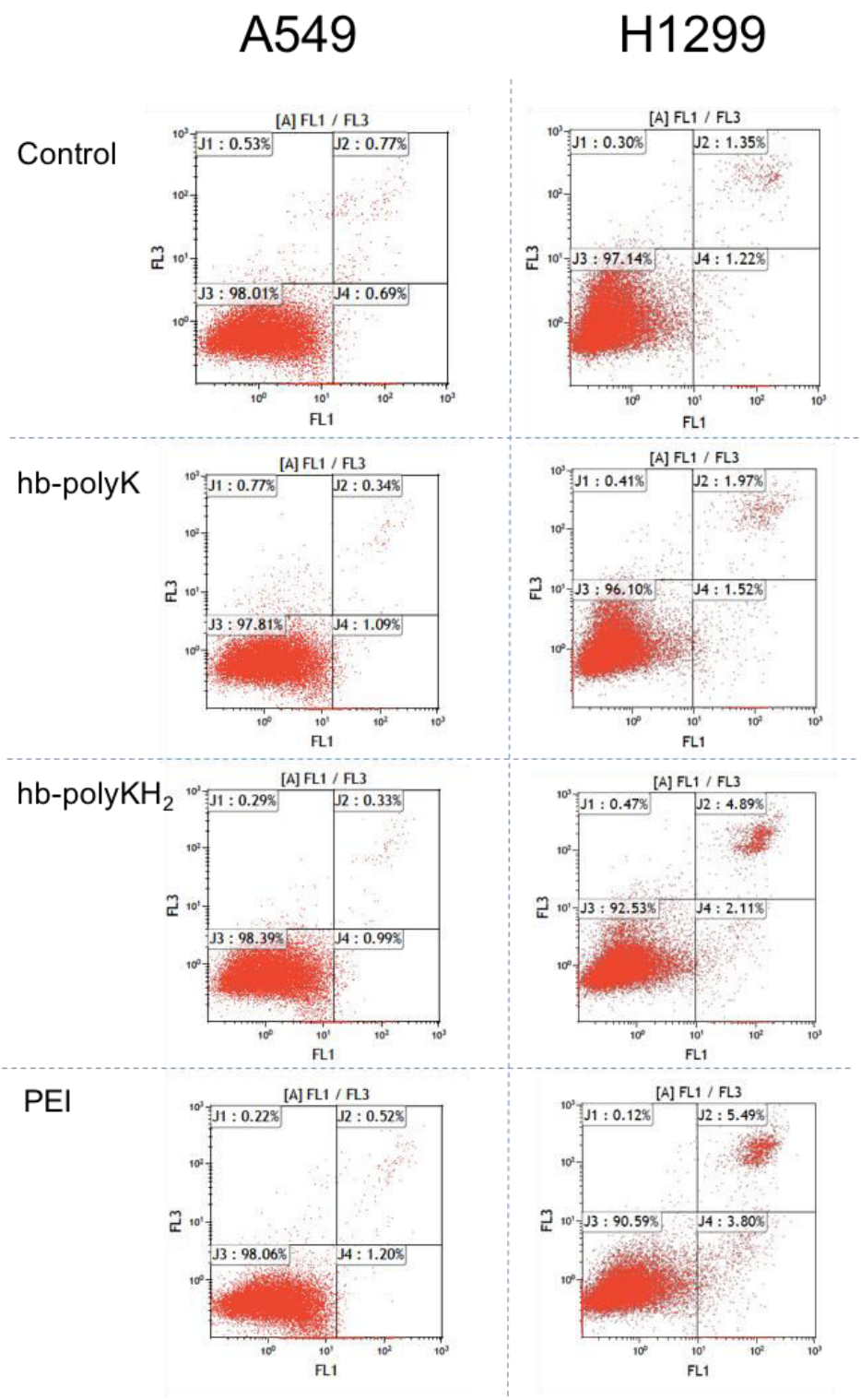


Figure 5-S3: Flow cytometry analysis of Annexin-V/PI apoptosis assays to measure the apoptotic and dead cells in A549 and H1299 cells after four hrs treatment with polyplexes of hb-polyK, hb-polyKH2 and PEI (the control group with FBS-free medium), and then 20 hrs of incubation without fully supplemented medium. The percentages of live, apoptotic, and dead cells were calculated from FL1/FL3. Annexin-V-FITC was used to detect apoptotic cells, and propidium iodide (PI) was used to detect dead cells. J1~ necrotic cells, J2 ~ dead cells, J3 ~ live cells, and J4 ~ apoptotic cell.

Table 5-S1: The metabolites that were changed significantly in A549 cells after the treatment with polyplexes, IDC: metabolite identification level according to the metabolomics standards initiative L1 – Level 1, L2 – Level 2. Colours in the table represent changes in metabolite levels with blue indicating a decrease and red denoting an increase.

Mass	Polarity	Mass error (PPM)	RT	FORMULA	Putative metabolite	IDC	Pathway	Control	Poly PEI	Poly K	Poly KH
89.0477	+	0.247308	11.01	C3H7NO2	L-Alanine	L1	Amino Acid Metabolism	1.00	0.70	1.00	1.00
90.0317	-	0.417857	7.42	C3H6O3	Lactate	L1	Carbohydrate Metabolism	1.00	0.52	0.78	0.90
103.0633	+	-0.17921	11.02	C4H9NO2	4-Amino-butanoate	L2	Amino Acid Metabolism	1.00	0.49	0.61	0.86
103.0997	+	-0.18211	10.23	C5H13NO	Choline	L2	Amino Acid Metabolism	1.00	0.74	0.83	0.76
104.0474	-	0.090649	7.42	C4H8O3	3-Hydroxy-butanoate	L2	Lipid Metabolism	1.00	0.75	1.17	1.02
113.0589	+	0.111963	8.47	C4H7N3O	Creatinine	L1	Amino Acid Metabolism	1.00	0.61	0.97	0.86
117.0426	-	0.260081	7.44	C4H7NO3	2-Amino-3-oxobutanoic acid	L2	Amino Acid Metabolism	1.00	0.51	0.89	1.06
117.0789	+	-0.42807	9.67	C5H11NO2	Valine	L1	Amino Acid Metabolism	1.00	0.62	0.89	0.88
125.0147	+	0.021564	10.7	C2H7NO3S	Taurine	L1	Lipid Metabolism	1.00	0.62	0.87	0.88
126.0429	-	-0.37997	7.49	C5H6N2O2	Thymine	L1	Nucleotide Metabolism	1.00	6.09	7.59	1.88
126.043	+	0.318535	8.67	C5H6N2O2	Imidazole-4-acetate	L1	Amino Acid Metabolism	1.00	0.41	0.76	1.10
130.1106	+	0.1079	16.69	C6H14N2O	N-Acetylputrescine	L2	Amino Acid Metabolism	1.00	0.43	0.60	0.81
131.0582	-	-0.09926	5.3	C5H9NO3	4-Amino-5-oxopentanoate	L2	Metabolism of Cofactors and Vitamins	1.00	0.49	0.71	0.86
131.0583	+	0.81444	10.58	C5H9NO3	Glutamate 5-semialdehyde	L2	Amino Acid Metabolism	1.00	0.65	0.80	0.90
131.0695	+	0.181322	10.77	C4H9N3O2	Creatine	L1	Amino Acid Metabolism	1.00	0.59	0.85	1.03
131.0946	+	0.113021	9.05	C6H13NO2	Leucine	L2	Amino Acid Metabolism	1.00	0.60	0.84	0.85
134.0216	+	-0.1023	10.44	C4H6O5	Malate	L1	Carbohydrate Metabolism	1.00	0.69	0.92	1.00
135.0545	+	-0.32059	8.53	C5H5N5	Adenine	L1	Nucleotide Metabolism	1.00	0.74	0.56	0.78
136.0524	-	0.096993	5.15	C8H8O2	Phenylacetic acid	L2	Amino Acid Metabolism	1.00	0.68	0.78	0.82
137.0476	-	-0.38995	7.35	C7H7NO2	Anthranilate	L2	Amino Acid Metabolism	1.00	6.11	6.55	1.54
141.0193	+	1.080585	10.68	C2H8NO4P	Ethanolamine phosphate	L1	Amino Acid Metabolism	1.00	1.47	1.59	1.22
145.0375	-	-0.3444	7.42	C5H7NO4	4-Oxoglutaramate	L2	Amino Acid Metabolism	1.00	0.53	0.68	1.05
145.0851	+	-0.23836	11.07	C5H11N3O2	4-Guanidinobutanoate	L2	Amino Acid Metabolism	1.00	0.58	0.88	0.92
145.1102	+	-0.31882	9.85	C7H15NO2	4-Trimethylammoniobutanoate	L1	Amino Acid Metabolism	1.00	0.64	0.96	1.08
146.0215	-	-0.36396	10.29	C5H6O5	2-Oxoglutarate	L1	Carbohydrate Metabolism	1.00	0.42	0.68	0.88
146.0691	+	-0.5994	10.71	C5H10N2O3	Glutamine	L1	Amino Acid Metabolism	1.00	1.26	1.12	0.93
147.0532	-	-0.00964	7.44	C5H9NO4	O-Acetyl-L-serine	L2	Amino Acid Metabolism	1.00	0.47	0.84	1.16

158.0439	-	-0.48709	10.65	C4H6N4O3	Allantoin	L2	Nucleotide Metabolism	1.00	0.59	0.92	0.70
159.0531	-	-0.39978	5.3	C6H9NO4	N-Methyl-2-oxoglutaramate	L2	-	1.00	0.47	0.59	0.68
160.1211	+	-0.33452	16.28	C7H16N2O2	N6-Methyl-L-lysine	L2	Amino Acid Metabolism	1.00	0.59	0.77	0.78
161.0688	+	-0.20004	8.87	C6H11NO4	O-Acetyl-L-homoserine	L2	Amino Acid Metabolism	1.00	0.37	0.80	0.85
161.1052	+	-0.24637	9.84	C7H15NO3	Carnitine	L1	Amino Acid Metabolism	1.00	0.63	0.94	1.01
163.0666	+	-0.40217	5.88	C6H13NO2S	Homomethionine	L2	Amino Acid Metabolism	1.00	0.52	0.60	0.81
165.0426	-	0.257381	4.89	C8H7NO3	Formylanthranilate	L2	Amino Acid Metabolism	1.00	54.7	33.7	1.18
165.079	+	0.148487	8.49	C9H11NO2	Phenylalanine	L2	Amino Acid Metabolism	1.00	0.61	0.84	0.92
169.0044	-	-0.34971	10.69	C3H7NO5S	Cysteate	L1	Amino Acid Metabolism	1.00	0.64	0.87	0.95
172.0137	-	-0.1157	9.97	C3H9O6P	Glycerol 3-phosphate	L1	Lipid Metabolism	1.00	0.56	0.92	0.79
173.0688	+	-0.03571	5.3	C7H11NO4	N-Acetyl-L-glutamate 5-semialdehyde	L2	Amino Acid Metabolism	1.00	0.57	0.74	1.02
174.0164	-	-0.28792	11.2	C6H6O6	cis-Aconitate	L2	Carbohydrate Metabolism	1.00	0.63	0.70	1.08
175.048	-	-0.17279	9.72	C6H9NO5	N-Acetyaspartate	L2	Amino Acid Metabolism	1.00	0.66	0.94	0.88
176.0432	-	-0.44438	10.8	C5H8N2O5	N-Carbamoyaspartate	L2	Nucleotide Metabolism	1.00	0.44	0.81	0.96
183.0661	+	0.490828	10.09	C5H14NO4P	Choline phosphate	L1	Lipid Metabolism	1.00	0.77	0.93	0.97
185.9928	-	-0.51588	11.02	C3H7O7P	3-Phospho-D-glycerate	L2	Carbohydrate Metabolism	1.00	0.39	0.59	1.05
189.0637	+	-0.11107	9.47	C7H11NO5	N-Acetyglutamate	L1	Amino Acid Metabolism	1.00	0.31	0.65	0.58
190.059	-	0.240851	10.58	C6H10N2O5	N-Carbamyglutamate	L2	Amino Acid Metabolism	1.00	0.39	0.49	0.92
204.0899	+	0.10895	9.56	C11H12N2O2	Tryptophan	L1	Amino Acid Metabolism	1.00	0.50	0.73	0.83
208.0848	+	-0.01681	9.05	C10H12N2O3	Kynurenine	L1	Amino Acid Metabolism	1.00	8.25	7.76	0.74
211.0358	+	0.131998	9.98	C4H10N3O5P	Phosphocreatine	L2	Amino Acid Metabolism	1.00	0.30	0.69	0.90
218.1266	+	-0.14451	10.42	C9H18N2O4	N2-(D-1-Carboxyethyl)-L-lysine	L2	Amino Acid Metabolism	1.00	0.45	0.63	0.97
219.0742	-	-0.61579	9.4	C8H13NO6	O-Succinyhomoserine	L2	Amino Acid Metabolism	1.00	0.27	0.54	0.59
220.0848	+	0.154061	7.52	C11H12N2O3	5-Hydroxy-tryptophan	L2	Amino Acid Metabolism	1.00	6.45	5.02	0.78
222.0674	+	-0.24604	11.33	C7H14N2O4S	Cystathionine	L1	Amino Acid Metabolism	1.00	0.63	0.57	1.07
227.0906	+	0.068625	7.56	C9H13N3O4	Deoxycytidine	L2	Nucleotide Metabolism	1.00	0.51	0.66	0.96
231.147	+	-0.33596	7.77	C11H21NO4	O-Butanoylcarnitine	L2	Lipids: Fatty Acyls	1.00	0.50	0.81	0.99
236.0797	+	-0.12813	8.38	C11H12N2O4	Formylkynurenine	L2	Amino Acid Metabolism	**0.00**	76.4	48.1	0.00
246.0504	-	-0.35348	9.07	C6H15O8P	Glycerophosphoglycerol	L2	-	1.00	0.28	0.62	0.90
246.1329	+	0.169951	10.44	C9H18N4O4	N2-(D-1-Carboxyethyl)-arginine	L2	Amino Acid Metabolism	1.00	0.41	0.55	0.83
247.142	+	0.122203	8.86	C11H21NO5	Hydroxybutyrylcarnitine	L2	-	1.00	0.61	0.82	1.14
257.1028	+	0.024194	10.26	C8H20NO6P	glycero-3-Phosphocholine	L1	Lipid Metabolism	1.00	0.74	0.78	0.74
260.0296	+	-0.4651	10.46	C6H13O9P	Glucose 6-phosphate	L1	Carbohydrate Metabolism	1.00	0.58	0.72	1.34
275.1733	+	0.207346	8.25	C13H25NO5	N-(3S-hydroxydecanoyl)-L-serine	L2	Lipids: Fatty Acyls	1.00	0.21	0.44	1.27
307.0838	+	-0.01621	9.82	C10H17N3O6S	Glutathione	L1	Amino Acid Metabolism	1.00	0.65	0.79	1.04
369.2877	+	-0.58459	5.2	C21H39NO4	5-Tetradecenoylcarnitine	L2	-	1.00	0.57	0.68	1.31
612.152	+	0.050963	10.86	C20H32N6O12S2	Glutathione disulfide	L1	Amino Acid Metabolism	1.00	0.51	0.58	0.81
663.1091	+	-0.00434	9.62	C21H27N7O14P2	NAD+	L2	Energy Metabolism	1.00	0.46	0.45	1.04
703.515	+	-0.26307	4.64	C38H74NO8P	PC (32:1)	L2	Lipids: Glycerophospholipids	1.00	0.77	0.83	0.94
704.5844	+	1.648575	4.74	C39H81N2O6P	SP (16:0)	L2	Lipids: Sphingolipids	1.00	1.78	1.64	1.26
719.5836	+	0.01342	4.84	C40H82NO7P	PC (32:2)	L2	Lipids: Glycerophospholipids	1.00	0.70	0.61	0.79
731.5462	+	-0.38157	4.63	C40H78NO8P	PC (32:1)	L2	Lipids: Glycerophospholipids	1.00	0.80	0.85	0.96

748.5254	-	0.001225	4.03	C40H77O10P	PG(34:1)		L2	Lipids: Glycerophospholipids	1.00	0.62	0.78	0.85
774.5412	-	0.145202	4.02	C42H79O10P	PG(36:2)		L2	Lipids: Glycerophospholipids	1.00	0.73	0.78	1.09

Table 5-S2: The metabolites that were changed significantly in H1299 cells after the treatment with polyplexes, IDC: metabolite identification level according to the metabolomics standards initiative L1 – Level 1, L2 – Level 2. Colours in the table represent changes in metabolite levels with blue indicating a decrease and red denoting an increase.

Mass	Polarity	Mass error (PPM)	RT	FORMULA	Putative metabolite	IDC	Pathway	Control	Poly PEI	Poly K	Poly KH
88.016	-	-0.00068	5.69	C3H4O3	3-Oxopropanoate	L2	Carbohydrate Metabolism	1.00	0.49	0.86	0.78
89.0477	-	-0.01326	10.06	C3H7NO2	beta-Alanine	L2	Nucleotide Metabolism	1.00	0.67	0.63	0.74
89.0477	+	0.20821	11.15	C3H7NO2	Alanine	L1	Amino Acid Metabolism	1.00	0.61	0.55	0.70
103.0997	+	-0.06347	17.54	C5H13NO	Choline	L2	Amino Acid Metabolism	1.00	2.88	1.77	1.81
105.0426	+	0.396434	11.52	C3H7NO3	Serine	L1	Amino Acid Metabolism	1.00	2.25	1.44	1.43
109.0198	+	0.074003	11.25	C2H7NO2S	Hypotaurine	L2	Amino Acid Metabolism	1.00	0.48	0.55	0.72
113.0477	-	0.283662	10.37	C5H7NO2	1-Pyrroline-5-carboxylate	L2	Amino Acid Metabolism	1.00	3.00	1.16	1.79
117.0538	+	-0.44225	11.86	C3H7N3O2	Guanidinoacetate	L1	Amino Acid Metabolism	1.00	1.62	1.00	1.02
119.0582	+	0.05021	10.76	C4H9NO3	Threonine	L1	Amino Acid Metabolism	1.00	1.67	1.00	1.13
125.0147	+	-0.05618	11.03	C2H7NO3S	Taurine	L1	Lipid Metabolism	1.00	0.39	0.49	0.63
130.1106	+	-0.1578	17.36	C6H14N2O	N-Acetylputrescine	L2	Amino Acid Metabolism	1.00	0.53	0.72	0.75
131.0582	+	-0.37712	7.41	C5H9NO3	5-Amino-2-oxopentanoic acid	L2	Amino Acid Metabolism	1.00	0.65	0.56	0.66
131.0582	+	-0.15717	5.66	C5H9NO3	N-Acetyl-beta-alanine	L2	Amino Acid Metabolism	1.00	0.63	0.42	0.63
131.0694	+	-0.3973	11.15	C4H9N3O2	Creatine	L1	Amino Acid Metabolism	1.00	0.44	0.46	0.60
131.0946	+	-0.26989	9.17	C6H13NO2	Leucine	L2	Amino Acid Metabolism	1.00	1.95	1.17	1.24
132.0535	-	0.062907	11.12	C4H8N2O3	Asparagine	L1	Amino Acid Metabolism	1.00	1.06	0.77	0.93
134.0215	-	0.085993	10.78	C4H6O5	Malate	L1	Carbohydrate Metabolism	1.00	0.63	0.53	0.79
145.0851	+	-0.46629	11.45	C5H11N3O2	4-Guanidinobutanoate	L2	Amino Acid Metabolism	1.00	0.73	0.72	0.83
145.1102	+	-0.34575	10.21	C7H15NO2	4-Trimethylammoniobutanoate	L1	Amino Acid Metabolism	1.00	0.90	0.71	0.76
146.0215	-	-0.23147	10.58	C5H6O5	2-Oxoglutarate	L1	Carbohydrate Metabolism	1.00	0.43	0.45	0.61
147.0531	+	-0.69791	7.99	C5H9NO4	Glutamate	L2	Amino Acid Metabolism	1.00	0.60	0.39	0.65
149.0511	-	0.039816	9.54	C5H11NO2S	Methionine	L1	Amino Acid Metabolism	1.00	1.77	1.26	1.34
151.0494	+	-0.27461	10.39	C5H5N5O	Guanine	L1	Nucleotide Metabolism	0.00	11.63	0.00	0.00
161.0687	+	-0.42558	9.1	C6H11NO4	O-Acetyl-L-homoserine	L2	Amino Acid Metabolism	1.00	0.50	0.44	0.70
161.1052	+	-0.11743	10.2	C7H15NO3	Carnitine	L1	Amino Acid Metabolism	1.00	0.68	0.66	0.73
165.079	+	0.015858	8.74	C9H11NO2	Phenylalanine	L2	Amino Acid Metabolism	1.00	2.20	1.33	1.36
169.0504	+	-0.15903	9.93	C4H12NO4P	Phosphodimethylethanolamine	L2	Lipid Metabolism	1.00	0.73	0.76	0.94
172.0137	-	-0.08564	10.61	C3H9O6P	Glycerol 3-phosphate	L1	Lipid Metabolism	1.00	1.57	1.55	1.22
174.0164	-	-0.49691	11.55	C6H6O6	cis-Aconitate	L2	Carbohydrate Metabolism	1.00	0.67	0.52	0.83
175.0481	+	0.069856	10.04	C6H9NO5	N-Acetyl-L-aspartate	L2	Amino Acid Metabolism	1.00	0.66	0.64	0.78
175.0957	+	0.019941	11.54	C6H13N3O3	Citrulline	L1	Amino Acid Metabolism	1.00	1.50	0.91	1.12
177.046	+	-0.06226	5.58	C6H11NO3S	N-Formymethionine	L2	Amino Acid Metabolism	1.00	0.88	0.65	0.70
179.0582	-	-0.05216	7.42	C9H9NO3	N-Acetylanthranilate	L2	-	1.00	0.69	0.59	0.72

181.0739	-	0.112349	10.4	C9H11NO3	Tyrosine	L1	Amino Acid Metabolism	1.00	1.72	0.94	1.32
183.0661	+	0.429736	10.42	C5H14NO4P	Choline phosphate	L1	Lipid Metabolism	1.00	0.64	0.85	0.87
189.0637	+	-0.05389	9.77	C7H11NO5	N-Acetyl-L-glutamate	L1	Amino Acid Metabolism	1.00	0.80	0.60	0.70
191.0616	+	0.116175	5.32	C7H13NO3S	N-Acetylmethionine	L2	-	1.00	0.72	0.44	0.65
195.0897	+	0.709481	5.65	C10H13NO3	Tyrosine methyl ester	L2	Amino Acid Metabolism	1.00	0.75	0.66	0.86
203.1158	+	0.26164	9.08	C9H17NO4	O-Acetylcarnitine	L1	Amino Acid Metabolism	1.00	0.63	0.48	0.64
204.0899	+	0.051584	9.88	C11H12N2O2	Tryptophan	L1	Amino Acid Metabolism	1.00	2.03	1.25	1.27
231.147	+	-0.114	8.05	C11H21NO4	O-Butanoylcarnitine	L2	Lipids: Fatty Acyls	1.00	0.56	0.58	0.70
243.0854	+	-0.34119	9.91	C9H13N3O5	Glutamyl-beta-cyanoalanine	L2	Amino Acid Metabolism	1.00	3.28	0.82	1.08
245.1626	+	-0.26101	7.71	C12H23NO4	N-(octanoyl)-L-homoserine	L2	-	1.00	0.77	0.75	0.85
245.1626	+	-0.25621	6.35	C12H23NO4	2-Methylbutyroylcarnitine	L2	-	1.00	0.69	0.63	0.70
246.0504	+	-0.17565	9.37	C6H15O8P	Glycerophosphoglycerol	L2	-	1.00	0.31	0.36	0.54
246.1329	+	0.467084	10.81	C9H18N4O4	N2-(D-1-Carboxyethyl)-L-arginine	L2	Amino Acid Metabolism	1.00	0.87	0.54	0.71
257.1029	+	0.15967	10.62	C8H20NO6P	sn-glycero-3-Phosphocholine	L1	Lipid Metabolism	1.00	1.41	1.41	1.19
267.0967	+	-0.19584	8.45	C10H13N5O4	Adenosine	L1	Nucleotide Metabolism	1.00	1.66	1.40	1.15
281.1124	+	-0.13102	12.23	C11H15N5O4	1-Methyladenosine	L2	-	1.00	1.93	0.88	0.96
307.0838	+	-0.15933	10.1	C10H17N3O6S	Glutathione	L1	Amino Acid Metabolism	1.00	0.55	0.64	0.81
347.063	+	-0.20359	9.66	C10H14N5O7P	AMP	L1	Nucleotide Metabolism	1.00	0.79	0.58	0.82
371.3036	+	0.200741	5.44	C21H41NO4	Tetradecanoylcarnitine	L2	-	1.00	2.12	2.20	1.01
397.3192	+	-0.05176	5.34	C23H43NO4	Hexadec-2-enoylcarnitine	L2	-	1.00	2.48	1.87	1.02
399.3349	+	0.08556	5.3	C23H45NO4	O-Palmitoyl-R-carnitine	L2	Lipids: Fatty Acyls	1.00	3.25	3.05	1.67
425.3505	+	-0.00153	5.23	C25H47NO4	Elaidiccarnitine	L2	-	1.00	3.99	3.41	1.62
427.3662	+	0.097364	5.18	C25H49NO4	Stearoylcarnitine	L2	-	1.00	3.83	5.58	2.07
466.3115	-	-0.29258	4.09	C27H46O4S	Cholesterolsulfate	L2	Lipids: Sterol lipids	1.00	0.87	0.61	0.64
467.3012	+	-0.05581	5.48	C22H46NO7P	PC (14:0)	L2	Lipids: Glycerophospholipids	1.00	1.43	0.68	0.81
481.3534	+	0.347655	5.38	C24H52NO6P	PC (16:2)	L2	Lipids: Glycerophospholipids	1.00	0.76	0.67	0.68
523.2909	+	-0.18379	4.42	C24H46NO9P	PS (18:1)	L2	Lipids: Glycerophospholipids	1.00	1.72	0.73	0.78
525.3067	+	-0.03636	4.4	C24H48NO9P	PS (18:0)	L2	Lipids: Glycerophospholipids	1.00	1.71	0.71	0.73
537.5121	+	0.029172	4.58	C34H67NO3	SP (16:0)	L2	Lipids: Sphingolipids	1.00	1.17	0.81	0.74
598.3119	-	0.09071	4.44	C27H51O12P	PI (18:1)	L2	Lipids: Glycerophospholipids	1.00	1.57	0.69	0.79
600.3277	-	0.454354	4.42	C27H53O12P	PI (18:0)	L2	Lipids: Glycerophospholipids	1.00	1.34	0.80	0.78
674.4886	-	-0.03932	4.11	C37H71O8P	PA(34:1)	L2	Lipids: Glycerophospholipids	1.00	0.64	0.38	0.49
689.4995	+	-0.0279	4.58	C37H72NO8P	PE(32:1)	L2	Lipids: Glycerophospholipids	1.00	0.73	0.58	0.63
705.5306	+	-0.33223	4.8	C38H76NO8P	PC(30:0)	L2	Lipids: Glycerophospholipids	1.00	0.82	0.72	0.85
717.5309	+	0.061038	4.57	C39H76NO8P	PE(34:1)	L2	Lipids: Glycerophospholipids	1.00	0.74	0.61	0.66
719.5833	+	0.539418	4.78	C40H82NO7P	PC (32:2)	L2	Lipids: Glycerophospholipids	1.00	0.80	0.63	0.71
731.5464	+	-0.10583	4.78	C40H78NO8P	PC(32:1)	L2	Lipids: Glycerophospholipids	1.00	0.81	0.73	0.81
733.4892	+	-0.20987	4.16	C38H72NO10P	PS(32:1)	L2	Lipids: Glycerophospholipids	1.00	0.67	0.47	0.66
748.5256	-	0.220898	4.06	C40H77O10P	PG(34:1)	L2	Lipids: Glycerophospholipids	1.00	0.69	0.48	0.68
761.5206	+	-0.06133	4.17	C40H76NO10P	PS(34:1)	L2	Lipids: Glycerophospholipids	1.00	0.76	0.50	0.58
819.6153	+	1.358911	4.7	C48H86NO7P	PC(40:5)	L2	Lipids: Glycerophospholipids	1.00	1.46	1.03	1.05
820.5258	-	0.496579	4.02	C46H77O10P	PG(40:7)	L2	Lipids: Glycerophospholipids	1.00	1.86	1.48	1.41

879.5841	+	0.4514	4.17	C45H86NO13P	PI (36:0)			L2	Lipids: Glycerophospholipids	1.00	0.86	0.55	0.70

Chapter six

Conclusion and future work

6.1 Conclusion

The use of nanotechnology in medicine, especially in drug delivery, is already developing rapidly. Polymeric materials are widely adopted to serve as investigational nanomedicines. Even though the most frequently used polymers are usually biocompatible and degradable, their fabrication/formulation into nanomaterials can alter their physicochemical properties which may, in turn, alter their safety profiles. In attempts to understand the impact of these nanomaterials on living tissue, many biocompatibility assays have been previously developed, but none of them can fully describe the impact of nanomaterials comprehensively. As a consequence of the latest advances in NMR spectroscopy and MS spectrometry, the field of metabolomics is now enhancing the understanding of the impact of nanomaterials at the cellular and molecular level.

In this work, global metabolic profiling was used to assess the effects of plain NPs, drug loaded NPs and cationic polymer polyplexes on human cells. PLGA was selected to fabricate the nanomaterials because it is the most frequently used polymer in nanomedicine development, it is an FDA approved, biocompatible and biodegradable polymer.

In order to be able to follow the cellular uptake of the fabricated NPs, fully fluorescently labelled PLGA was synthesised. Three

different fluorophores were used as initiators in a single step ROP under solvent-free conditions. The synthesised PLGA polymers were able to self-assemble into highly bright NPs upon controlled nanoprecipitation. The cytotoxicity study showed that the fluorescently labelled polymers demonstrated a comparable toxicity profile to commercially available PLGA *in vitro*. The cellular uptake of NPs was observed using confocal microscopy and they were readily internalised by the THP-1 derived macrophages. The results of the aforementioned assays conclude that the synthesized polymers can be utilised to fabricate NPs for drug delivery purposes, with the ability to track them intracellularly. NPs' intestinal delivery in *C. elegans* nematodes was observed using fluorescent microscopy, the NPs were accumulating in the gastro-intestinal tract of the nematodes (Chapter 2).

Cell-based metabolomics approach was applied to investigate the biological impact of blank PLGA NPs which are repeatedly reported as safe. In addition, different coatings were applied to the NPs. THP-1 derived macrophages were used as a cell model because macrophages are the main responsible for NPs clearance from the body. The metabolomics method revealed that plain PLGA NPs and surface modified ones were well tolerated by the cell, nevertheless there were several metabolic changes that are comparable to what

was caused by some metal oxide NPs and other nanomaterials; exposure to plain and Pluronic coated PLGA NPs caused alterations in amino acid metabolism, which could tamper with urea cycle and induce signs of oxidative stress. Pluronic coated and PEGylated NPs have altered some glycerophospholipids lipids, which are core membrane component, such effects are could lead to growth arrest and membrane integrity alterations. PEGylated NPs had the least impact on the cellular metabolism in terms of metabolite levels fold changes, which agrees with the fact that PEGylation improves NPs biocompatibility. These findings are in alignment with the previous reports about PLGA NPs biocompatibility, nevertheless, the ability of the fabricated PLGA NPs with different surface functionalities to alter some main metabolic pathways including amino acid metabolism and glycerophospholipids synthesis indicate that these implications results from the physicochemical properties of the NPs themselves rather than their bulk counterparts, in other words, the biocompatibility of certain material does not mean that it will still be biocompatible once fabricated in the Nano range (Chapter 3).

Global metabolic profiling was used to compare the cellular responses of cancer cells and macrophages to free and polymer-encapsulated methotrexate. THP-1 derived macrophages and A549 lung carcinoma cells were exposed to subtoxic concentrations of

free MTX and MTX loaded NPs. The results showed that free MTX had higher impacts on the metabolome than MTX-loaded NPs in THP-1 derived macrophages. In these cells, MTX induced oxidative stress, a drop in glycolytic activity, reduction in the TCA cycle, and inhibition of nucleotide metabolism. In contrast, the effects of MTX-loaded NPs were limited to alteration of nucleotide metabolism and inhibition of TCA cycle. In comparison, A549 cancer cells were more susceptible to MTX-loaded NPs than to the free drug, in terms of purine synthesis suppression, which we suggest was linked to the different entry mechanisms for nanoparticles compared to free MTX, and lack of efflux pumps for the NPs. The results showed that administering the drug in the free form is more efficient if the target cells were phagocytic such as microphages, in case of administering a vaccine or a chemotherapeutic targeting a cancer in the immune system, loading the vaccine/drug into NPs might enhance uptake but decrease the activity. The presented work shows that metabolomics is a valuable analytical technique that can be used to understand mechanisms of action of drugs and formulations in various clinically important cell lines. (Chapter 4).

The global metabolic profiling approach was also applied to evaluate the impact of three cationic polymer plasmid DNA polyplexes hyperbranched poly lysine, poly lysine co histidine and

polyethyleneimine. Two lung cancer cell lines (A549 and H1299) were exposed to subtoxic concentrations of the polyplexes with equal polymer nitrogen to DNA phosphate ratio. Polyplexes made of hb-polyKH were the better tolerated than the other two polyplexes, whereas hb-polyK and PEI polyplexes tampered with energy metabolism and caused oxidative stress on both cell types, in addition, signs indicating apoptosis were detected in H1299 cells after the exposure to these two polyplexes. The results indicated a relation with the transfection efficiency of the polyplexes and their toxicities. (Chapter 5).

Finally, this work suggests that the metabolomics approach is a powerful safety assessment tool, as these assays were able to detect potential toxicity markers at sub-toxic concentrations where the traditional methods are insensitive. Also, this method provided insight into the molecular mechanism of toxicity and therapeutic effect alike, which might accelerate the design of more efficient and applicable delivery systems. Although metabolomics studies of delivery systems are still in their infancy, we believe that this approach is highly promising and in the future can enhance our understanding of the efficacy and safety of drug delivery materials.

6.2 Future work

This work showed the ability of cell-based metabolomics to assess the safety and up to certain extent the efficiency of polymer nanomedicine at the molecular level. This was done by mainly monitoring the changes in the hydrophilic metabolites. Despite the success of the used approach, adding global lipidomics to the analysis would make the assessment more comprehensive. That is because lipids functions are not limited to energy storage and membrane structure, but also have very important rules in signalling, metabolism and are precursor of several classes of hormones.

In vitro cell lines based assays are very important tools for toxicological studies, however, biological reaction to nanomaterials involves systemic effects that can be only assessed by animal testing. Applying the developed global metabolic profiling approach to test the impact of nanomaterials on both blood plasma and various tissues metabolomes is very important step before starting clinical trials. So, repeating the experiments on animal models would be a good next step to assess the safety and biocompatibility of the developed nanomaterials.

The results from chapter five indicated that the cationic polymer polyplexes have induced oxidative stress and inflammatory

response, and this effect was noted solely in A549 cells, in order to suppress the inflammatory response, both cell lines were treated with Aspirin, the treatment did not affect the transfection results of A549 cells significantly, however, the transfection efficiency in H1299 cells has increased 3-4 folds with the different polyplexes formulation, Figure 6-1, taking into account that H1299 cells did not show any inflammatory response, Aspirin seems to enhance the transfection efficiency by other means than its anti-inflammatory activity. In the future this effect will be thoroughly studied by a control vs treatment experiment whereas some cells will be treated with Aspirin alone and different transfection agents will be put into test. Since the major challenges facing gene delivery systems and limiting their FDA approval have been delivery of DNA to the target cells and duration of expression, Aspirin gene transfection enhancement will be worth assessing

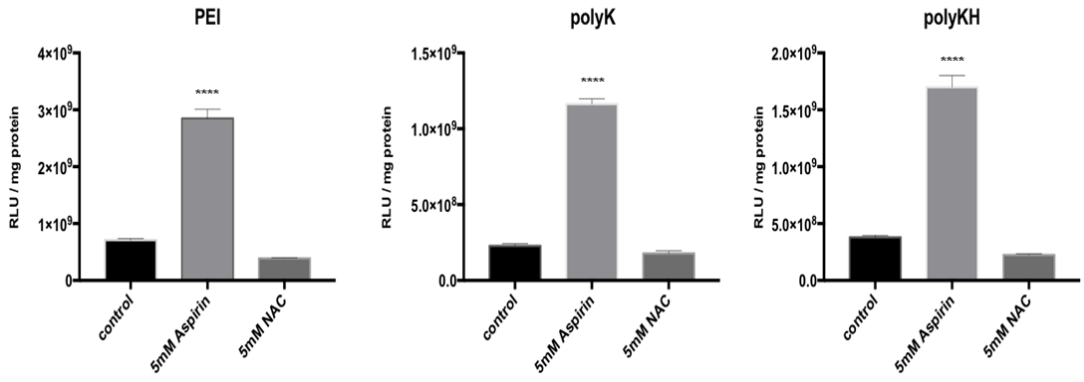


Figure 6-1: The effect of 5mM Aspirin treatment on the transfection efficiency of polycationic polymer polyplexes loaded with lecuferase coding plasmid DNA on H1299 cells. The cells were treated with the predetermied concentration of Aspirin for 1 hour prior to the transfection assay, the trasfection assay was curried out as dicribed in chapter 5.

5-Aaminofluorescein-PLGA (PLGA-5AF) was one of the synthesised fluorescently labelled polymers. FA-PLGA showed a pH-dependent linear increase in fluorescence intensity (Figure 6-1), this characteristic can be used to develop PLGA nanoparticles that can simultaneously deliver drugs to subcellular spaces and quantify changes in pH microenvironments, which is a critical biochemical marker that affects the success of a pharmaceutical formulations.

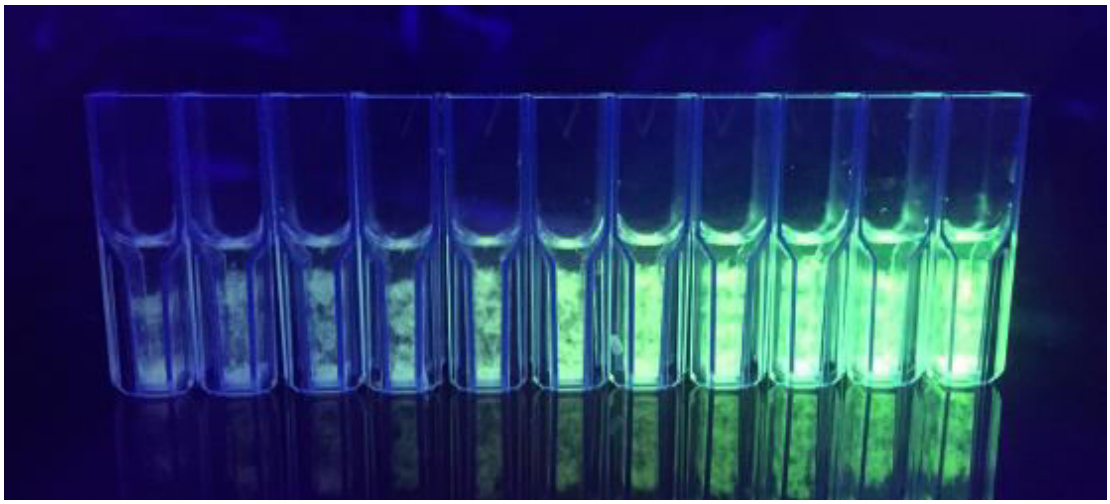


Figure 6-2: Increasing the fluorescence intensity of PLGA-FA NPs with increasing the pH from 4 to 9 left to right.

References

1. Pelaz B, Alexiou C, Alvarez-Puebla RA, Alves F, Andrews AM, Ashraf S, et al. Diverse Applications of Nanomedicine. ACS Nano. 2017;11(3):2313-81.

2. Yao C, Lu J. 1 - Introduction to nanomedicine. In: Webster TJ, editor. Nanomedicine: Woodhead Publishing; 2012. p. 3-19.

3. Wu X, Liu J, Yang L, Wang F. Photothermally controlled drug release system with high dose loading for synergistic chemo-photothermal therapy of multidrug resistance cancer. Colloids Surf B Biointerfaces. 2018;175:239-47.

4. Singh RK, Patel KD, Mahapatra C, Parthiban SP, Kim TH, Kim HW. Combinatory Cancer Therapeutics with Nanoceria-capped Mesoporous Silica Nanocarriers Through pH-triggered Drug Release and Redox Activity. ACS Appl Mater Interfaces. 2018.

5. Huang Y, Chen Q, Ma P, Song H, Ma X, Ma Y, et al. Facile Fabrication of Oxidation-Responsive Polymeric Nanoparticles for Effective Anticancer Drug Delivery. Mol Pharm. 2018.

6. Chinnaiyan SK, Karthikeyan D, Gadela VR. Combined synergetic potential of metformin loaded pectin-chitosan biohybrids nanoparticle for NIDDM. Int J Biol Macromol. 2018.

7. Fernández Fernández E, Santos-Carballal B, de Santi C, Ramsey JM, MacLoughlin R, Cryan S-A, et al. Biopolymer-Based Nanoparticles for Cystic Fibrosis Lung Gene Therapy Studies. Materials (Basel, Switzerland). 2018;11(1):122.

8. Pandey R, Sharma A, Zahoor A, Sharma S, Khuller GK, Prasad B. Poly (DL-lactide-co-glycolide) nanoparticle-based inhalable sustained drug delivery system for experimental tuberculosis. J Antimicrob Chemother. 2003;52(6):981-6.

9. Ehmann F, Sakai-Kato K, Duncan R, Ossa DHPdl, Pita R, Vidal J-M, et al. Next-generation nanomedicines and nanosimilars: EU regulators' initiatives relating to the development and evaluation of nanomedicines. Nanomedicine. 2013;8(5):849-56.

10. https://www.britishsocietynanomedicine.org/what-is-nanomedicine/. (accessed November 30, 2018).

11. Sanjuan-Alberte P, Alexander MR, Hague RJM, Rawson FJ. Electrochemically stimulating developments in bioelectronic medicine. Bioelectronic Medicine. 2018;4(1):1.

12. Duncan R, Gaspar R. Nanomedicine(s) under the microscope. Mol Pharm. 2011;8(6):2101-41.

13. Gaudin A, Andrieux K, Couvreur P. Nanomedicines and stroke: Toward translational research. Journal of Drug Delivery Science and Technology. 2015;30:278-99.

14. Wang X, Tu M, Yan K, Li P, Pang L, Gong Y, et al. Tri-functional polymeric nanocomposites incorporated with Fe3O4/iodine-containing rare earth complex for CT, MR, and optical imaging. ACS applied materials & interfaces. 2015.

15. Godin B, Sakamoto JH, Serda RE, Grattoni A, Bouamrani A, Ferrari M. Emerging applications of nanomedicine for the diagnosis and treatment of cardiovascular diseases. Trends in pharmacological sciences. 2010;31(5):199-205.

16. Sajja HK, East MP, Mao H, Wang YA, Nie S, Yang L. Development of multifunctional nanoparticles for targeted drug delivery and noninvasive imaging of therapeutic effect. Current drug discovery technologies. 2009;6(1):43-51.

17. Lu XY, Wu DC, Li ZJ, Chen GQ. Polymer nanoparticles. Prog Mol Biol Transl Sci. 2011;104:299-323.

18. Gonzalez-Paredes A, Sitia L, Ruyra A, Morris C, Wheeler GN, McArthur M, et al. Solid lipid nanoparticles for the delivery of anti-microbial oligonucleotides. Eur J Pharm Biopharm. 2018.

19. Lee Y, Fukushima S, Bae Y, Hiki S, Ishii T, Kataoka K. A Protein Nanocarrier from Charge-Conversion Polymer in Response to Endosomal pH. Journal of the American Chemical Society. 2007;129(17):5362-3.

20. Guo P. The emerging field of RNA nanotechnology. Nat Nanotechnol. 2010;5(12):833-42.

21. Baker SN, Baker GA. Luminescent carbon nanodots: emergent nanolights. Angew Chem Int Ed Engl. 2010;49(38):6726-44.

22. Parak WJ, Pellegrino T, Plank C. Labelling of cells with quantum dots. Nanotechnology. 2005;16(2):R9-R25.

23. Lin C-AJ, Yang T-Y, Lee C-H, Huang SH, Sperling RA, Zanella M, et al. Synthesis, Characterization, and Bioconjugation of Fluorescent Gold Nanoclusters toward Biological Labeling Applications. ACS Nano. 2009;3(2):395-401.

24. Alazzo A, Lovato T, Collins H, Taresco V, Stolnik S, Soliman M, et al. Structural variations in hyperbranched polymers prepared via thermal polycondensation of lysine and histidine and their effects on DNA delivery. Journal of Interdisciplinary Nanomedicine. 2018;3(2):38-54.

25. Ngoune R, Peters A, von Elverfeldt D, Winkler K, Putz G. Accumulating nanoparticles by EPR: A route of no return. J Control Release. 2016;238:58-70.

26. Theek B, Baues M, Ojha T, Möckel D, Veettil SK, Steitz J, et al. Sonoporation enhances liposome accumulation and penetration in tumors with low EPR. Journal of controlled release : official journal of the Controlled Release Society. 2016;231:77-85.

27. Bartlett DW, Su H, Hildebrandt IJ, Weber WA, Davis ME. Impact of tumor-specific targeting on the biodistribution and efficacy of siRNA nanoparticles measured by multimodality in vivo imaging. Proceedings of the National Academy of Sciences of the United States of America. 2007;104(39):15549-54.

28. Singh R, Lillard JW, Jr. Nanoparticle-based targeted drug delivery. Experimental and molecular pathology. 2009;86(3):215-23.

29. Bahrami B, Hojjat-Farsangi M, Mohammadi H, Anvari E, Ghalamfarsa G, Yousefi M, et al. Nanoparticles and targeted drug delivery in cancer therapy. Immunology Letters. 2017;190:64-83.

30. Yao J, Feng J, Chen J. External-stimuli responsive systems for cancer theranostic. Asian Journal of Pharmaceutical Sciences. 2016;11(5):585-95.

31. Cheah HY, Gallon E, Dumoulin F, Hoe SZ, Japundžić-Žigon N, Glumac S, et al. Near-Infrared Activatable Phthalocyanine–Poly-L-Glutamic Acid Conjugate: Enhanced in Vivo Safety and Antitumor Efficacy

toward an Effective Photodynamic Cancer Therapy. Molecular Pharmaceutics. 2018;15(7):2594-605.

32. Suri K, Wolfram J, Shen H, Ferrari M. Chapter 3 - Advances in Nanotechnology-Based Drug Delivery Platforms and Novel Drug Delivery Systems. In: Singh M, Salnikova M, editors. Novel Approaches and Strategies for Biologics, Vaccines and Cancer Therapies. San Diego: Academic Press; 2015. p. 41-58.

33. Pangalos MN, Schechter LE, Hurko O. Drug development for CNS disorders: strategies for balancing risk and reducing attrition. Nature reviews Drug discovery. 2007;6(7):521-32.

34. Sands MS, Haskins ME. CNS-directed gene therapy for lysosomal storage diseases. Acta Paediatr. 2008;97(457):22-7.

35. Xiao JF, Zhou B, Ressom HW. Metabolite identification and quantitation in LC-MS/MS-based metabolomics. TrAC Trends in Analytical Chemistry. 2012;32:1-14.

36. Ryu J-H, Chacko RT, Jiwpanich S, Bickerton S, Babu RP, Thayumanavan S. Self-Cross-Linked Polymer Nanogels: A Versatile Nanoscopic Drug Delivery Platform. Journal of the American Chemical Society. 2010;132(48):17227-35.

37. Danhier F, Ansorena E, Silva JM, Coco R, Le Breton A, Préat V. PLGA-based nanoparticles: An overview of biomedical applications. Journal of Controlled Release. 2012;161(2):505-22.

38. Lee JH, Yeo Y. Controlled drug release from pharmaceutical nanocarriers. Chemical Engineering Science. 2015;125:75-84.

39. Qi F, Wu J, Li H, Ma G. Recent research and development of PLGA/PLA microspheres/nanoparticles: A review in scientific and industrial aspects. Frontiers of Chemical Science and Engineering. 2018.

40. da Luz CM, Boyles MSP, Falagan-Lotsch P, Pereira MR, Tutumi HR, de Oliveira Santos E, et al. Poly-lactic acid nanoparticles (PLA-NP) promote physiological modifications in lung epithelial cells and are internalized by clathrin-coated pits and lipid rafts. Journal of Nanobiotechnology. 2017;15(1):11.

41. Prado LB, Huber SC, Barnab, #xe9, A, Bassora FDS, et al. Characterization of PCL and Chitosan Nanoparticles as Carriers of

Enoxaparin and Its Antithrombotic Effect in Animal Models of Venous Thrombosis. Journal of Nanotechnology. 2017;2017:7.

42. Ventola CL. Progress in Nanomedicine: Approved and Investigational Nanodrugs. P T. 2017;42(12):742-55.

43. Seigneuric R, Markey L, Nuyten DS, Dubernet C, Evelo CT, Finot E, et al. From nanotechnology to nanomedicine: applications to cancer research. Curr Mol Med. 2010;10(7):640-52.

44. Pang L, Zhu Y, Qin J, Zhao W, Wang J. Primary M1 macrophages as multifunctional carrier combined with PLGA nanoparticle delivering anticancer drug for efficient glioma therapy. Drug Deliv. 2018;25(1):1922-31.

45. Sokol MB, Nikolskaya ED, Yabbarov NG, Zenin VA, Faustova MR, Belov AV, et al. Development of novel PLGA nanoparticles with co-encapsulation of docetaxel and abiraterone acetate for a highly efficient delivery into tumor cells. J Biomed Mater Res B Appl Biomater. 2018.

46. Hung H-I, Klein OJ, Peterson SW, Rokosh SR, Osseiran S, Nowell NH, et al. PLGA nanoparticle encapsulation reduces toxicity while retaining the therapeutic efficacy of EtNBS-PDT in vitro. Scientific Reports. 2016;6:33234.

47. Zheng N, Lian B, Xu G, Liu X, Li X, Ji J. Development a subcellular semi-mechanism based pharmacokinetic/pharmacodynamic model to characterize paclitaxel effects delivered by polymeric micelles. J Pharm Sci. 2018.

48. Andima M, Costabile G, Isert L, Ndakala AJ, Derese S, Merkel OM. Evaluation of beta-Sitosterol Loaded PLGA and PEG-PLA Nanoparticles for Effective Treatment of Breast Cancer: Preparation, Physicochemical Characterization, and Antitumor Activity. Pharmaceutics. 2018;10(4).

49. Gulfam M, Matini T, Monteiro PF, Riva R, Collins H, Spriggs K, et al. Bioreducible cross-linked core polymer micelles enhance in vitro activity of methotrexate in breast cancer cells. Biomaterials Science. 2017;5(3):532-50.

50. Stuart MAC, Huck WTS, Genzer J, Müller M, Ober C, Stamm M, et al. Emerging applications of stimuli-responsive polymer materials. Nature Materials. 2010;9:101.

51. Alexis F, Pridgen E, Molnar LK, Farokhzad OC. Factors Affecting the Clearance and Biodistribution of Polymeric Nanoparticles. Molecular Pharmaceutics. 2008;5(4):505-15.

52. Hume DA, Ross IL, Himes SR, Sasmono RT, Wells CA, Ravasi T. The mononuclear phagocyte system revisited. Journal of leukocyte biology. 2002;72(4):621-7.

53. Aggarwal P, Hall JB, McLeland CB, Dobrovolskaia MA, McNeil SE. Nanoparticle interaction with plasma proteins as it relates to particle biodistribution, biocompatibility and therapeutic efficacy. Advanced Drug Delivery Reviews. 2009;61(6):428-37.

54. Cedervall T, Lynch I, Lindman S, Berggård T, Thulin E, Nilsson H, et al. Understanding the nanoparticle–protein corona using methods to quantify exchange rates and affinities of proteins for nanoparticles. Proceedings of the National Academy of Sciences. 2007;104(7):2050-5.

55. Sempf K, Arrey T, Gelperina S, Schorge T, Meyer B, Karas M, et al. Adsorption of plasma proteins on uncoated PLGA nanoparticles. European Journal of Pharmaceutics and Biopharmaceutics. 2013;85(1):53-60.

56. Moghimi SM, Hunter AC, Murray JC. Long-circulating and target-specific nanoparticles: theory to practice. Pharmacological reviews. 2001;53(2):283-318.

57. Frank MM, Fries LF. The role of complement in inflammation and phagocytosis. Immunology today. 1991;12(9):322-6.

58. Jokerst JV, Lobovkina T, Zare RN, Gambhir SS. Nanoparticle PEGylation for imaging and therapy. Nanomedicine (London, England). 2011;6(4):715-28.

59. Dong X, Mumper RJ. Nanomedicinal strategies to treat multidrug-resistant tumors: current progress. Nanomedicine (London, England). 2010;5(4):597-615.

60. Alakhova DY, Kabanov AV. Pluronics and MDR reversal: an update. Molecular pharmaceutics. 2014;11(8):2566-78.

61. Jackson JK, Springate CMK, Hunter WL, Burt HM. Neutrophil activation by plasma opsonized polymeric microspheres: inhibitory effect of Pluronic F127. Biomaterials. 2000;21(14):1483-91.

62. Njuguna J, Ansari F, Sachse S, Zhu H, Rodriguez VM. 1 - Nanomaterials, nanofillers, and nanocomposites: types and properties. In: Njuguna J, Pielichowski K, Zhu H, editors. Health and Environmental Safety of Nanomaterials: Woodhead Publishing; 2014. p. 3-27.

63. van Schooneveld MM, Vucic E, Koole R, Zhou Y, Stocks J, Cormode DP, et al. Improved biocompatibility and pharmacokinetics of silica nanoparticles by means of a lipid coating: a multimodality investigation. Nano letters. 2008;8(8):2517-25.

64. Krug HF. Nanosafety research--are we on the right track? Angew Chem Int Ed Engl. 2014;53(46):12304-19.

65. Xia T, Li N, Nel AE. Potential health impact of nanoparticles. Annual Review of Public Health2009. p. 137-50.

66. Hussain SM, Hess KL, Gearhart JM, Geiss KT, Schlager JJ. In vitro toxicity of nanoparticles in BRL 3A rat liver cells. Toxicology in Vitro. 2005;19(7):975-83.

67. Choi J, Wang NS. Nanoparticles in Biomedical Applications and Their Safety Concerns2011 2011-08-29.

68. Nel AE, Mädler L, Velegol D, Xia T, Hoek EMV, Somasundaran P, et al. Understanding biophysicochemical interactions at the nano-bio interface. Nature Materials. 2009;8(7):543-57.

69. Walczyk D, Bombelli FB, Monopoli MP, Lynch I, Dawson KA. What the cell "sees" in bionanoscience. Journal of the American Chemical Society. 2010;132(16):5761-8.

70. Hauck TS, Ghazani AA, Chan WCW. Assessing the effect of surface chemistry on gold nanorod uptake, toxicity, and gene expression in mammalian cells. Small. 2008;4(1):153-9.

71. Linse S, Cabaleiro-Lago C, Xue WF, Lynch I, Lindman S, Thulin E, et al. Nucleation of protein fibrillation by nanoparticles. Proceedings of the National Academy of Sciences of the United States of America. 2007;104(21):8691-6.

72. Leroueil PR, Berry SA, Duthie K, Han G, Rotello VM, McNerny DQ, et al. Wide varieties of cationic nanoparticles induce defects in supported lipid bilayers. Nano letters. 2008;8(2):420-4.

73. Navarro E, Baun A, Behra R, Hartmann NB, Filser J, Miao AJ, et al. Environmental behavior and ecotoxicity of engineered nanoparticles to algae, plants, and fungi. Ecotoxicology. 2008;17(5):372-86.

74. Øvrevik J, Låg M, Schwarze P, Refsnes M. p38 and Src-ERK1/2 pathways regulate crystalline silica-induced chemokine release in pulmonary epithelial cells. Toxicological Sciences. 2004;81(2):480-90.

75. Xia T, Kovochich M, Liong M, Mädler L, Gilbert B, Shi H, et al. Comparison of the mechanism of toxicity of zinc oxide and cerium oxide nanoparticles based on dissolution and oxidative stress properties. ACS Nano. 2008;2(10):2121-34.

76. Uchino T, Tokunaga H, Ando M, Utsumi H. Quantitative determination of OH radical generation and its cytotoxicity induced by TiO2-UVA treatment. Toxicology in Vitro. 2002;16(5):629-35.

77. Auffan M, Achouak W, Rose J, Roncato MA, Chanéac C, Waite DT, et al. Relation between the redox state of iron-based nanoparticles and their cytotoxicity toward Escherichia coli. Environmental Science and Technology. 2008;42(17):6730-5.

78. Gou N, Onnis-Hayden A, Gu AZ. Mechanistic toxicity assessment of nanomaterials by whole-cell-array stress genes expression analysis. Environmental Science and Technology. 2010;44(15):5964-70.

79. Tucci P, Porta G, Agostini M, Dinsdale D, Iavicoli I, Cain K, et al. Metabolic effects of TiO2 nanoparticles, a common component of sunscreens and cosmetics, on human keratinocytes. Cell Death Dis. 2013;4:e549.

80. Mariani V, Ponti J, Giudetti G, Broggi F, Marmorato P, Gioria S, et al. Online monitoring of cell metabolism to assess the toxicity of nanoparticles: the case of cobalt ferrite. Nanotoxicology. 2012;6(3):272-87.

81. Oliver SG, Winson MK, Kell DB, Baganz F. Systematic functional analysis of the yeast genome. Trends in Biotechnology. 1998;16(9):373-8.

82. Ramautar R, Mayboroda OA, Somsen GW, de Jong GJ. CE-MS for metabolomics: Developments and applications in the period 2008-2010. Electrophoresis. 2011;32(1):52-65.

83. Patti GJ, Yanes O, Siuzdak G. Innovation: Metabolomics: the apogee of the omics trilogy. Nat Rev Mol Cell Biol. 2012;13(4):263-9.

84. Wishart DS, Tzur D, Knox C, Eisner R, Guo AC, Young N, et al. HMDB: the Human Metabolome Database. Nucleic Acids Research. 2007;35(Database issue):D521-D6.

85. Han X, Jiang X. A review of lipidomic technologies applicable to sphingolipidomics and their relevant applications. European Journal of Lipid Science and Technology. 2009;111(1):39-52.

86. German JB, Hammock BD, Watkins SM. Metabolomics: building on a century of biochemistry to guide human health. Metabolomics : Official journal of the Metabolomic Society. 2005;1(1):3-9.

87. Ring J, Sommer C, Carmona-Gutierrez D, Ruckenstuhl C, Eisenberg T, Madeo F. The metabolism beyond programmed cell death in yeast. Experimental Cell Research. 2012;318(11):1193-200.

88. https://www.scopus.com. (accessed November 30, 2018.).

89. Theodoridis G, Gika HG, Wilson ID. LC-MS-based methodology for global metabolite profiling in metabonomics/metabolomics. Trac-Trends in Analytical Chemistry. 2008;27(3):251-60.

90. Lu W, Bennett BD, Rabinowitz JD. Analytical strategies for LC-MS-based targeted metabolomics. Journal of Chromatography B-Analytical Technologies in the Biomedical and Life Sciences. 2008;871(2):236-42.

91. Lenz EM, Wilson ID. Analytical strategies in metabonomics. Journal of Proteome Research. 2007;6(2):443-58.

92. Nicholson JK, Lindon JC. Systems biology - Metabonomics. Nature. 2008;455(7216):1054-6.

93. Want EJ, Masson P, Michopoulos F, Wilson ID, Theodoridis G, Plumb RS, et al. Global metabolic profiling of animal and human tissues via UPLC-MS. Nature Protocols. 2013;8(1):17-32.

94. Lee JH, Okuno Y, Cavagnero S. Sensitivity enhancement in solution NMR: emerging ideas and new frontiers. Journal of magnetic resonance (San Diego, Calif : 1997). 2014;241:18-31.

95. Emwas A-HM, Salek RM, Griffin JL, Merzaban J. NMR-based metabolomics in human disease diagnosis: applications, limitations, and recommendations. 2013;9(5):1048-72.

96. Emwas AH. The strengths and weaknesses of NMR spectroscopy and mass spectrometry with particular focus on metabolomics research. Methods Mol Biol. 2015;1277:161-93.

97. Cordeau E, Arnaudguilhem C, Bouyssiere B, Hagege A, Martinez J, Subra G, et al. Investigation of Elemental Mass Spectrometry in Pharmacology for Peptide Quantitation at Femtomolar Levels. PLoS One. 2016;11(6):e0157943.

98. Clarke CJ, Haselden JN. Metabolic profiling as a tool for understanding mechanisms of toxicity. Toxicologic pathology. 2008;36(1):140-7.

99. Huang MZ, Yuan CH, Cheng SC, Cho YT, Shiea J. Ambient ionization mass spectrometry. Annu Rev Anal Chem (Palo Alto Calif). 2010;3:43-65.

100. Wang H, Hanash S. Electrospray mass spectrometry for quantitative plasma proteome analysis. Methods in molecular biology (Clifton, NJ). 2009;564:227-42.

101. Furey A, Moriarty M, Bane V, Kinsella B, Lehane M. Ion suppression; A critical review on causes, evaluation, prevention and applications. Talanta. 2013;115:104-22.

102. Gowda GAN, Djukovic D. Overview of mass spectrometry-based metabolomics: opportunities and challenges. Methods in molecular biology (Clifton, NJ). 2014;1198:3-12.

103. Cai Y, Zhu ZJ. A High-Throughput Targeted Metabolomics Workflow for the Detection of 200 Polar Metabolites in Central Carbon Metabolism. Methods Mol Biol. 2019;1859:263-74.

104. Yumba Mpanga A, Siluk D, Jacyna J, Szerkus O, Wawrzyniak R, Markuszewski M, et al. Targeted metabolomics in bladder cancer: From analytical methods development and validation towards application to clinical samples. Anal Chim Acta. 2018;1037:188-99.

105. Ho J, Sharma A, Mandal R, Wishart DS, Wiebe C, Storsley L, et al. Detecting Renal Allograft Inflammation Using Quantitative Urine Metabolomics and CXCL10. Transplant Direct. 2016;2(6):e78.

106. Sawada Y, Akiyama K, Sakata A, Kuwahara A, Otsuki H, Sakurai T, et al. Widely targeted metabolomics based on large-scale MS/MS data for elucidating metabolite accumulation patterns in plants. Plant Cell Physiol. 2009;50(1):37-47.

107. Yang W, Mu T, Jiang J, Sun Q, Hou X, Sun Y, et al. Identification of Potential Biomarkers and Metabolic Profiling of Serum in Ovarian Cancer Patients Using UPLC/Q-TOF MS. Cell Physiol Biochem. 2018;51(3):1134-48.

108. Zhao H, Li X, Zhang D, Chen H, Chao Y, Wu K, et al. Integrative Bone Metabolomics-Lipidomics Strategy for Pathological Mechanism of Postmenopausal Osteoporosis Mouse Model. Sci Rep. 2018;8(1):16456.

109. Surrati A, Linforth R, Fisk ID, Sottile V, Kim D-H. Non-destructive characterisation of mesenchymal stem cell differentiation using LC-MS-based metabolite footprinting. Analyst. 2016;141(12):3776-87.

110. Zubarev RA, Makarov A. Orbitrap Mass Spectrometry. Analytical Chemistry. 2013;85(11):5288-96.

111. Grinfeld D, Monastyrskiy M, Makarov A. Control of Aberration and Space-Charge Effects in the Orbitrap Mass Analyzer. Microscopy and Microanalysis. 2015;21(S4):176-81.

112. Jones DM, Smith JR, Huck WTS, Alexander C. Variable Adhesion of Micropatterned Thermoresponsive Polymer Brushes: AFM Investigations of Poly(N-isopropylacrylamide) Brushes Prepared by Surface-Initiated Polymerizations. Advanced Materials. 2002;14(16):1130-4.

113. Wang WW, Balk M, Deng ZJ, Wischke C, Gossen M, Behl M, et al. Engineering biodegradable micelles of polyethylenimine-based amphiphilic block copolymers for efficient DNA and siRNA delivery. Journal of Controlled Release. 2016;242:71-9.

114. Breunig M, Lungwitz U, Liebl R, Goepferich A. Breaking up the correlation between efficacy and toxicity for nonviral gene delivery. Proceedings of the National Academy of Sciences of the United States of America. 2007;104(36):14454-9.

115. Cunliffe D, de las Heras Alarcón C, Peters V, Smith JR, Alexander C. Thermoresponsive Surface-Grafted Poly(N−isopropylacrylamide) Copolymers: Effect of Phase Transitions on Protein and Bacterial Attachment. Langmuir. 2003;19(7):2888-99.

116. Cunliffe D, Pennadam S, Alexander C. Synthetic and biological polymers––merging the interface. European Polymer Journal. 2004;40(1):5-25.

117. Saeed AO, Dey S, Howdle SM, Thurecht KJ, Alexander C. One-pot controlled synthesis of biodegradable and biocompatible co-polymer micelles. Journal of Materials Chemistry. 2009;19(26):4529-35.

118. Louzao I, Koch B, Taresco V, Ruiz-Cantu L, Irvine DJ, Roberts CJ, et al. Identification of Novel "Inks" for 3D Printing Using High-Throughput Screening: Bioresorbable Photocurable Polymers for Controlled Drug Delivery. ACS Applied Materials & Interfaces. 2018;10(8):6841-8.

119. Dhawan A, Sharma V. Toxicity assessment of nanomaterials: methods and challenges. Analytical and bioanalytical chemistry. 2010;398(2):589-605.

120. Klaper R, Arndt D, Bozich J, Dominguez G. Molecular interactions of nanomaterials and organisms: defining biomarkers for toxicity and high-throughput screening using traditional and next-generation sequencing approaches. Analyst. 2014;139(5):882-95.

121. Patti GJ, Yanes O, Siuzdak G. Innovation: Metabolomics: the apogee of the omics trilogy. Nat Rev Mol Cell Biol. 2012;13(4):263-9.

122. Keun HC. Metabonomic modeling of drug toxicity. Pharmacol Ther. 2006;109(1-2):92-106.

123. Bain JR, Stevens RD, Wenner BR, Ilkayeva O, Muoio DM, Newgard CB. Metabolomics applied to diabetes research: moving from information to knowledge. Diabetes. 2009;58(11):2429-43.

124. Beckonert O, Keun HC, Ebbels TM, Bundy J, Holmes E, Lindon JC, et al. Metabolic profiling, metabolomic and metabonomic procedures for NMR spectroscopy of urine, plasma, serum and tissue extracts. Nat Protoc. 2007;2(11):2692-703.

125. Fiehn O. Metabolomics--the link between genotypes and phenotypes. Plant Mol Biol. 2002;48(1-2):155-71.

126. Lv M, Huang W, Chen Z, Jiang H, Chen J, Tian Y, et al. Metabolomics techniques for nanotoxicity investigations. Bioanalysis. 2015;7(12):1527-44.

127. Taylor NS, Merrifield R, Williams TD, Chipman JK, Lead JR, Viant MR. Molecular toxicity of cerium oxide nanoparticles to the freshwater alga Chlamydomonas reinhardtii is associated with supra-environmental exposure concentrations. Nanotoxicology. 2015:1-10.

128. Li L, Wu H, Ji C, van Gestel CA, Allen HE, Peijnenburg WJ. A metabolomic study on the responses of daphnia magna exposed to silver nitrate and coated silver nanoparticles. Ecotoxicology and environmental safety. 2015;119:66-73.

129. Carrola J, Bastos V, Ferreira de Oliveira JMP, Oliveira H, Santos C, Gil AM, et al. Insights into the impact of silver nanoparticles on human keratinocytes metabolism through NMR metabolomics. Archives of Biochemistry and Biophysics. 2015.

130. Garcia-Contreras R, Sugimoto M, Umemura N, Kaneko M, Hatakeyama Y, Soga T, et al. Alteration of metabolomic profiles by titanium dioxide nanoparticles in human gingivitis model. Biomaterials. 2015;57:33-40.

131. Song Y, Zhao R, Hu Y, Hao F, Li N, Nie G, et al. Assessment of the Biological Effects of a Multifunctional Nano-Drug-Carrier and Its Encapsulated Drugs. Journal of Proteome Research. 2015;14(12):5193-201.

132. Saborano R, Wongpinyochit T, Totten JD, Johnston BF, Seib FP, Duarte IF. Metabolic Reprogramming of Macrophages Exposed to Silk, Poly(lactic-co-glycolic acid), and Silica Nanoparticles. Advanced Healthcare Materials. 2017;6(14):1601240.

133. Armiñán A, Palomino-Schätzlein M, Deladriere C, Arroyo-Crespo JJ, Vicente-Ruiz S, Vicent MJ, et al. Metabolomics facilitates the discrimination of the specific anti-cancer effects of free- and polymer-conjugated doxorubicin in breast cancer models. Biomaterials. 2018;162:144-53.

134. Creek DJ, Jankevics A, Breitling R, Watson DG, Barrett MP, Burgess KE. Toward global metabolomics analysis with hydrophilic interaction liquid chromatography-mass spectrometry: improved metabolite identification by retention time prediction. Anal Chem. 2011;83(22):8703-10.

135. Surrati A, Linforth R, Fisk ID, Sottile V, Kim DH. Non-destructive characterisation of mesenchymal stem cell differentiation using LC-MS-based metabolite footprinting. Analyst. 2016;141(12):3776-87.

136. Xu P, Gullotti E, Tong L, Highley CB, Errabelli DR, Hasan T, et al. Intracellular drug delivery by poly(lactic-co-glycolic acid) nanoparticles, revisited. Molecular pharmaceutics. 2009;6(1):190-201.

137. Martins C, Sousa F, Araujo F, Sarmento B. Functionalizing PLGA and PLGA Derivatives for Drug Delivery and Tissue Regeneration Applications. Advanced Healthcare Materials. 2018;7(1).

138. Ding DW, Zhu QD. Recent advances of PLGA micro/nanoparticles for the delivery of biomacromolecular therapeutics. Materials Science & Engineering C-Materials for Biological Applications. 2018;92:1041-60.

139. Mir M, Ahmed N, Rehman AU. Recent applications of PLGA based nanostructures in drug delivery. Colloids and Surfaces B-Biointerfaces. 2017;159:217-31.

140. Man DKW, Casettari L, Cesp M, Bonacucina G, Palmieri GF, Sze SCW, et al. Oleanolic Acid Loaded PEGylated PLA and PLGA Nanoparticles with Enhanced Cytotoxic Activity against Cancer Cells. Molecular Pharmaceutics. 2015;12(6):2112-25.

141. Fu J, Sun F, Liu W, Liu Y, Gedam M, Hu Q, et al. Subconjunctival Delivery of Dorzolamide-Loaded Poly(ether-anhydride) Microparticles Produces Sustained Lowering of Intraocular Pressure in Rabbits. Mol Pharm. 2016;13(9):2987-95.

142. Thomas C, Rawat A, Hope-Weeks L, Ahsan F. Aerosolized PLA and PLGA Nanoparticles Enhance Humoral, Mucosal and Cytokine Responses to Hepatitis B Vaccine. Molecular Pharmaceutics. 2011;8(2):405-15.

143. Cun D, Jensen DK, Maltesen MJ, Bunker M, Whiteside P, Scurr D, et al. High loading efficiency and sustained release of siRNA encapsulated in PLGA nanoparticles: quality by design optimization and characterization. European Journal of Pharmaceutics and Biopharmaceutics. 2011;77(1):26-35.

144. Wang W, Liang H, Cheikh Al Ghanami R, Hamilton L, Fraylich M, Shakesheff KM, et al. Biodegradable Thermoresponsive Microparticle Dispersions for Injectable Cell Delivery Prepared Using a Single-Step Process. Advanced Materials. 2009;21(18):1809-13.

145. Qiao MX, Chen DW, Ma XC, Liu YJ. Injectable biodegradable temperature-responsive PLGA-PEG-PLGA copolymers: Synthesis and effect of copolymer composition on the drug release from the copolymer-

based hydrogels. International Journal Of Pharmaceutics. 2005;294(1-2):103-12.

146. Fu C, Bai HT, Zhu JQ, Niu ZH, Wang Y, Li JN, et al. Enhanced cell proliferation and osteogenic differentiation in electrospun PLGA/hydroxyapatite nanofibre scaffolds incorporated with graphene oxide. Plos One. 2017;12(11).

147. Michalet X, Pinaud FF, Bentolila LA, Tsay JM, Doose S, Li JJ, et al. Quantum dots for live cells, in vivo imaging, and diagnostics. Science. 2005;307(5709):538-44.

148. Escobedo JO, Rusin O, Lim S, Strongin RM. NIR dyes for bioimaging applications. Curr Opin Chem Biol. 2010;14(1):64-70.

149. Artzi N, Oliva N, Puron C, Shitreet S, Artzi S, bon Ramos A, et al. In vivo and in vitro tracking of erosion in biodegradable materials using non-invasive fluorescence imaging. Nat Mater. 2011;10(9):704-9.

150. Jaiswal JK, Mattoussi H, Mauro JM, Simon SM. Long-term multiple color imaging of live cells using quantum dot bioconjugates. Nat Biotechnol. 2003;21(1):47-51.

151. Zhang Y, Yang J. Design Strategies for Fluorescent Biodegradable Polymeric Biomaterials. J Mater Chem B. 2013;1(2):132-48.

152. Hu J, Guo J, Xie Z, Shan D, Gerhard E, Qian G, et al. Fluorescence imaging enabled poly(lactide-co-glycolide). Acta biomaterialia. 2016;29:307-19.

153. Panyam J, Labhasetwar V. Dynamics of endocytosis and exocytosis of poly(D,L-lactide-co-glycolide) nanoparticles in vascular smooth muscle cells. Pharm Res. 2003;20(2):212-20.

154. Kakde D, Powell LG, Bansal KK, Howdle S, Irvine D, Mantovani G, et al. Synthesis, characterization and evaluation of in vitro toxicity in hepatocytes of linear polyesters with varied aromatic and aliphatic co-monomers. Journal of Controlled Release. 2016;244:214-28.

155. Abdel-Mottaleb MMA, Beduneau A, Pellequer Y, Lamprecht A. Stability of fluorescent labels in PLGA polymeric nanoparticles: Quantum dots versus organic dyes. International Journal of Pharmaceutics. 2015;494(1):471-8.

156. Chauhan VM, Burnett GR, Aylott JW. Dual-fluorophore ratiometric pH nanosensor with tuneable pK(a) and extended dynamic range. Analyst. 2011;136(9):1799-801.

157. Horisawa E, Kubota K, Tuboi I, Sato K, Yamamoto H, Takeuchi H, et al. Size-dependency of DL-lactide/glycolide copolymer particulates for intra-articular delivery system on phagocytosis in rat synovium. Pharm Res. 2002;19(2):132-9.

158. Weiss B, Schaefer UF, Zapp J, Lamprecht A, Stallmach A, Lehr CM. Nanoparticles made of fluorescence-labelled Poly(L-lactide-co-glycolide): preparation, stability, and biocompatibility. J Nanosci Nanotechnol. 2006;6(9-10):3048-56.

159. Ratzinger G, Fillafer C, Kerleta V, Wirth M, Gabor F. The role of surface functionalization in the design of PLGA micro-and nanoparticles. Critical Reviews™ in Therapeutic Drug Carrier Systems. 2010;27(1).

160. Brenner S. Nobel lecture. Nature's gift to science. Biosci Rep. 2003;23(5-6):225-37.

161. Brenner S. The genetics of Caenorhabditis elegans. Genetics. 1974;77(1):71-94.

162. Leung MCK, Williams PL, Benedetto A, Au C, Helmcke KJ, Aschner M, et al. Caenorhabditis elegans: an emerging model in biomedical and environmental toxicology. Toxicological sciences : an official journal of the Society of Toxicology. 2008;106(1):5-28.

163. Colmenares D, Sun Q, Shen P, Yue Y, McClements DJ, Park Y. Delivery of dietary triglycerides to Caenorhabditis elegans using lipid nanoparticles: Nanoemulsion-based delivery systems. Food Chem. 2016;202:451-7.

164. Schwach G, Coudane J, Engel R, Vert M. More about the polymerization of lactides in the presence of stannous octoate. Journal of Polymer Science Part A: Polymer Chemistry. 1997;35(16):3431-40.

165. Labet M, Thielemans W. Synthesis of polycaprolactone: a review. Chemical Society Reviews. 2009;38(12):3484-504.

166. Fessi H, Puisieux F, Devissaguet JP, Ammoury N, Benita S. Nanocapsule formation by interfacial polymer deposition following solvent displacement. International Journal of Pharmaceutics. 1989;55(1):R1-R4.

167. Chauhan VM, Orsi G, Brown A, Pritchard DI, Aylott JW. Mapping the Pharyngeal and Intestinal pH of Caenorhabditis elegans and Real-Time Luminal pH Oscillations Using Extended Dynamic Range pH-Sensitive Nanosensors. Acs Nano. 2013;7(6):5577-87.

168. Conte C, Mastrotto F, Taresco V, Tchoryk A, Quaglia F, Stolnik S, et al. Enhanced uptake in 2D- and 3D- lung cancer cell models of redox responsive PEGylated nanoparticles with sensitivity to reducing extra- and intracellular environments. Journal of Controlled Release. 2018;277:126-41.

169. Redhead HM, Davis SS, Illum L. Drug delivery in poly(lactide-co-glycolide) nanoparticles surface modified with poloxamer 407 and poloxamine 908: in vitro characterisation and in vivo evaluation. Journal of Controlled Release. 2001;70(3):353-63.

170. Auwerx J. THE HUMAN LEUKEMIA-CELL LINE, THP-1 - A MULTIFACETED MODEL FOR THE STUDY OF MONOCYTE-MACROPHAGE DIFFERENTIATION. Experientia. 1991;47(1):22-31.

171. Peng Z-H, Kopeček J. Enhancing Accumulation and Penetration of HPMA Copolymer–Doxorubicin Conjugates in 2D and 3D Prostate Cancer Cells via iRGD Conjugation with an MMP-2 Cleavable Spacer. Journal of the American Chemical Society. 2015;137(21):6726-9.

172. Basuki JS, Duong HTT, Macmillan A, Erlich RB, Esser L, Akerfeldt MC, et al. Using Fluorescence Lifetime Imaging Microscopy to Monitor Theranostic Nanoparticle Uptake and Intracellular Doxorubicin Release. Acs Nano. 2013;7(11):10175-89.

173. Zhao Y-X, Shaw A, Zeng X, Benson E, Nystrom AM, Hogberg B. DNA Origami Delivery System for Cancer Therapy with Tunable Release Properties. Acs Nano. 2012;6(10):8684–91.

174. Wibroe PP, Ahmadvand D, Oghabian MA, Yaghmur A, Moghimi SM. An integrated assessment of morphology, size, and complement activation of the PEGylated liposomal doxorubicin products Doxil®, Caelyx®, DOXOrubicin, and SinaDoxosome. Journal of Controlled Release. 2016;221:1-8.

175. Vicent MJ, Ringsdorf H, Duncan R. Polymer therapeutics: Clinical applications and challenges for development. Advanced Drug Delivery Reviews. 2009;61(13):1117-20.

176. Dhal PK, Polomoscanik SC, Avila LZ, Holmes-Farley SR, Miller RJ. Functional polymers as therapeutic agents: Concept to market place. Advanced Drug Delivery Reviews. 2009;61(13):1121-30.

177. Ventola CL. Progress in Nanomedicine: Approved and Investigational Nanodrugs. P & T : a peer-reviewed journal for formulary management. 2017;42(12):742-55.

178. Nair LS, Laurencin CT. Polymers as biomaterials for tissue engineering and controlled drug delivery. Adv Biochem Eng Biotechnol. 2006;102:47-90.

179. Makadia HK, Siegel SJ. Poly Lactic-co-Glycolic Acid (PLGA) as Biodegradable Controlled Drug Delivery Carrier. Polymers. 2011;3(3):1377-97.

180. Bala I, Hariharan S, Kumar MN. PLGA nanoparticles in drug delivery: the state of the art. Crit Rev Ther Drug Carrier Syst. 2004;21(5):387-422.

181. Azizi M, Farahmandghavi F, Joghataei M, Zandi M, Imani M, Bakhtiary M, et al. Fabrication of protein-loaded PLGA nanoparticles: effect of selected formulation variables on particle size and release profile. Journal of Polymer Research. 2013;20(4):1-14.

182. Nafee N, Taetz S, Schneider M, Schaefer UF, Lehr C-M. Chitosan-coated PLGA nanoparticles for DNA/RNA delivery: effect of the formulation parameters on complexation and transfection of antisense oligonucleotides. Nanomedicine: Nanotechnology, Biology and Medicine. 2007;3(3):173-83.

183. Dhawan A, Sharma V, Parmar D. Nanomaterials: A challenge for toxicologists. Nanotoxicology. 2009;3(1):1-9.

184. Anreddy RN, Yellu NR, Devarakonda KR. Oxidative biomarkers to assess the nanoparticle-induced oxidative stress. Methods Mol Biol. 2013;1028:205-19.

185. Siddiqui MA, Alhadlaq HA, Ahmad J, Al-Khedhairy AA, Musarrat J, Ahamed M. Copper oxide nanoparticles induced mitochondria mediated apoptosis in human hepatocarcinoma cells. PLoS One. 2013;8(8):e69534.

186. Trouiller B, Reliene R, Westbrook A, Solaimani P, Schiestl RH. Titanium dioxide nanoparticles induce DNA damage and genetic

instability in vivo in mice. Cancer research. 2009;69(22):10.1158/0008-5472.CAN-09-2496.

187. Gioria S, Lobo Vicente J, Barboro P, La Spina R, Tomasi G, Urbán P, et al. A combined proteomics and metabolomics approach to assess the effects of gold nanoparticles in vitro. Nanotoxicology. 2016;10(6):736-48.

188. Hirsch C, Roesslein M, Krug HF, Wick P. Nanomaterial cell interactions: are current in vitro tests reliable? Nanomedicine. 2011;6(5):837-47.

189. Kong B, Seog JH, Graham LM, Lee SB. Experimental considerations on the cytotoxicity of nanoparticles. Nanomedicine (London, England). 2011;6(5):929-41.

190. Jiao G, Li X, Zhang N, Qiu J, Xu H, Liu S. Metabolomics study on the cytotoxicity of graphene. RSC Advances. 2014;4(84):44712-7.

191. Hadrup N, Lam HR, Loeschner K, Mortensen A, Larsen EH, Frandsen H. Nanoparticulate silver increases uric acid and allantoin excretion in rats, as identified by metabolomics. J Appl Toxicol. 2012;32(11):929-33.

192. Feng J, Li J, Wu H, Chen Z. Metabolic responses of HeLa cells to silica nanoparticles by NMR-based metabolomic analyses. Metabolomics. 2013;9(4):874-86.

193. Ratnasekhar C, Sonane M, Satish A, Mudiam MK. Metabolomics reveals the perturbations in the metabolome of Caenorhabditis elegans exposed to titanium dioxide nanoparticles. Nanotoxicology. 2015;9(8):994-1004.

194. Lindeque JZ, Matthyser A, Mason S, Louw R, Taute CJF. Metabolomics reveals the depletion of intracellular metabolites in HepG2 cells after treatment with gold nanoparticles. Nanotoxicology. 2018;12(3):251-62.

195. Wu B, Zhu L, Le XC. Metabolomics analysis of TiO2 nanoparticles induced toxicological effects on rice (Oryza sativa L.). Environmental Pollution. 2017;230:302-10.

196. Chavez Soria NG, Montes A, Bisson MA, Atilla-Gokcumen GE, Aga DS. Mass spectrometry-based metabolomics to assess uptake of silver

nanoparticles by Arabidopsis thaliana. Environmental Science: Nano. 2017;4(10):1944-53.

197. Havel HA. Where Are the Nanodrugs? An Industry Perspective on Development of Drug Products Containing Nanomaterials. AAPS J. 2016;18(6):1351-3.

198. Chan JM, Valencia PM, Zhang L, Langer R, Farokhzad OC. Polymeric nanoparticles for drug delivery. Methods Mol Biol. 2010;624:163-75.

199. Meiser J, Krämer L, Sapcariu SC, Battello N, Ghelfi J, D'Herouel AF, et al. Pro-inflammatory Macrophages Sustain Pyruvate Oxidation through Pyruvate Dehydrogenase for the Synthesis of Itaconate and to Enable Cytokine Expression. The Journal of biological chemistry. 2016;291(8):3932-46.

200. Grabowski N, Hillaireau H, Vergnaud J, Santiago LA, Kerdine-Romer S, Pallardy M, et al. Toxicity of surface-modified PLGA nanoparticles toward lung alveolar epithelial cells. Int J Pharm. 2013;454(2):686-94.

201. Jones CF, Grainger DW. In vitro assessments of nanomaterial toxicity. Advanced Drug Delivery Reviews. 2009;61(6):438-56.

202. Menon JU, Kona S, Wadajkar AS, Desai F, Vadla A, Nguyen KT. Effects of surfactants on the properties of PLGA nanoparticles. J Biomed Mater Res A. 2012;100(8):1998-2005.

203. Batrakova EV, Li S, Elmquist WF, Miller DW, Alakhov VY, Kabanov AV. Mechanism of sensitization of MDR cancer cells by Pluronic block copolymers: Selective energy depletion. British journal of cancer. 2001;85(12):1987-97.

204. Erbetta CDAC, Alves RJ, Resende JMe, Freitas RFdS, Sousa RGd. Synthesis and Characterization of Poly(D,L-Lactide-co-Glycolide) Copolymer. Journal of Biomaterials and Nanobiotechnology. 2012;Vol.03No.02:18.

205. Li T, Ci T, Chen L, Yu L, Ding J. Salt-induced reentrant hydrogel of poly(ethylene glycol)-poly(lactide-co-glycolide) block copolymers. Polymer Chemistry. 2014;5(3):979-91.

206. Park EK, Jung HS, Yang HI, Yoo MC, Kim C, Kim KS. Optimized THP-1 differentiation is required for the detection of responses to weak stimuli. Inflamm Res. 2007;56(1):45-50.

207. Want EJ, Wilson ID, Gika H, Theodoridis G, Plumb RS, Shockcor J, et al. Global metabolic profiling procedures for urine using UPLC-MS. Nat Protoc. 2010;5(6):1005-18.

208. Tautenhahn R, Böttcher C, Neumann S. Highly sensitive feature detection for high resolution LC/MS. BMC Bioinformatics. 2008;9:504-.

209. Scheltema RA, Jankevics A, Jansen RC, Swertz MA, Breitling R. PeakML/mzMatch: a file format, Java library, R library, and tool-chain for mass spectrometry data analysis. Anal Chem. 2011;83(7):2786-93.

210. Creek DJ, Jankevics A, Burgess KE, Breitling R, Barrett MP. IDEOM: an Excel interface for analysis of LC-MS-based metabolomics data. Bioinformatics. 2012;28(7):1048-9.

211. Sumner LW, Amberg A, Barrett D, Beale MH, Beger R, Daykin CA, et al. Proposed minimum reporting standards for chemical analysis Chemical Analysis Working Group (CAWG) Metabolomics Standards Initiative (MSI). Metabolomics : Official journal of the Metabolomic Society. 2007;3(3):211-21.

212. Sumner LW, Lei Z, Nikolau BJ, Saito K, Roessner U, Trengove R. Proposed quantitative and alphanumeric metabolite identification metrics. Metabolomics. 2014;10(6):0.

213. Boccard J, Rutledge DN. A consensus orthogonal partial least squares discriminant analysis (OPLS-DA) strategy for multiblock Omics data fusion. Analytica Chimica Acta. 2013;769:30-9.

214. Xia J, Sinelnikov IV, Han B, Wishart DS. MetaboAnalyst 3.0--making metabolomics more meaningful. Nucleic Acids Res. 2015;43(W1):W251-7.

215. Kanehisa M, Goto S, Sato Y, Kawashima M, Furumichi M, Tanabe M. Data, information, knowledge and principle: back to metabolism in KEGG. Nucleic Acids Res. 2014;42(Database issue):D199-205.

216. Barnes TJ, Prestidge CA. PEO-PPO-PEO block copolymers at the emulsion droplet-water interface. Langmuir. 2000;16(9):4116-21.

217. Xu J, Hu F-L, Wang W, Wan X-C, Bao G-H. Investigation on biochemical compositional changes during the microbial fermentation process of Fu brick tea by LC–MS based metabolomics. Food Chemistry. 2015;186:176-84.

218. Newsholme P, Procopio J, Lima MM, Pithon-Curi TC, Curi R. Glutamine and glutamate--their central role in cell metabolism and function. Cell Biochem Funct. 2003;21(1):1-9.

219. Wu G. Amino acids: metabolism, functions, and nutrition. Amino Acids. 2009;37(1):1-17.

220. Visek WJ. Arginine needs, physiological state and usual diets. A reevaluation. The Journal of nutrition. 1986;116(1):36-46.

221. Morris SM, Jr. Arginine metabolism: boundaries of our knowledge. J Nutr. 2007;137(6 Suppl 2):1602S-9S.

222. Tapiero H, Mathé G, Couvreur P, Tew KD. I. Arginine. Biomedicine & Pharmacotherapy. 2002;56(9):439-45.

223. Du L, Miao X, Jia H, Gao Y, Liu K, Zhang X, et al. Detection of nitric oxide in macrophage cells for the assessment of the cytotoxicity of gold nanoparticles. Talanta. 2012;101(Supplement C):11-6.

224. Wu G, Morris SM. Arginine metabolism: nitric oxide and beyond. Biochemical Journal. 1998;336(Pt 1):1-17.

225. Morris Jr SM. Recent advances in arginine metabolism: roles and regulation of the arginases. British Journal of Pharmacology. 2009;157(6):922-30.

226. Wood PL, Khan MA, Moskal JR. The concept of "aldehyde load" in neurodegenerative mechanisms: Cytotoxicity of the polyamine degradation products hydrogen peroxide, acrolein, 3-aminopropanal, 3-acetamidopropanal and 4-aminobutanal in a retinal ganglion cell line. Brain Research. 2007;1145:150-6.

227. Radosavac D, Graf P, Polidori MC, Sies H, Stahl W. Tocopherol metabolites 2, 5, 7, 8-tetramethyl-2-(2'-carboxyethyl)-6-hydroxychroman (alpha-CEHC) and 2, 7, 8-trimethyl-2-(2'-carboxyethyl)-6-hydroxychroman (gamma-CEHC) in human serum after a single dose of natural vitamin E. Eur J Nutr. 2002;41(3):119-24.

228. van Meer G, Voelker DR, Feigenson GW. Membrane lipids: where they are and how they behave. Nature reviews Molecular cell biology. 2008;9(2):112-24.

229. Carrola J, Bastos V, Ferreira de Oliveira JM, Oliveira H, Santos C, Gil AM, et al. Insights into the impact of silver nanoparticles on human keratinocytes metabolism through NMR metabolomics. Arch Biochem Biophys. 2016;589:53-61.

230. Haase A, Arlinghaus HF, Tentschert J, Jungnickel H, Graf P, Mantion A, et al. Application of laser postionization secondary neutral mass spectrometry/time-of-flight secondary ion mass spectrometry in nanotoxicology: visualization of nanosilver in human macrophages and cellular responses. ACS Nano. 2011;5(4):3059-68.

231. Suk JS, Xu Q, Kim N, Hanes J, Ensign LM. PEGylation as a strategy for improving nanoparticle-based drug and gene delivery. Advanced drug delivery reviews. 2016;99(Pt A):28-51.

232. Abbina S, Parambath A. 14 - PEGylation and its alternatives: A summary. In: Parambath A, editor. Engineering of Biomaterials for Drug Delivery Systems: Woodhead Publishing; 2018. p. 363-76.

233. Wojtuszkiewicz A, Peters GJ, van Woerden NL, Dubbelman B, Escherich G, Schmiegelow K, et al. Methotrexate resistance in relation to treatment outcome in childhood acute lymphoblastic leukemia. J Hematol Oncol. 2015;8:61.

234. Lin Y, Gerson SL. Chapter 26 - Clinical Trials Using LV-P140K-MGMT for Gliomas. In: Lattime EC, Gerson SL, editors. Gene Therapy of Cancer (Third Edition). San Diego: Academic Press; 2014. p. 379-91.

235. Quéméneur L, Gerland L-M, Flacher M, Ffrench M, Revillard J-P, Genestier L. Differential Control of Cell Cycle, Proliferation, and Survival of Primary T Lymphocytes by Purine and Pyrimidine Nucleotides. The Journal of Immunology. 2003;170(10):4986.

236. Lonnerholm G, Valsecchi MG, De Lorenzo P, Schrappe M, Hovi L, Campbell M, et al. Pharmacokinetics of high-dose methotrexate in infants treated for acute lymphoblastic leukemia. Pediatr Blood Cancer. 2009;52(5):596-601.

237. Canellos GP, Skarin AT, Rosenthal DS, Moloney WC, Frei E, 3rd. Methotrexate as a single agent and in combination chemotherapy for the

treatment of non-Hodgkin's lymphoma of unfavorable histology. Cancer Treat Rep. 1981;65 Suppl 1:125-9.

238. van Dalen EC, de Camargo B. Methotrexate for high-grade osteosarcoma in children and young adults. Cochrane Database Syst Rev. 2009(1):CD006325.

239. Singh R, Fouladi-Nashta AA, Li D, Halliday N, Barrett DA, Sinclair KD. Methotrexate induced differentiation in colon cancer cells is primarily due to purine deprivation. J Cell Biochem. 2006;99(1):146-55.

240. Mikkelsen TS, Thorn CF, Yang JJ, Ulrich CM, French D, Zaza G, et al. PharmGKB summary: methotrexate pathway. Pharmacogenet Genomics. 2011;21(10):679-86.

241. Wang Z, Chen ZHE, Yang S, Wang YU, Yu L, Zhang B, et al. (1)H NMR-based metabolomic analysis for identifying serum biomarkers to evaluate methotrexate treatment in patients with early rheumatoid arthritis. Experimental and Therapeutic Medicine. 2012;4(1):165-71.

242. Brody M, Böhm I, Bauer R. Mechanism of Action of Methotrexate: Experimental Evidence that Methotrexate Blocks the Binding of Interleukin 1β to the Interleukin 1 Receptor on Target Cells. Clinical Chemistry and Laboratory Medicine1993. p. 667.

243. Böhm I. Increased peripheral blood B-cells expressing the CD5 molecules in association to autoantibodies in patients with lupus erythematosus and evidence to selectively down-modulate them. Biomedicine & Pharmacotherapy. 2004;58(5):338-43.

244. Wessels JAM, Huizinga TWJ, Guchelaar HJ. Recent insights in the pharmacological actions of methotrexate in the treatment of rheumatoid arthritis. Rheumatology. 2008;47(3):249-55.

245. Tong X, Zhao F, Thompson CB. The molecular determinants of de novo nucleotide biosynthesis in cancer cells. Current opinion in genetics & development. 2009;19(1):32-7.

246. Evans WE, Crom WR, Abromowitch M, Dodge R, Look AT, Bowman WP, et al. Clinical Pharmacodynamics of High-Dose Methotrexate in Acute Lymphocytic Leukemia. New England Journal of Medicine. 1986;314(8):471-7.

247. Matherly LH, Hou Z. Structure and function of the reduced folate carrier a paradigm of a major facilitator superfamily mammalian nutrient transporter. Vitamins and hormones. 2008;79:145-84.

248. McBride A, Antonia SJ, Haura EB, Goetz D. Suspected Methotrexate Toxicity From Omeprazole:A Case Review of Carboxypeptidase G2 Use in a Methotrexate-Experienced Patient With Methotrexate Toxicity and a Review of the Literature. Journal of Pharmacy Practice. 2012;25(4):477-85.

249. Maleki H, Dorkoosh F, Adabi M, Khosravani M, Arzani H, Kamali M. Methotrexate-loaded plga nanoparticles: Preparation, characterization and their cytotoxicity effect on human glioblastoma U87MG cells. Int J Med Nano Res. 2017;4(1):020.

250. Nicholson JK, Lindon JC. Systems biology: Metabonomics. Nature. 2008;455(7216):1054-6.

251. Tiziani S, Kang Y, Choi JS, Roberts W, Paternostro G. Metabolomic high-content nuclear magnetic resonance-based drug screening of a kinase inhibitor library. Nat Commun. 2011;2:545.

252. Richter E, Ventz K, Harms M, Mostertz J, Hochgräfe F. Induction of Macrophage Function in Human THP-1 Cells Is Associated with Rewiring of MAPK Signaling and Activation of MAP3K7 (TAK1) Protein Kinase. Frontiers in cell and developmental biology. 2016;4:21-.

253. Huang SC, Everts B, Ivanova Y, O'Sullivan D, Nascimento M, Smith AM, et al. Cell-intrinsic lysosomal lipolysis is essential for alternative activation of macrophages. Nat Immunol. 2014;15(9):846-55.

254. Pearce EL, Pearce EJ. Metabolic pathways in immune cell activation and quiescence. Immunity. 2013;38(4):633-43.

255. Barisci S, Turkay O, Ulusoy E, Dimoglo A. Degradation of the cytostatic methotrexate by electrosynthesized ferrate (VI): Identification of oxidation by-products2015.

256. Halama A, Riesen N, Möller G, Hrabě de Angelis M, Adamski J. Identification of biomarkers for apoptosis in cancer cell lines using metabolomics: tools for individualized medicine. J Intern Med. 2013;274(5):425-39.

257. Halama A, Riesen N, Moller G, Hrabe de Angelis M, Adamski J. Identification of biomarkers for apoptosis in cancer cell lines using

metabolomics: tools for individualized medicine. the Journal of Internal Medicine. 2013;274(5):425-39.

258. Rainaldi G, Romano R, Indovina P, Ferrante A, Motta A, Indovina PL, et al. Metabolomics using 1H-NMR of apoptosis and Necrosis in HL60 leukemia cells: differences between the two types of cell death and independence from the stimulus of apoptosis used. Radiation research. 2008;169(2):170-80.

259. Carracedo A, Cantley LC, Pandolfi PP. Cancer metabolism: fatty acid oxidation in the limelight. Nature reviews Cancer. 2013;13(4):227-32.

260. Vander Heiden MG, Cantley LC, Thompson CB. Understanding the Warburg effect: the metabolic requirements of cell proliferation. Science (New York, NY). 2009;324(5930):1029-33.

261. Akacha A, Rebai T, Zourgui L, Amri M. Preventive effect of ethanolic extract of cactus (Opuntia ficus-indica) cladodes on methotrexate-induced oxidative damage of the small intestine in Wistar rats. J Cancer Res Ther. 2018;14(Supplement):S779-S84.

262. Meng Z, O'Keeffe-Ahern J, Lyu J, Pierucci L, Zhou D, Wang W. A new developing class of gene delivery: messenger RNA-based therapeutics. Biomaterials Science. 2017;5(12):2381-92.

263. Keles E, Song Y, Du D, Dong W-J, Lin Y. Recent progress in nanomaterials for gene delivery applications. Biomaterials Science. 2016;4(9):1291-309.

264. Zelikin AN, Ehrhardt C, Healy AM. Materials and methods for delivery of biological drugs. Nat Chem. 2016;8(11):997-1007.

265. Scholz C, Wagner E. Therapeutic plasmid DNA versus siRNA delivery: Common and different tasks for synthetic carriers. Journal of Controlled Release. 2012(0).

266. Yin H, Kanasty RL, Eltoukhy AA, Vegas AJ, Dorkin JR, Anderson DG. Non-viral vectors for gene-based therapy. Nat Rev Genet. 2014;15(8):541-55.

267. Islam MA, Reesor EKG, Xu YJ, Zope HR, Zetter BR, Shi JJ. Biomaterials for mRNA delivery. Biomaterials Science. 2015;3(12):1519-33.

268. Zhang Y, Chan HF, Leong KW. Advanced materials and processing for drug delivery: The past and the future. Advanced Drug Delivery Reviews. 2013;65(1):104-20.

269. Chen J, Guo Z, Tian H, Chen X. Production and clinical development of nanoparticles for gene delivery. Molecular Therapy - Methods & Clinical Development. 2016;3:Article 16023.

270. Samal SK, Dash M, Van Vlierberghe S, Kaplan DL, Chiellini E, van Blitterswijk C, et al. Cationic polymers and their therapeutic potential. Chemical Society Reviews. 2012;41(21):7147-94.

271. Kudsiova L, Welser K, Campbell F, Mohammadi A, Dawson N, Cui LL, et al. Delivery of siRNA using ternary complexes containing branched cationic peptides: the role of peptide sequence, branching and targeting. Molecular Biosystems. 2016;12(3):934-51.

272. De Smedt SC, Demeester J, Hennink WE. Cationic Polymer Based Gene Delivery Systems. Pharmaceutical Research. 2000;17(2):113-26.

273. Oupicky D, Konak C, Ulbrich K, Wolfert MA, Seymour LW. Dna Delivery Systems Based on Complexes of Dna With Synthetic Polycations and Their Copolymers. Journal of Controlled Release. 2000;65(1-2):149-71.

274. Bansal R, Tayal S, Gupta KC, Kumar P. Bioreducible polyethylenimine nanoparticles for the efficient delivery of nucleic acids. Organic & Biomolecular Chemistry. 2015;13(10):3128-35.

275. Wang T, Upponi JR, Torchilin VP. Design of multifunctional non-viral gene vectors to overcome physiological barriers: dilemmas and strategies. Int J Pharm. 2012;427(1):3-20.

276. Morille M, Passirani C, Vonarbourg A, Clavreul A, Benoit JP. Progress in developing cationic vectors for non-viral systemic gene therapy against cancer. Biomaterials. 2008;29(24-25):3477-96.

277. Moghimi SM, Symonds P, Murray JC, Hunter AC, Debska G, Szewczyk A. A two-stage poly(ethylenimine)-mediated cytotoxicity: implications for gene transfer/therapy. Molecular therapy : the journal of the American Society of Gene Therapy. 2005;11(6):990-5.

278. Symonds P, Murray JC, Hunter AC, Debska G, Szewczyk A, Moghimi SM. Low and high molecular weight poly(L-lysine)s/poly(L-

lysine)-DNA complexes initiate mitochondrial-mediated apoptosis differently. FEBS letters. 2005;579(27):6191-8.

279. Hall A, Parhamifar L, Lange MK, Meyle KD, Sanderhoff M, Andersen H, et al. Polyethylenimine architecture-dependent metabolic imprints and perturbation of cellular redox homeostasis. Biochimica et biophysica acta. 2015;1847(3):328-42.

280. Caballero-Díaz E, Valcárcel Cases M. Analytical methodologies for nanotoxicity assessment. TrAC Trends in Analytical Chemistry. 2016;84:160-71.

281. Meyer UA, Zanger UM, Schwab M. Omics and drug response. Annual review of pharmacology and toxicology. 2013;53:475-502.

282. Creek D-HKDJ. What role can metabolomics play in the discovery and development of new medicines for infectious diseases? Bioanalysis. 2015;7(6):629-31.

283. Huang SM, Zuo XB, Li JJ, Li SFY, Bay BH, Ong CN. Metabolomics Studies Show Dose-Dependent Toxicity Induced by SiO2 Nanoparticles in MRC-5 Human Fetal Lung Fibroblasts. Adv Healthc Mater. 2012;1(6):779-84.

284. Hunter AC, Moghimi SM. Cationic carriers of genetic material and cell death: a mitochondrial tale. Biochimica et biophysica acta. 2010;1797(6-7):1203-9.

285. Kadlecova Z, Rajendra Y, Matasci M, Baldi L, Hacker DL, Wurm FM, et al. DNA delivery with hyperbranched polylysine: a comparative study with linear and dendritic polylysine. J Control Release. 2013;169(3):276-88.

286. Contrepois K, Jiang L, Snyder M. Optimized Analytical Procedures for the Untargeted Metabolomic Profiling of Human Urine and Plasma by Combining Hydrophilic Interaction (HILIC) and Reverse-Phase Liquid Chromatography (RPLC)-Mass Spectrometry. Molecular & cellular proteomics : MCP. 2015;14(6):1684-95.

287. Wang Y, Liu S, Hu Y, Li P, Wan J-B. Current state of the art of mass spectrometry-based metabolomics studies – a review focusing on wide coverage, high throughput and easy identification. RSC Advances. 2015;5(96):78728-37.

288. Nagana Gowda GA, Raftery D. Can NMR solve some significant challenges in metabolomics? Journal of magnetic resonance (San Diego, Calif : 1997). 2015;260:144-60.

289. Kadlecova Z, Baldi L, Hacker D, Wurm FM, Klok HA. Comparative study on the in vitro cytotoxicity of linear, dendritic, and hyperbranched polylysine analogues. Biomacromolecules. 2012;13(10):3127-37.

290. Grandinetti G, Smith AE, Reineke TM. Membrane and nuclear permeabilization by polymeric pDNA vehicles: efficient method for gene delivery or mechanism of cytotoxicity? Molecular pharmaceutics. 2012;9(3):523-38.

291. Vaidyanathan S, Orr BG, Banaszak Holl MM. Role of Cell Membrane-Vector Interactions in Successful Gene Delivery. Accounts of chemical research. 2016;49(8):1486-93.

292. Almulathanon AAY, Ranucci E, Ferruti P, Garnett MC, Bosquillon C. Comparison of Gene Transfection and Cytotoxicity Mechanisms of Linear Poly(amidoamine) and Branched Poly(ethyleneimine) Polyplexes. Pharm Res. 2018;35(4):86.

293. Panieri E, Santoro MM. ROS homeostasis and metabolism: a dangerous liason in cancer cells. Cell death & disease. 2016;7(6):e2253.

294. Hall A, Lachelt U, Bartek J, Wagner E, Moghimi SM. Polyplex Evolution: Understanding Biology, Optimizing Performance. Molecular therapy : the journal of the American Society of Gene Therapy. 2017;25(7):1476-90.

295. Choi YM, Kim HK, Shim W, Anwar MA, Kwon JW, Kwon HK, et al. Mechanism of Cisplatin-Induced Cytotoxicity Is Correlated to Impaired Metabolism Due to Mitochondrial ROS Generation. PloS one. 2015;10(8):e0135083.

296. Hoppel C. The role of carnitine in normal and altered fatty acid metabolism. Am J Kidney Dis. 2003;41(4 Suppl 4):S4-12.

297. Fukao T, Mitchell G, Sass JO, Hori T, Orii K, Aoyama Y. Ketone body metabolism and its defects. Journal of Inherited Metabolic Disease. 2014;37(4):541-51.

298. Ciccarese F, Ciminale V. Escaping Death: Mitochondrial Redox Homeostasis in Cancer Cells. Frontiers in Oncology. 2017;7:117.

299. Winkler BS, DeSantis N, Solomon F. Multiple NADPH-producing pathways control glutathione (GSH) content in retina. Exp Eye Res. 1986;43(5):829-47.

300. Mailloux RJ, Bériault R, Lemire J, Singh R, Chénier DR, Hamel RD, et al. The Tricarboxylic Acid Cycle, an Ancient Metabolic Network with a Novel Twist. PLOS ONE. 2007;2(8):e690.

301. Ramen T M. Depletion of Glutathione during Oxidative Stress and Efficacy of N-Acetyl Cysteine: An Old Drug with New Approaches2015.

302. Lee MS, Kim NW, Lee K, Kim H, Jeong JH. Enhanced Transfection by Antioxidative Polymeric Gene Carrier that Reduces Polyplex-Mediated Cellular Oxidative Stress. Pharm Res. 2013;30(6):1642-51.

303. Hall A, Wu LP, Parhamifar L, Moghimi SM. Differential Modulation of Cellular Bioenergetics by Poly(L-lysine)s of Different Molecular Weights. Biomacromolecules. 2015;16(7):2119-26.

304. Morel Y, Barouki R. Repression of gene expression by oxidative stress. The Biochemical journal. 1999;342 Pt 3:481-96.

305. Halama A, Riesen N, Moller G, Hrabe de Angelis M, Adamski J. Identification of biomarkers for apoptosis in cancer cell lines using metabolomics: tools for individualized medicine. Journal of internal medicine. 2013;274(5):425-39.

306. Rainaldi G, Romano R, Indovina P, Ferrante A, Motta A, Indovina PL, et al. Metabolomics using 1H-NMR of apoptosis and Necrosis in HL60 leukemia cells: differences between the two types of cell death and independence from the stimulus of apoptosis used. Radiation research. 2008;169(2):170-80.

307. Takikawa O. Biochemical and medical aspects of the indoleamine 2,3-dioxygenase-initiated L-tryptophan metabolism. Biochemical and biophysical research communications. 2005;338(1):12-9.

308. Thomas SR, Stocker R. Redox reactions related to indoleamine 2,3-dioxygenase and tryptophan metabolism along the kynurenine pathway. Redox report : communications in free radical research. 1999;4(5):199-220.

309. Stone TW, Darlington LG. Endogenous kynurenines as targets for drug discovery and development. Nature Reviews Drug Discovery. 2002;1:609.

310. Matz RL, Erickson B, Vaidyanathan S, Kukowska-Latallo JF, Baker JR, Jr., Orr BG, et al. Polyplex exposure inhibits cell cycle, increases inflammatory response, and can cause protein expression without cell division. Molecular pharmaceutics. 2013;10(4):1306-17.

Appendix

General methods

Proton nuclear magnetic resonance (1H-NMR) spectroscopy

^{1}H-NMR spectroscopy was performed at 400 MHz using a Brüker DPX400 Ultrashield spectrometer and deuterated chloroform ($CDCl_3$) as a solvent. All the chemical shifts were recorded in ppm with reference to $CDCl_3$. The spectra were analysed using MestRENova (6.0.2, Mestrelab Research S.L., 2009).

Particle size and Zeta potential measurement

Mean hydrodynamic diameters of NPs were obtained by measuring the light scattering at 173° angle to incident radiation at 25 °C after diluting the samples with water using Malvern (TM) Zetasizer equipped with 10 mW He-Ne laser operating at a wavelength of 633 nm. The zeta potential for the NPs was measured in water using the same Malvern (TM) Zetasizer.

Transmission electron microscopy (TEM)

NPs' morphological was evaluated using a Tecnai G2 (FEI, Oregon, USA) Transmission Electron Microscopy (TEM). 17 µl of NPs suspension in water were added onto a copper grid and wicked off

after 10 minutes, and then 3% wt/v uranyl acetate was used as negative stain prior to imaging.